Dominik Hemmer, BSc

Alginate Acoustics

Development and analysis of micro perforated foils based on a sustainable material

master's thesis

submitted to

Graz University of Technology

Supervisors

Dipl.-Ing. Dr.techn. Jamilla Balint
Dipl.-Ing. Dr.techn. Werner Weselak

Signal Processing and Speech Communication Laboratory
Head: Univ.-Prof. Dipl.-Ing. Dr.techn. Gernot Kubin

in cooperation with

Institute of Architecture and Media
Institute for Chemistry and Biobased Systems

Graz, September 2023

Affidavit

I declare that I have authored this thesis independently, that I have not used other than the declared sources/resources, and that I have explicitly indicated all material which has been quoted either literally or by content from the sources used. The text document uploaded to TUGRAZonline is identical to the present master's thesis.

date	(signature)

Danksagung

Da sich nun eine große Reise dem Ende neigt, möchte ich meiner tiefen Dankbarkeit gegenüber den Menschen Ausdruck verleihen, die mich während des großen Projekts Masterarbeit unterstützt und geleitet haben.

Zuerst möchte ich meiner Betreuerin, Dr. Jamilla Balint, meinen aufrichtigen Dank aussprechen für ihre unschätzbare Unterstützung, ihr Fachwissen und ihre Geduld. Die Hingabe, das konstruktive Feedback und die wertvollen Ratschläge haben eine entscheidende Rolle bei der Gestaltung dieser Arbeit gespielt.
Weiters bedanken möchte ich mich bei Dr. Werner Weselak, für seine großartige Unterstützung, die unschätzbare Erfahrung und sein kritisches Auge als Betreuer, Dipl.-Ing Eric Kurz vom SPSC (Signal Processing and Speech Communication Laboratory) und Dr. Milena Stavric vom IAM (Institut für Architektur und Medien) für ihre tatkräftige Unterstützung sowie speziell bei Cornelia Ott, BSc, die neben den Fragen zu Architektur, praktischem Aufbau und Design auch den besten Kaffee zubereitete.

Besonderer Dank geht auch an meine Familie, insbesondere an meine Eltern Sonja und Gerhard für die unermüdliche Unterstützung in allen Lebenslagen. Ihr Glaube an mein Potenzial haben eine entscheidende Rolle bei der Gestaltung meines Lebensweges gespielt. Meinem Bruder Marcel möchte ich ebenso meine Wertschätzung aussprechen für seinen scharfen Hausverstand und die lustigen Unterhaltungen.

Zu guter Letzt bin ich meiner geliebten Gattin Natalie zutiefst dankbar für ihre unermüdliche Unterstützung, das notwendige Verständnis und den positiven Zuspruch. Ohne sie wäre es nicht möglich gewesen, die gemeinsame Firma neben dem Studienabschluss weiterzuführen. Ihre Geduld und ihr Zuspruch waren von unschätzbarem Wert und gaben mir die Kraft und Motivation, in den herausfordernden Momenten durchzuhalten.

Allen Genannten und vielen anderen, die mich auf dieser Reise unterstützt haben, möchte ich meinen herzlichen Dank aussprechen. Eure Beiträge haben diese Leistung möglich gemacht, und ich bin dafür sehr dankbar.

Abstract

This work deals with the fabrication, analysis and modelling of microperforated films made from alginate, an irreversibly hardening elastic moldable material which is found in brown algae cell walls. In an interdisciplinary project connecting architecture, chemistry, and acoustics, the properties of alginate are explored for the use as acoustic absorbers. As the substance alginate can be classified as a sustainable material, the challenging fight against the plastic flood is always in need for biodegradable alternatives. Also in real world scenarios, there are only a few translucent solutions available that provide acoustic absorption.
First, the associated theory is examined in detail. Therefore models for resonance absorbers and microperforated absorbers are introduced. Then, especially the fabrication process of microperforated, translucent films will be discussed in this thesis. The samples made from alginate will then be evaluated by measuring the absorption coefficient in the impedance tube. The obtained data will be compared against established theoretical models, providing valuable insights and potential directions for future research. By exploring the capabilities of alginate, this work tries to promote environmentally friendly materials and encourage further development in the field of biodegradable alternatives.

Kurzfassung

Diese Arbeit beschäftigt sich mit der Herstellung, Analyse und Modellierung von mikroperforierten Folien, die aus dem Grundstoff Alginat hergestellt sind. Vermischt man Alginatpulver mit Wasser, bildet sich ein durchsichtiger Stoff, der nach Trocknung aushärtet und sich plastikähnlich verhält. In einem interdisziplinären Projekt, das die Bereiche Architektur, Chemie und Akustik umspannt, sollen die Eigenschaften des Alginats erkundet werden und ihr Einsatz als akustischer Absorber evaluiert werden. Da das Material als nachhaltiger Grundstoff klassifiziert werden kann, könnte sich eine dringend gesuchte Alternative als Grundstoff in einer Zeit des Plastiküberflusses finden. Ebenso sucht die Architektur stets nach Designmöglichkeiten mit optisch transparenten Lösungen, die auch akustische Wirksamkeit einbringen.
Zuerst wird die zugehörige Theorie der Resonanzabsorber und der mikroperforierten Absorber untersucht. Im Detail werden anschließend der Herstellungsprozess der durchsichtigen Folien, die Mikroperforation und die Vergleiche mit bestehenden Theorien zu mikroperforierten Absorbern beschrieben. Der Absorptionsgrad der Testfolien soll im Messrohr bestimmt werden. Abschließend werden die Ergebnisse diskutiert und Impulse für zukünftige Arbeiten gegeben. Mit der Untersuchung der Eignung als Absorbergrundstoff, wird der Einsatz umweltfreundlicher Stoffe unterstützt und der Anstoß für zukünftige Arbeiten gegeben.

Contents

1 Introduction

.

1.1 Motivation

As the need for plastic-free alternatives increases in various aspects of life and industries, the acoustic properties of the biodegradable substance *alginate* were examined. It reflects the growing concern about the environmental impact of plastic waste and the desire to reduce plastic usage by replacing it with more sustainable alternatives. A special motivation was a recent study made by the environmental initiative **Back to Blue** on the consumption of plastics. Back to Blue is an organisation to improve evidence-based approaches and solutions to the issues faced by the oceans, and to restoring ocean health [Org, 2023]. They revealed alarming findings in their study: without further steps, plastic consumption is expected to double by 2050, reaching an astonishing 451 million tons annually. These incredible large numbers emphasize the urgent need for immediate action to address the escalating plastic crisis. Efforts to reduce, recycle and find sustainable alternatives are crucial to secure a healthier future for generations to come.
The control of reverberance has been a topic of interest for a very long time. If we think of large spaces like railway stations or shopping malls with their excessive reverberation times, it can be difficult to communicate in this noisy environments. People tend to slow down their speech, talk louder and try to pronounce words more precisely to make the received speech understandable. Reverberation is the decay of sound after a sound source has stopped and it is a key feature in room acoustics [Kuttruff, 2019]. In spaces with hard surfaces, reverberation is most audible. In small spaces with soft acoustically absorbent materials, such as living rooms, the materials absorb the sound energy, and the sound dies away rapidly. When people talk about rooms being 'live' or 'dead' this is usually a description of the perception of reverberance. The amount of reverberation in a space depends on the size of the room and the amount of sound absorption. Controlling the right amount of reverberation in a space is vital to most rooms, whether the aim is to reduce noise levels, to optimize a room for communication purposes, to optimize for good sounding musical performances or simply to make a space a pleasant place to be in [Cox and D'Antonio, 2009]. Therefore **sound absorbers** are used, to

- **increase the transmission loss** of walls,
- **decrease the reverberation time** of rooms, or to
- **attenuate the noise** generated by internal sound sources.

In modern design, there is a growing focus on creating attractive spaces while controlling the acoustics and still taking care of our environment. At the same time, acoustic engineers are looking for ways to use less plastic in their applications, both indoors and outdoors, to reduce plastic waste and protect the planet. There is great potential for contributing to plastic-free acoustic solutions.
The aim of this research was to imitate the acoustic behavior of perforated absorber film and to replace traditional materials made of plastic with the sustainable alternative, namely *alginate*.

During the experimental phase we were searching for thin, tear- and waterresistent alginate films that could be used as the basis for translucent absorbers. Due to the comprehensive interdisciplinary project involving architecture, chemistry and acoustics, a part of the research work was performed at the facilities of the **Institute for Architecture and Media** (IAM) and the **Institute of Chemistry and Technology of Biobased Systems** (iBioSys) of TU Graz with special support from Univ.-Prof. Dr. Milena Stavric, Univ.-Prof. Dr. Karin Stana Kleinschek and Dr. Tamilselvan Mohan.
Throughout the work on this thesis, the fabrication process of microperforated absorbers made from alginate is discussed. We tried to optimize the stability of the resulting films as well as the tear-resistance. As we deal with submillimetric dimensions to obtain broadband absorption, different types of perforation methods were discussed. With the design approach and the need for optically transparent devices in mind, the focus lies on the fabrication of the films and the evaluation of different design parameters. Therefore an intensive recap of the theory of microperforated absorbers is given. First, the theoretical framework was implemented in Matlab providing quick evaluation of the measurements and a way to predict the acoustic behaviour by tuning certain material parameters. Then, a detailed parameter-study supported the selection of the design parameters to receive broadband sound absorption. After performing measurements in the impedance tube with the fabricated films, the expected and the measured results for the absorption coefficient were compared and discussed. Additionally, we investigated the potential of double-layer arrangements for increased absorption.

1.2 Overview

Chapter 2 - Absorber principles
An insight to the theories used in different acoustic applications is given in this chapter. Therefore the principles of sound propagation and absorption are explained. It continues with the mathematical background of different absorber principles, namely porous sound absorbers, resonant absorbers and finally, microperforated absorbers. The later are discussed in detail. A parameter-study is performed and shows the necessary relations between different material parameters to obtain broadband sound absorption within the boundaries of microperforated panels. Finally the multi-layer arrangement of microperforated films and their applications are considered.

Chapter 3 - Sustainable materials in acoustics
First, sustainable materials are presented that are already in use for acoustic applications. Then, the extraction and occurrence as well as the background of the substance *alginate* is explained in this section. The different steps of the fabrication process are shown in detail that finally lead to the specimen for further measurement. Starting from just alginate powder and water, different mixtures are considered with the aim to obtain a translucent absorber film that comes close to the feeling and behaviour of plastic. Also several perforation techniques are discussed.

Chapter 4 - Results and discussion
In this chapter, the focus is on the measurement of the absorption coefficient, and particularly on examining individual specimens of alginate films. To accomplish this, the absorption coefficient is determined using an impedance tube. The obtained results are then compared to the expected behavior predicted by the theory discussed in Chap. 2. Various plots are used to visualize and analyze the comparison between the individual samples and the theoretical predictions. Furthermore, the chapter shows the behavior of a two-layer arrangement of alginate films and discusses the results.

Chapter 5 - Conclusion and outlook
Within the final section, a short summary of the theory and the corresponding results of the previous chapters is presented. A future outlook shows some of the difficulties during the fabrication process and provides ideas for possible applications and future research.

2 Absorber principles

In this work, we consider two types of absorbers: porous absorbers and resonant absorbers. We evaluate their performance by using an absorption coefficient. It's value varies from 0 to 1, representing no and complete absorption. Porous absorbers are the most used materials because of their high performance-to-cost ratio in the frequency band of interest and the ease of use. Microperforated panels (MPPs) in front of a rigid surface with an enclosed air cavity instead offer a fiber-free alternative to porous absorbers in cases where small particle discharge can be an issue, like pharmaceutical, food and microelectric industries. In general MPPs with broadband absorption require many small holes distributed over a panel or film of also submillimetric thickness.
In this chapter we will first consider some theoretical aspects of sound propagation, give a short description of porous absorbers and then discuss the theory which is needed to describe resonant absorbers in detail. Also, the theoretical approaches to obtain the acoustic impedance of microperforated panels are considered. In a parameter study we examine favorable parameter sets that are later used in the design process of microperforated films. We distinguish single layer and multi layer arrangements of MPPs and show further some of their applications.

2.1 Sound propagation

2.1.1 Impedance

For the design of absorbers, knowledge on sound propagation is important. The following sections follow the derivations as presented in [Cox and D'Antonio, 2009] and [Kuttruff, 2019]. Therefore we use the complex number representation of waves as a fundamental mathematical construct. The pressure $\underline{p}$ of a plane wave propagating in a direction $\mathbf{r}$ can be written as:

$$\underline{p}(t, \mathbf{r}) = Ae^{j(\omega t - \mathbf{kr})} = Ae^{j(\omega t - k_x x - k_y y - k_z z)} \quad \left[Pa\right] \tag{2.1}$$

where

- $\mathbf{k} = \{k_x, k_y, k_z\}$ is the wavenumber, with k_x being the component in x direction
- A is a constant for the magnitude of the wave,
- $\mathbf{r} = \{x, y, z\}$ is the direction of the propagating wave,
- t is time and $\omega = 2\pi f = kc$ the angular frequency with
- f being the frequency and c the speed of sound.

If we consider a plane wave propagating through an acoustic medium only in the x-direction, the pressure $\underline{p}$ and particle velocity $\underline{v}$ are given as:

$$\underline{p}(t,x) = Ae^{j(\omega t - kx)} \quad \left[Pa\right] \tag{2.2}$$

and

$$\underline{v}(t,x) = \frac{A}{\rho c} e^{j(\omega t - kx)} \quad \left[\frac{m}{s}\right] \tag{2.3}$$

with ρ being the density and c the speed of sound of the acoustic medium.
A useful property of a material is the **characteristic acoustic impedance** $\underline{Z}_c$. It is given by the ratio of pressure to velocity. Acoustic impedance is the opposition of a medium to a sound wave motion.

$$\boxed{\underline{Z}_c = \frac{\underline{p}}{\underline{v}} = \underline{\rho c} \quad \left[\frac{Ns}{m^3}\right]} \tag{2.4}$$

Thus, the acoustic impedance that is acting in opposition to the wave propagation increases with an increase in medium density as well as an increase in the speed of sound. It is useful when calculating the transmission of waves between and within different media. The specific acoustic impedance of air changes with temperature since both the medium density and the speed of sound depend on temperature. For a plane wave in air, the term is real with a value of about 415 $\left[\frac{Ns}{m^3}\right]$ at $18°C$. In a porous material, it will be complex, with a characteristic resistance and reactance, which are the real and imaginary parts of the characteristic impedance.

2.1.2 Effect of a surface

Three acoustic parameters, that are interrelated, can be used to characterize the impact of a surface to an acoustic wave:

- Wall impedance $\underline{W}$
- Reflection factor $\underline{R}$
- Absorption coefficient α

The first two parameters contain the information on the magnitude and phase change on the reflection, whereas the last parameter gives only information about the energy change on reflection and does not contain phase data.

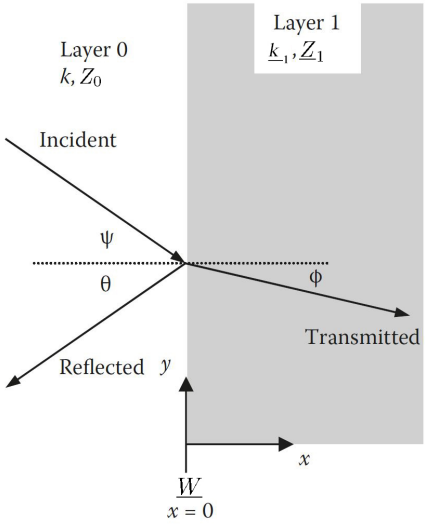

Figure 2.1: Sound incident on a surface and being reflected and transmitted [Cox and D'Antonio, 2009].

A simple model for a porous medium assumes that it behaves like air, only with complex speed of sound $\underline{c}$ and density $\underline{\rho}$. We consider plane wave incident at an angle ψ to a boundary between two acoustic media at $x = 0$ as shown in figure 2.1, representing air as layer 0 and a porous medium as an infinitely extended layer 1, leading to a wall impedance

$$\underline{W} = \underline{Z}_1 \quad \left[\frac{Ns}{m^3}\right], \tag{2.5}$$

equal to the characteristic impedance of the porous medium (layer 1), extended to infinity. The reflection factor, sometimes referred to reflection coefficient $\underline{R}$ gives the ratio of the reflected and incident pressure:

$$\underline{R} = \frac{\underline{p}_r}{\underline{p}_i} \tag{2.6}$$

The wall impedance $\underline{W}$ is often used normalized to the characteristic impedance of air Z_0, for that we write $\underline{w} = \frac{\underline{W}}{Z_0}$. The relationship between reflection factor and the wall impedance for oblique incidences are:

$$\boxed{\underline{R} = \frac{\underline{W}\cos\psi - Z_0}{\underline{W}\cos\psi + Z_0} = \frac{\underline{w}\cos\psi - 1}{\underline{w}\cos\psi + 1}} \tag{2.7}$$

For a given angle ψ, the best fit is found with $|\underline{W}| \geq Z_0$. The absorption coefficient α is a ratio of the absorbed and incident energy and can be derived to:

$$\alpha = 1 - |\underline{R}|^2 \tag{2.8}$$

with $|\underline{R}|$ being the magnitude of the reflection coefficient.

$$\boxed{\alpha = \frac{4 \cdot \mathrm{Re}\{\underline{w}\} \cdot \cos\psi}{[1 + \mathrm{Re}\{\underline{w}\} \cdot \cos\psi]^2 + [\mathrm{Im}\{\underline{w}\} \cdot \cos\psi]^2}} \tag{2.9}$$

The real term of the wall impedance is associated with energy losses, and the imaginary term with changes in phase. To get a brief insight on the absorbing properties of a material, the wall impedance can be used as an alternative to the absorption coefficient.

2.2 Porous sound absorbers

Porous absorbers are commonly associated with acoustic absorption, as many materials possess natural porosity and therefore absorb sound. When attempting to build a home studio or implement basic acoustic treatment in a room, people often use common items such as thick curtains, carpets, and sofas to regulate the reverberation time. They are often made from materials with open pores and work as porous absorbers. An example of a fibrous porous absorber is mineral wool, which is created by spinning molten minerals, such as sand, into fibres and weaving them together to produce a complex structure of pores. This pore network creates a highly porous material that is often used for both acoustic and fire insulation. Its open pores restrict the flow of air through the material, allowing it to absorb sound and prevent heat exchange. Another example for porous materials are all kinds of foams with open cells. If the cells are closed, these foams have either closed pores so there is no propagation path or pores that are too small for the sound wave to propagate through. As waves cannot propagate through the material there will be no viscous and thermal losses and the material will act as a reflector. Figure 2.2 shows the structure of foam with open and closed cells.

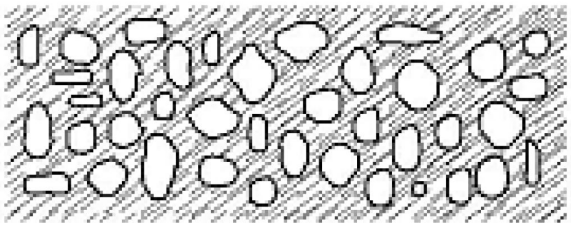

(a) Closed cell foam, pores are closed

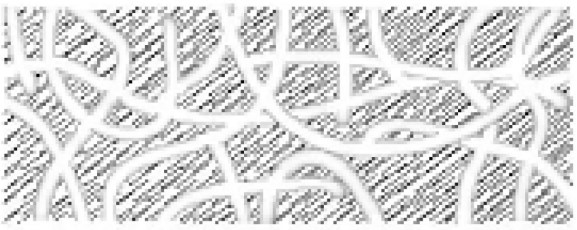

(b) Open cell foam, pores allow for acoustic propagation and thermal and viscous losses

Figure 2.2: Porous materials [Cox and D'Antonio, 2009]

When sound propagates in small spaces there are losses in energy, primarily caused by viscous boundary layer effects, i.e. the friction of the air passing through the orifice of a small pore. This friction causes viscous and heat losses in porous materials making them suitable for room acoustic applications.
The absorption effect of a porous device is most effective placed at the space where the sound particle velocity has its maximum. This maximum can be found with a distance of $x = \frac{\lambda}{4}$ to a rigid backing. Therefore to obtain decent sound absorption at $100\,Hz$ a depth of 85 cm is necessary. To develop a theoretical model for sound propagation through a porous material, it is crucial to obtain measurements that characterize the properties of the absorber as an acoustic medium. However, the wavenumber and characteristic impedance cannot be directly measured. Therefore, absorber designers require other parameters. Typically, when working with a porous material, research begins by measuring the flow resistivity Ξ, and porosity σ. Sometimes also the structure factor χ is also taken into account.

The porosity σ quantifies the volume of open space available within the absorber for sound waves to propagate and can be written as relation of the volume of the acoustic relevant air volume V_{air} to the whole absorber volume V_{total}.

$$\sigma = \frac{V_{air}}{V_{total}} < 1 \tag{2.10}$$

The flow resistivity Ξ measures the resistance to flow that the porous absorber presents. The unit is expressed in terms of Pascal-seconds per square meter ($Pa*s/m^2$). Table 2.1 shows some common values.

$$\Xi = \frac{\Delta p}{v \Delta x} \quad \left[\frac{Pa*s}{m^2}\right] \tag{2.11}$$

Δp is the pressure difference measured while constantly streaming air through an absorbing layer with a certain thickness Δx and a flow velocity v.

Material	Flow resistivity Ξ
Fiberglass insulation	$5 - 25kPa*s/m^2$
Mineral wool insulation	$8 - 40kPa*s/m^2$
Acoustic foam (Melamin)	$5 - 50kPa*s/m^2$

Table 2.1: Absorbing materials and typical values for Ξ. [ISO 11654:1997, 1997]

Depending on the addressed frequency range of the absorber and the possibility of using different panel-thickness, the following relationships for the applications arise:

- With thin material thicknesses up to 10 cm, a high length-specific flow resistance Ξ allows for more sound energy absorption (fig. 2.3).
- Absorbers with a thickness of 50 cm or more and lower flow resistance can absorb even lower frequencies up to $\geq 100\,\text{Hz}$. The increased difficulty of penetration at lower frequencies and high flow resistance becomes noticeable (fig. 2.4).

Furthermore, Fig. 2.3 and 2.4 show the effect of the length-specific flow resistance on the absorption coefficient for the same material thickness. We can observe that with a smaller thickness, for example, 10 cm, a higher flow resistance leads to improved absorption performance at lower frequencies, although the maximum absorption coefficient is not reached. With a material thickness of 50 cm, the absorption coefficient gets reduced at lower frequencies compared to the material with lower flow resistance since the sound waves are no longer able to get into the absorber effectively.

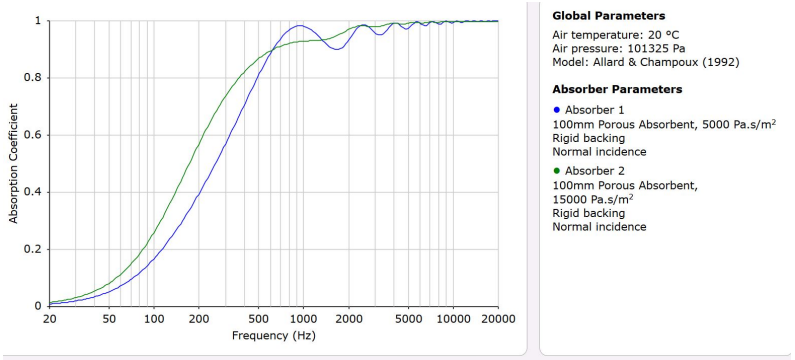

Figure 2.3: Comparing panels made of e.g. melamine resin ($5kPa*s/m^2$, blue) and mineral wool ($15kPa*s/m^2$, green), panel thickness 10 cm. Calculated with the online available tool "Porous absorber calculator" by acoustic modelling [PCal, 2023]

.

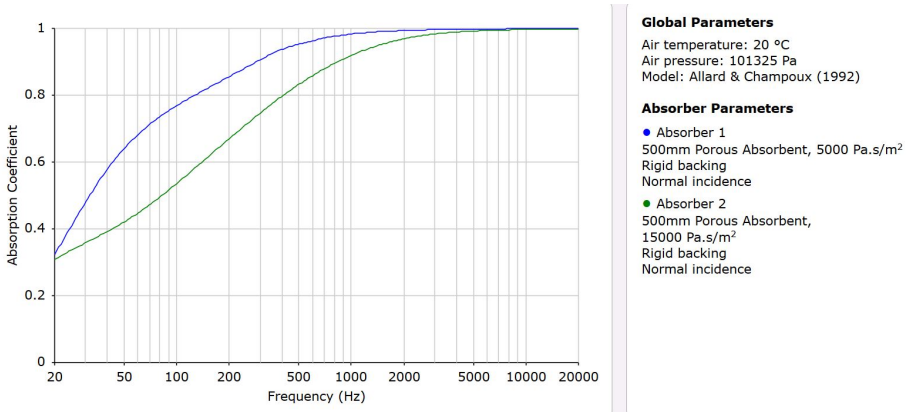

Figure 2.4: Comparing panels made of e.g. melamine resin ($5kPa*s/m^2$, blue) and mineral wool ($15kPa*s/m^2$, green), panel thickness 50 cm. Calculated with the online available tool "Porous absorber calculator" by acoustic modelling [PCal, 2023]

.

We aim for a model to describe the porous material with the characteristic impedance of the absorber $\underline{Z}_A$ and a complex propagation constant $\underline{\Gamma}_A$. The **Delany-Bazley-Modell** shall later be used for further calculations. It is an empirically obtained model from a large number of measurements on fibrous materials with porosities close to 1.00, [Delany and Bazley, 1970] have proposed empirical expressions for the values of $\underline{\Gamma}_A$ and $\underline{Z}_A$.

$$\boxed{\underline{Z}_A = Z_0 \left[1 + 0,057\left(\frac{\Xi}{\rho \cdot f}\right)^{0.75} - j0.087\left(\frac{\Xi}{\rho \cdot f}\right)^{0.73}\right] \left[\frac{Ns}{m^3}\right]} \tag{2.12}$$

$$\boxed{\underline{\Gamma}_A = k\left[0,189\left(\frac{\Xi}{\rho \cdot f}\right)^{0.59} + j\left(1 + 0.098\left(\frac{\Xi}{\rho \cdot f}\right)^{0.70}\right)\right] \left[\frac{1}{m}\right]} \tag{2.13}$$

This is valid for the following range:

$$0,01 \leq \frac{\rho \cdot f}{\Xi} \leq 1 \tag{2.14}$$

and as example for mineral wool with $\Xi = 10400 \left[\frac{Pa*s}{m^2}\right]$ for

$$87\,[Hz] \leq f \leq 8667\,[Hz]. \tag{2.15}$$

To obtain a wall impedance $\underline{W}_d$, leading towards the absorption coefficient, the known relationship from [TA, 2023] for a porous layer with thickness d in front of a rigid wall is used:

$$\boxed{\underline{W}_d = -j\underline{Z}_A \cdot \cot\left(-j\underline{\Gamma}_A \cdot d\right) \left[\frac{Ns}{m^3}\right]} \tag{2.16}$$

2.3 Resonant sound absorbers

Acoustic panel absorbers are a type of sound absorber that use a thin, flexible membrane to convert sound energy into heat. When sound waves strike the membrane, they cause it to vibrate, which in turn dissipates the sound energy into heat. Absorbers working on that principle are called resonant absorbers more generally. While porous absorption is mainly used for mid to high frequency sound absorption, resonant absorption is predominantly used for addressing low frequency acoustic issues. Resonant absorption can also be utilized for higher frequency situations where porous absorbers are not feasible due to potential damage or clogging of the pores by external elements such as weather or fumes. However, using resonant absorption for higher frequency issues is not typical because the bandwidth of absorption is generally narrow compared to that of porous absorption in order to achieve high absorption coefficients.
There are two main types of resonant absorption, namely membrane absorbers and the Helmholtz absorbers named after Hermann von Helmholtz (1821-1894). Both are commonly used in room applications and also as silencers in engines or ventilation. An overview on the theory of both concepts is presented in the following section [Cox and D'Antonio, 2009].

2.3.1 Membrane absorbers

Membrane absorbers are mass-spring systems. The vibrating mass is a flexible membrane and the spring is the enclosed air cavity behind the membrane. The air gap can also be filled with a porous absorbent. A basic design of a membrane absorber is shown in Fig. 2.5. Acoustic waves that meet the surface of a membrane cause it to oscillate at a frequency, determined by its mass, and the stiffness of the air spring of the cavity. And while some devices such as Helmholtz absorbers can be predicted with reasonable accuracy, membrane devices are still designed by trial and error through experimentation. This is because the exact mounting conditions and properties of the membrane are hard to predict and model [Oldfield, 2006].
The volume in the cavity can be filled with damping material, e.g. fiberglass or other porous material. The damping will have the following effects: First, the bandwidth of the resonator will be wider. Second, the dissipation of energy in the cavity will be more effective. A simple construction is formed by a cavity with a covering sheet.

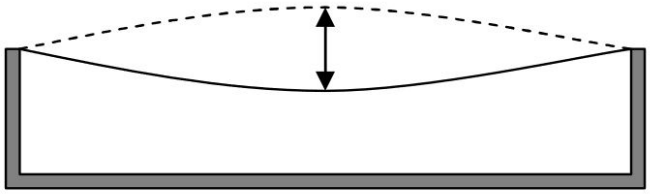

Figure 2.5: Schematic representation of a membrane absorber

The surface impedance of the resonant system is given as [Cox and D'Antonio, 2009]:

$$\boxed{\underline{W} = r + j[\omega m' - \rho_0 c_0 \cot(kD)] \quad \left[\frac{Ns}{m^3}\right]} \tag{2.17}$$

In our spring-mass system, the acoustic mass and resistance due to the membrane come into play. The losses resulting in a resistance term (r), a mass term ($\omega m'$) and a spring term ($-\rho_0 c_0 \cot(kD)$) occur. In the equation, $k = 2\frac{\pi}{\lambda}$ is the wavenumber in air, D is the cavity depth, $m' \quad \left[\frac{kg}{m^2}\right]$ is the acoustic mass per unit of the area of the panel, ρ_0 is the density of air, ω is the angular frequency and c_0 is the speed of sound in air. We consider a case without porous

absorbent material and cavity size much smaller than the acoustic wavelength.
We use the assumption $kD \leq 1$ which simplifies the term to $\cot(kD) \longrightarrow \frac{1}{kD}$. This leads to the spring behaviour. In comparison to Eq. 2.16, we notice the similarity in the appearance of the last term with the cotangent. The difference of its argument comes from the medium itself. We now consider a lossless medium and use jk instead of the complex propagation constant $\underline{\Gamma}$.
Systems resonate when the imaginary part of the impedance is 0, so to obtain the resonant frequency we set the imaginary part of Eq. 2.17 to 0. The resonance frequency f is given by:

$$\boxed{f = \frac{c_0}{2\pi}\sqrt{\frac{\rho_0}{m'D}}} \tag{2.18}$$

By using the constants $c_0 = 343\,\frac{m}{s}$ and $\rho_0 = 1.204\frac{kg}{m^3}$, with the cavity depth D in cm, mass per unit of area m' in $\frac{kg}{m^2}$ this can be further simplified to the following simplification by [Cox and D'Antonio, 2009]:

$$f \approx \frac{600}{\sqrt{m'D}} \tag{2.19}$$

In [Fuchs, 2017] we find the same approximation with d in mm:

$$f \approx \frac{1900}{\sqrt{m'D}} \tag{2.20}$$

Table 2.2 compares two membrane configurations leading to f_{res1} and f_{res2}.

	f_{res1} [Hz]	D [cm]	m' $[\frac{kg}{m^2}]$	f_{res2} [Hz]	D [cm]	m' $[\frac{kg}{m^2}]$
	281	5	0.912	971	3	0.1273

Table 2.2: Approximated resonance frequency of a membrane absorber.

2.3.2 Helmholtz absorbers

A typical Helmholtz absorber consists of a plate with numerous equally spaced holes. These are typically treated with porous absorption, unless they are small enough to generate enough absorption on their own. The resulting plug of air inside the holes is the resonating mass, while the air of the volume between the front and back plates acts as the spring. Fig. 2.6 illustrates the structure of a common Helmholtz absorber.

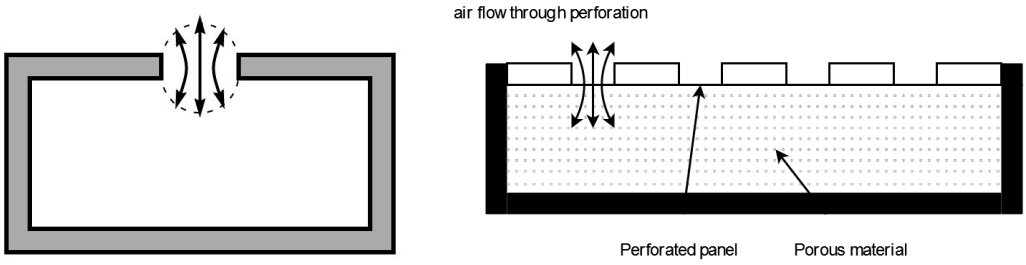

(a) Principle of the Helmholtz resonator: The air plug in the opening oscillates on the elastic "bed" formed by the air in the backing.

(b) Schematic representation of a Helmholtz absorber

Figure 2.6: Helmholtz absorber, drawn with draw.io

The resonant frequency of Helmholtz absorbers can be predicted to a high degree of accuracy by considering each orifice to be a short tube forming individual Helmholtz resonators. The perforated surface is divided into individual cells that are assumed to behave independently with a repeat distance b. For b and other describing parameters see Fig. 2.7. The absorber is assumed to be perforated in two directions, with the repeat length being the same in both directions. The individual cells will not be entirely independent at low frequency, as the wavelength becomes large.

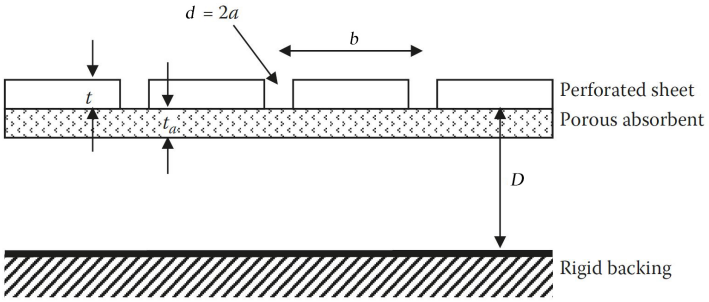

Figure 2.7: Cross-section through Helmholtz absorber [Cox and D'Antonio, 2009]

The perforated area on the panel's surface allows the determination of the porosity. This porosity ϵ is the ratio of open surface to total surface, also called open area ratio or perforation rate. The geometry of the perforation influences the porosity. It is given by:

$$\epsilon = \frac{\text{open surface}}{\text{total surface}} \tag{2.21}$$

For circular shaped holes this leads to:

$$\epsilon = \frac{\pi \cdot a^2}{b^2} \tag{2.22}$$

The hole spacing b should be large compared to the hole diameter $2a$. The acoustic mass per unit m' is then [Cox and D'Antonio, 2009]

$$m' = \rho_0 b^2 \frac{t}{\pi a^2} \quad \left[\frac{kg}{m^2}\right], \tag{2.23}$$

where t is the thickness of the perforated sheet. The mass of the device comes from the vibrating plug of air within the perforations. The length of the plug is more than just the perforated plate thickness and the effect of radiation impedance must be considered. Therefore, the vibrating plug of air has a certain length given by the thickness of the panel plus additional end corrections that describe the radiation impedance of the orifice. For the mass we obtain:

$$\boxed{m' = \frac{\rho_0}{\epsilon} \cdot (t + 2\Delta a)} \tag{2.24}$$

Δ is the end correction factor, which is usually taken as $\Delta = 0.85$. The interaction of neighboring orifices is not taken into account, therefore other more accurate formulations exist. Also for unusual shapes, the radiation impedance of the plug of air can be evaluated using finite element models.
The sheet thickness and the hole radius a are assumed to be a lot smaller than the wavelength of sound in air.

This leads to the resonant frequency as

$$f = \frac{c_0}{2\pi}\sqrt{\frac{S}{tV}} \tag{2.25}$$

with $V = b^2 D$ being the volume of each individual cell and $S = \pi a^2$ being the hole area. Sometimes another formulation is used, using the fraction of the open area of the perforated sheet ϵ.

$$\boxed{f = \frac{c_0}{2\pi}\sqrt{\frac{\epsilon}{tD}}} \tag{2.26}$$

So far, the theory allows for the calculation of the resonant frequency.

For the design process of these resonant absorbers, again the surface impedance must be determined to obtain the absorption coefficient. We find the surface impedance for the Helmholtz-resonator from Eq. 2.17 with the approximation of $\cot x = \frac{1}{x}$ according to [TA, 2023]:

$$\boxed{\underline{W} = r + j(\omega m' - \frac{s'}{\omega})} \tag{2.27}$$

with

$$\boxed{s' = \frac{\rho_0 c_0^2}{D} \quad \left[\frac{N}{m^3}\right]} \tag{2.28}$$

being the spring component related to the perforation ratio and hole area. Additionally, also the losses within the devices must be modelled. Those are determined by the resistance term r of Eq. 2.27. Without further porous absorbent, this can be written as [TA, 2023]:

$$\boxed{r = \frac{t}{\epsilon a}\sqrt{2\rho_0 \eta \omega} \quad \left[\frac{Ns}{m^3}\right]} \tag{2.29}$$

The dynamic viscosity of air η has a value of 1.84 x 10^{-5} $Pa \cdot s$.

In order to get good absorption with resonant devices, it is necessary to add further porous material. It should be placed where the particle velocity is at its maximum. For a Helmholtz resonator this means the porous layer should be as close to the opening as possible. For a membrane absorber, the porous layer should be just behind but not touching the membrane. Too much absorption however might prevent resonance.

2.4 Microperforated panel absorbers

A micro-perforated panel (MPP) absorber is an alternative concept to traditional porous sound absorbers. It consists of a panel with small perforations, or holes, that are used to absorb energy and reduce the amount of sound that is transmitted through the panel. Microperforated devices provide absorption through high viscous losses as air passes through the holes that are in the size of the boundary layer or even smaller. The basic concepts of microperforation were developed by D.Y. Maa in the 1960s. According to this theory, the perforations convert acoustic energy into heat [D. Y. Maa, 1975].
MPPs are absorbers, that require an air space between the perforated panel or foil and the backing wall. Unlike Helmholtz resonators, the absorption of an MPP covers a wide frequency range. A microperforated panel presents various advantages compared to porous materials: it is thin, hygienic and can be washed or cleaned. For this reasons, MPP's can be used for noise absorption purposes replacing porous materials. The lack of fibrous or porous materials, allows designing absorbing systems adequate for food courts, hospitals, air conditioning systems and rooms for microelectronics. A big advantage of MPPs is, that they can be built optically transparent. In the German Bundestag in Bonn, transparent acrylglass panels with a thickness $t = 5$ mm have been used for the improvement of the acoustics [Fuchs and Zha, 1997].

2.4.1 Theory

The MPP can be fully described by the following set of parameters according to fig. 2.8.

- t ... Panel thickness or length of drill hole,
- d ... hole diameter,
- b ... spacing between the center of the holes,
- D ... Air space behind the panel,

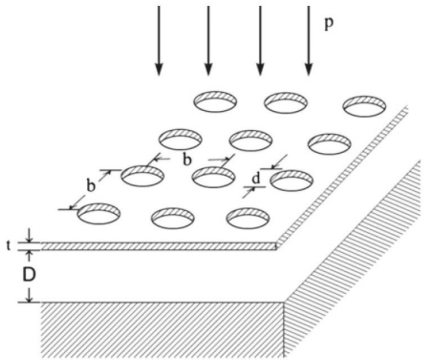

Figure 2.8: MPP scheme with parameters [Qian et al., 2013]

The perforated area on the panel's surface allows the determination of the porosity ϵ. For circular holes, the open surface $\sigma_s = \pi a^2$ where $a = \frac{d}{2}$. For perforation with slits $\sigma_s = d \cdot l$ with l being the length of the slit.
It has been proven that MPP absorber can be equivalently described by an electric circuit with the equivalent analogy [D. Y. Maa, 1975]. The acoustic impedance, the pressure difference and velocity of the particles are associated with the electric impedance, the voltage and the electric current respectively. The global circuit impedance is the result of the series between the impedance of the perforated panel $\underline{Z}_1$ with the impedance occurring from the air behind it $\underline{W}_D$ as shown in Fig. 2.9.

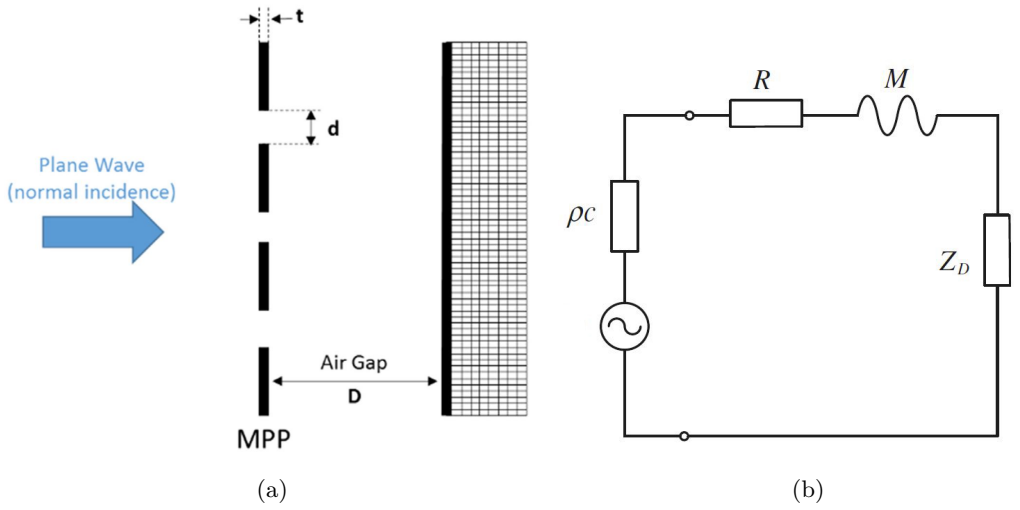

Figure 2.9: A single MPP absorber with the equivalent electro-acoustical circuit [Bucciarelli et al., 2019]

The impedance of the panel $\underline{Z}_1$ is always in series with the corresponding air cavity and its impedance $\underline{W}_D$. The equivalent impedance of the circuit can be estimated to

$$\boxed{\underline{W}_{MPP} = \frac{\underline{Z}_1}{\epsilon} + \underline{W}_D \quad \left[\frac{Ns}{m^3}\right]} \tag{2.30}$$

where $\underline{W}_{MPP}$ represents the impedance of a model for a single MPP layer. Similar to Eq. 2.17, $\underline{Z}_1$ describes the mass and resistance term and $\underline{W}_D$ the "spring" term.
The impedance $\underline{W}_{MPP}$ in total contains the following effects:

- The visco-thermal dissipation within the holes, $\underline{Z}_{hole}$
- The resonances in the air cavity, $\underline{W}_D$
- The distortion of the flow around the perforation edges, $\underline{Z}_{edge}$

For the air cavity of thickness D close to a rigid wall, the impedance $\underline{W}_D$ is given by

$$\underline{W}_D = -jZ_0 \cot(kD), \tag{2.31}$$

with $k = \frac{\omega}{c_0}$ being the same as the the last term of Eq. 2.17.

$\underline{Z}_{hole}$ and $\underline{Z}_{edge}$ provide the impedance $\underline{Z}_1$ according to:

$$\underline{Z}_1 = \underline{Z}_{hole} + \underline{Z}_{edge} \tag{2.32}$$

A typically studied configuration consists of a flat rigid surface with periodically arranged circular holes. The holes can be regarded as short tubes. Maa proposed the perforation impedance $\underline{Z}_{hole}$ from solving the wave equations in a cylindrical tube as proposed by [Rayleigh, 1945] for short tubes, compared to the wavelength. With $\underline{v}$ being the average particle velocity inside the tube and Δp the pressure difference on both sides of the tube [D.-Y. Maa, 1998]

$$\underline{v} = \frac{1}{j\omega\rho_0}\left[1 - \frac{2}{x\sqrt{-j}}\frac{J_1(x\sqrt{-j})}{J_0(x\sqrt{-j})}\right]\frac{\Delta p}{t} \quad \left[\frac{m}{s}\right] \tag{2.33}$$

we obtain the hole impedance $\underline{Z}_{hole} = \frac{\Delta p}{\underline{v}}$ as [D.-Y. Maa, 1998]:

$$\underline{Z}_{hole} = \frac{j\omega\rho_0 t}{1 - \frac{2}{x\sqrt{-j}} \cdot \frac{J_1\left(x\sqrt{-j}\right)}{J_0\left(x\sqrt{-j}\right)}} \quad \left[\frac{Ns}{m^3}\right] \tag{2.34}$$

J_1 is Bessel's function of the first kind and first order, J_0 is Bessel's function of the first kind and zeroth order, and x the dimensionless relation of the holeradius a to the acoustic boundary layer. This quantity x is also called perforation constant and can be written according to [Zwikker and Kosten, 1949, D.-Y. Maa, 1998]:

$$\boxed{x = d\sqrt{\frac{\rho_0\omega}{4\eta}} = 0,65\left[\frac{\sqrt{s}}{m}\right] \cdot a \cdot \sqrt{f}} \tag{2.35}$$

In order to extract energy from the sound wave, it is necessary to have a hole diameter in the same range as the boundary layer. Depending on the frequency, the flowing air ranges from laminar air flow to turbulent whirling movements. Similar to water flowing through a pipe, the outermost layer adheres to the pipe wall [Fuchs, 2007].
The approximation of Eq. 2.34 uses a general approach for the sequence development of the Bessel functions. As the terms get very small, almost vanishing, the development is aborted after the third term [Zwicker and Zollner, 1993].

$$J_0(x\sqrt{-j}) = 1 + \frac{1}{4}jx^2 - \frac{1}{64}x^4 \tag{2.36}$$

$$J_1(x\sqrt{-j}) = \frac{1}{2}x\sqrt{-j} \cdot \left(1 + \frac{1}{8}jx^2 - \frac{1}{192}x^4\right) \tag{2.37}$$

We obtain the approximation by inserting Eq. 2.36 and Eq. 2.37 into Eq. 2.34 leading to the following result, that was also stated by [Crandall, 1926]. He proposed a formula for $\underline{Z}_{hole}$ of very narrow ($x << 1$) tubes using the aborted series expansion from above:

$$\underline{Z}_{hole} = \frac{32\eta t}{d^2} + \frac{4}{3}j\omega\rho_0 t \quad \text{for} \quad x << 1 \tag{2.38}$$

For relatively wide tubes ($x >> 10$) he stated the following formula:

$$\underline{Z}_{hole} = \frac{4\eta t}{d}\sqrt{\frac{\omega\rho_0}{2\eta}}(1 + j) + j\omega\rho_0 t \quad \text{for} \quad x >> 10 \tag{2.39}$$

[D. Y. Maa, 1975] used these formulas but observed higher deviations from measurements with these two cases. With common designs of microperforated panels, and especially smaller hole sizes he developed an approximation for sub-millimetric perforation and the more practical range $1 < x < 10$:

$$\underline{Z}_{hole} = \frac{32\eta t}{d^2}\sqrt{1 + \frac{x^2}{32}} + j\omega\rho_0 t\left(1 + \frac{1}{\sqrt{3^2 + \frac{x^2}{2}}}\right) \quad \text{for } 1 < x < 10 \tag{2.40}$$

To get a better insight on the value range, we calculate x in Tab. 2.3 for a common design approach [$d = 0.3\,\mathrm{mm}$].

f [Hz]	x
50	0.7
270	1.6
483	2.1
700	2.5
920	2.9
1130	3.2
1350	3.5
1570	3.8
1780	4
2000	4.3

Table 2.3: Value range for the perforation constant x.

However, for simulation of the MPP behaviour in this thesis we use Eq. 2.34 as the Bessel functions can be solved numerically with Matlab.
Maa further considered a correction term $\underline{Z}_{edge}$ due to edge effects that consists of the two correction factors K_r and K_m leading to the following relation:

$$\underline{Z}_{edge} = K_r + jK_m \quad \left[\frac{Ns}{m^3}\right] \tag{2.41}$$

The end correction K_r of the acoustic resistance is produced by the flow friction of the panel when the flow is forced to pass through the micro holes. The correction factor to this so called surface resistance was proposed as [Ingard, 1953]:

$$K_r = \frac{\sqrt{2\eta\omega\rho_0}}{2} \quad \left[\frac{Ns}{m^3}\right] \tag{2.42}$$

Moreover, [Rayleigh, 1945] showed that the acoustic radiation of the perforation adds a mass of air to the motion. The correction factor for this so called mass reactance is [Ingard, 1953]:

$$K_m = 0.85\omega\rho_0 d \quad \left[\frac{Ns}{m^3}\right] \tag{2.43}$$

which can also be found as a corrective term on the effective acoustic mass of the Helmholtz resonator (Eq. 2.24). The corresponding impedance to the end correction is then:

$$\underline{Z}_{edge} = \frac{\sqrt{2\eta\omega\rho_0}}{2} + j0.85\omega\rho_0 d \tag{2.44}$$

The formulation for the wall impedance $\underline{W}_{MPP}$ of an MPP with end correction and air cavity to a rigid wall is then extended to:

$$\boxed{\underline{W}_{MPP} = \frac{\sqrt{2\eta\omega\rho_0}}{2\epsilon} + \frac{j\omega\rho_0}{\epsilon}\left[\frac{t}{1 - \frac{2}{x\sqrt{-j}}\cdot\frac{J_1\left(x\sqrt{-j}\right)}{J_0\left(x\sqrt{-j}\right)}} + 0.85d\right] - j\rho_0 c_0 \cot\left(kD\right)} \tag{2.45}$$

The normalized impedance $\underline{w}_{MPP}$ is obtained dividing $\underline{Z}_1$ and $\underline{W}_D$ by the characteristic impedance of air, $Z_0 = \rho_0 \cdot c_0$ and can be written as:

$$\underline{w}_{MPP} = r' + j\Big(\omega m'' - \cot(kD)\Big) \tag{2.46}$$

In extension to a basic mass-spring system, the term $\cot(kD)$ determines the impact of the backing cavity on high frequencies forming a tube resonator. The approximated equation (Eq. 2.40) by Maa and also Eq. 2.45 can only be applied at low perforation rates $\leq 20\%$ and circular perforation. In this case, the perforations are separated from each other far enough so that the borders do not interact. For higher perforation rates, this interaction has to be considered. On medium and high sound levels, this hole-interaction effect modifies both acoustic resistance and reactance and leads to a decrease of the maximum absorption coefficient [Tayong et al., 2011]. As with the traditional Helmholtz-resonator, a reactance part m'' and resistance part r' of the normalized wall impedance can be formed. The difference to the Helmholtz-resonator lies in the frequency dependence of r' and m'' [Fuchs, 2017].

So called micro slit absorbers (MSA) have rectangular shape perforations. The shape can be approximated to an ellipse where the length of the slit is much greater than the width. The ratio between the length and width is significantly larger than one, which impacts the wide band properties of the MSA. The equation leading to an equivalent of $\underline{Z}_{hole}$ (Eq. 2.34) for a single slit and normal sound incidence is [D. Maa, 2000]:

$$\underline{Z}_{slit} = \frac{j\omega\rho_0 t}{1 - \frac{1}{x\sqrt{-j}} \cdot \tanh\left(x\sqrt{-j}\right)} \quad \left[\frac{Ns}{m^3}\right] \tag{2.47}$$

Instead of the Bessel functions for circular holes the hyperbolic tangent function is used to approximate the rectangular shape perforation [D. Maa, 2000].
While the end correction term K_r remains the same, the reactive end correction K_m alters. For an elliptic aperture it follows Rayleigh's derivation [Rayleigh, 1945] and is defined using the incomplete elliptic integral of first kind $F_{(e)}$:

$$F_{(e)} = \int_0^{\frac{\pi}{2}} \frac{1}{\sqrt{1 - e^2 \sin^2\phi}} d\phi \tag{2.48}$$

with $e = \sqrt{1 - (\frac{d}{l})^2}$ being related to the slit length l and the slit width d. The angle ϕ is a parameter coming from studies on ellipsoids and refers to a *modular angle* measured from the z-axis [Byrd and Friedman, 1971]. K_m for slit perforation can be written as [D. Maa, 2000]:

$$K_m = \frac{F_{(e)}}{2} \cdot \omega\rho_0 d \quad \left[\frac{Ns}{m^3}\right] \tag{2.49}$$

Although the equations for an MSA and MPP are similar, the resistance of an MSA is lower. Consequently, the performance of an MPP is better to that of an MSA. The formula for the impedance of an MSA with end correction corresponds to Eq. 2.45 and leads to [D. Maa, 2000]:

$$\boxed{\underline{W}_{MSA} = \frac{\sqrt{2\eta\omega\rho_0}}{2\epsilon} + \frac{j\omega\rho_0}{\epsilon}\left[\frac{t}{1 - \frac{1}{x\sqrt{j}}\tanh\left(x\sqrt{j}\right)} + \frac{F_{(e)}d}{2}\right] - j\rho_0 c_0 \cot(kD) \quad \left[\frac{Ns}{m^3}\right]} \tag{2.50}$$

2.4.2 Parameter study

This section shows a study on the different design parameters of a MPP by varying only one parameter and keeping the others constant. We examine the effect of panel thickness t, air gap D, hole size d and hole spacing b. The impact of the geometry of the perforation is shown by comparing circular perforation and slit perforation.

Effect of panel thickness

The parameter thickness affects the acoustic impedance. Thicker panels have greater total mass of air inside the perforation while the stiffness of the resonator system is unchanged due to the same air cavity depth. Therefore, the resonant frequency becomes lower. The maximum absorption requires the resistance component of the acoustic impedance to be close to 1 and the reactance part to be close to 0. The results in Tab. 2.4 show the panel thickness t, the resonance frequency f_0, the maximum absorption coefficient α_{max} and the corresponding normalized impedance values r' and $\mathrm{Im}\{\underline{w}_{MPP}\}$. A MPP with r' close to 1 has the highest absorption coefficient, whilst higher values reduce the absorption peak as proven in the table. In Fig. 2.10 we see a representation of alpha by varying the panel thickness.

	t [mm]	f_0 [Hz]	α_{max}	r'	$\mathrm{Im}\{\underline{w}_{MPP}\}$
	0.15	953	0.98	0.77	-0.02
	0.75	591	0.69	3.49	-0.05
	1.5	471	0.44	6.80	0.21
	2	411	0.36	9.16	0.19
	3	351	0.25	13.7	0.41

Table 2.4: Properties of a MPP, effect of thickness t

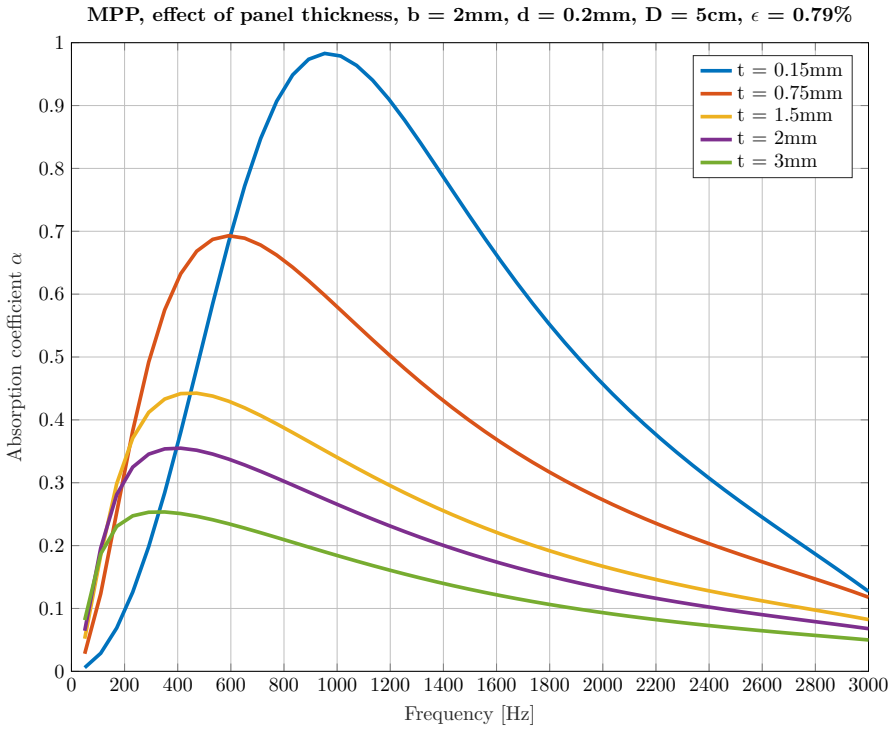

Figure 2.10: Comparing the effect of panel thickness t

Effect of perforation ratio

Similar to the panel thickness, the perforation ratio affects both center frequency and bandwidth. However, the best trade-off between a high absorption peak and a broad bandwidth can be observed for values of $\epsilon = 0.79\,\%$ and $\epsilon = 1.4\,\%$. Values $\geq 1.4\,\%$ further broaden the curve, but lower the absorption peak and shift the center towards higher frequencies as Fig. 2.11 shows.

b [mm]	ϵ [%]	f_0 [Hz]	α_{max}	r'	Im$\{\underline{w}_{MPP}\}$
4	0.20	532	0.75	2.97	-0.05
2	0.79	953	0.98	0.77	-0.02
1.5	1.40	1194	0.85	0.44	0.06
1	3.14	1435	0.55	0.20	0.05
0.5	12.6	1676	0.19	0.05	0.05

Table 2.5: Properties of a MPP, effect of perforation ratio ϵ

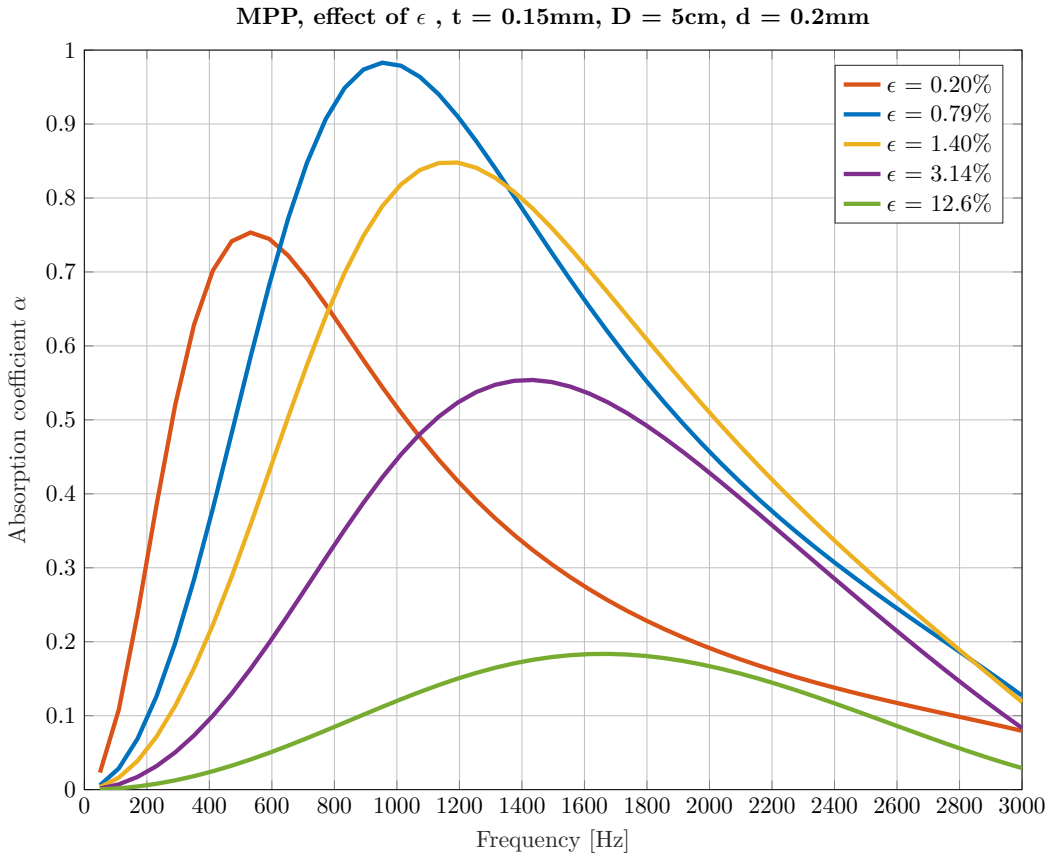

Figure 2.11: Comparing the effect of ϵ

Effect of hole diameter

Figure 2.12 and the corresponding Tab. 2.6 show the effect of modifying the hole diameter d while keeping all other parameters constant. We notice a shift of the center frequency to higher frequencies while the diameter is increased. The peak value of the absorption coefficient α reaches its maximum around the sweet spot with a porosity $\epsilon \approx 1\%$ and decreases with greater deviation from it, as stated by [D.-Y. Maa, 1998]. In correlation to the hole diameter d, increasing porosity ϵ moves the central frequency higher in the frequency spectrum. We further notice the influence of the imaginary part of the normalized impedance.

	d [mm]	f_0 [Hz]	α_{max}	ϵ [%]	r'	Im$\{\underline{w}_{MPP}\}$
	0.1	592	0.30	0.20	0.75	-1.15
	0.15	772	0.85	0.44	0.76	-0.50
	0.2	953	0.98	0.79	0.77	-0.02
	0.3	1194	0.53	1.77	0.78	0.51
	0.5	1495	0.15	4.91	0.80	1.08

Table 2.6: Effect of hole diameter and perforation

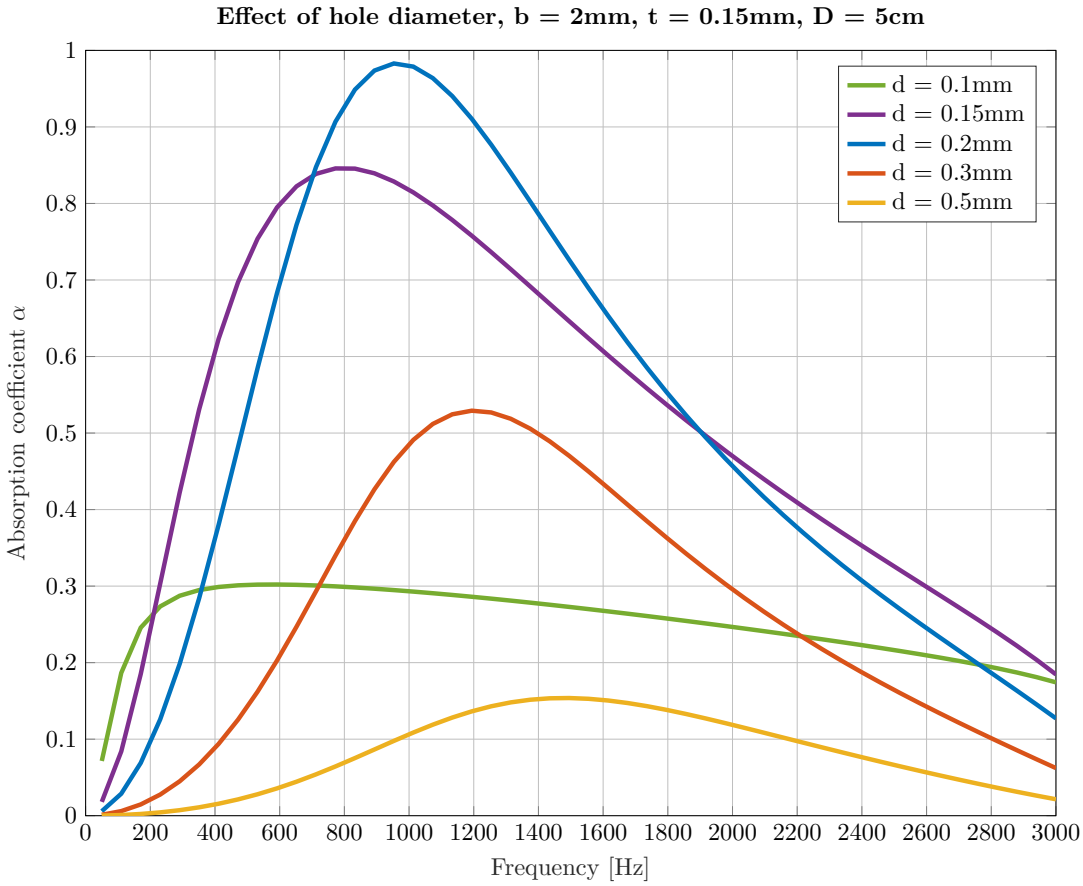

Figure 2.12: Comparing the effect of hole diameter d

Effect of the air gap

Figure 2.13 and the corresponding Tab. 2.7 show the effect of increasing the length of the enclosed air gap D from 3 cm to 7 cm while keeping all other parameters constant. With increasing depth the center frequency shifts to the lower frequency range, so a better absorption at low frequencies can be achieved by increasing the entity of the backing air space. The peak value of α is not affected but the frequency range covered reduces slightly. One can observe that a second absorption peak occurs for $D = 3\,\text{cm}$ as a resulting $\frac{\lambda}{4}$ cavity resonator.

	D [mm]	f_0 [Hz]	α_{max}	r'	Im$\{\underline{w}_{MPP}\}$
	30	1314	0.99	0.79	0
	50	953	0.98	0.77	-0.02
	70	772	0.98	0.88	-0.03

Table 2.7: Effect of different air gaps

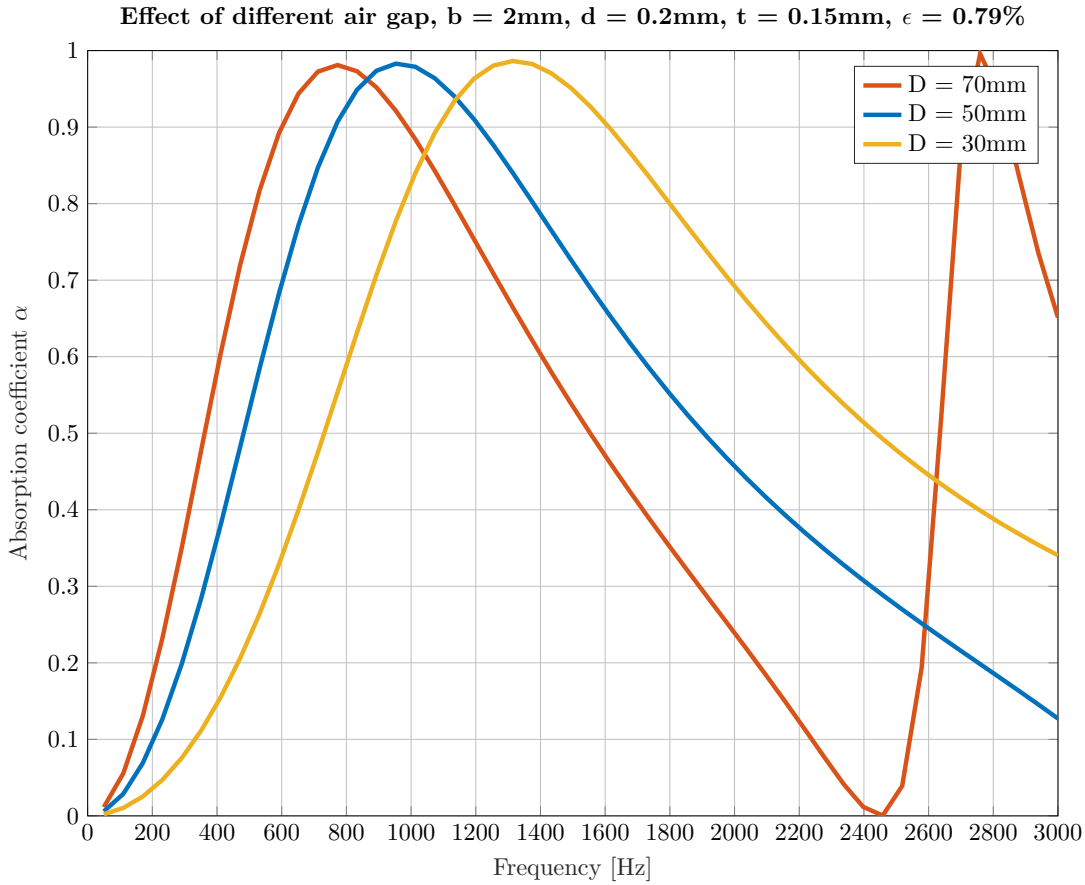

Figure 2.13: Comparing the effect of different air gaps D

Effect of hole separation

Figure 2.14 and the corresponding Tab. 2.8 show the effect of increasing the spacing between the holes from 1 mm to 4 mm, also effecting the perforation ratio ϵ. With increasing distance between the holes, the center frequency shifts to the lower frequency range but this also affects the peak value of α. We find the highest peak of α at 0.98 with a perforation ϵ close to 1% and $b = 2$ mm while the peak decreases for bigger or smaller hole spacing. Sufficient absorption is also found for $b = 3$ mm and $\alpha = 0.93$ with a lower center frequency at $712\,Hz$. Also the bandwidth of α is affected by varying the hole spacing.

	b [mm]	f_0 [Hz]	α_{max}	ϵ [%]	r'	Im$\{\underline{w}_{MPP}\}$
	1	1435	0.53	3.14	0.20	0.04
	2	953	0.98	0.79	0.77	-0.02
	3	712	0.93	0.35	1.70	0.07
	4	532	0.75	0.20	2.97	-0.05

Table 2.8: Effect of hole separation and perforation

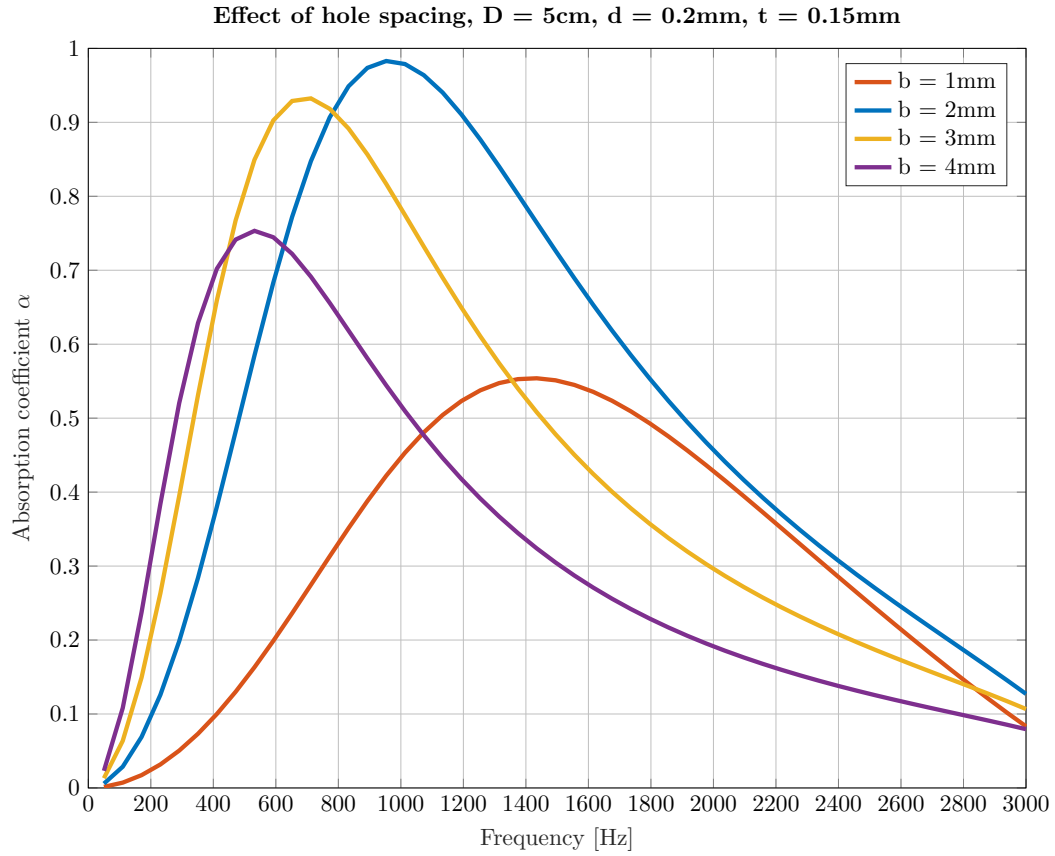

Figure 2.14: Comparing the effect of the hole spacing b

Effect of ultra-micro perforation

Modern manufacturing techniques open up new possibilities for the use of MPPs. Test series with laser-cutter perforation, micro needles or chemical insulting techniques proved further controlled decrease of the hole diameter to µm range. If we go back to Maa's theory, the resistance part of the acoustic impedance r' varies inversely with the perforation diameter. If the perforation diameter is reduced to a certain value, sufficient acoustic resistance and lower reactance can be obtained to get good wide band sound absorption. To observe the impact, we use the theory of Maa for the following five cases in Tab. 2.9. The maximum perforation ratio is 20%, meeting the basic assumptions of Maa's theory. For higher perforation rates, the effect of over-perforation has to be taken into account. By decreasing the perforation diameter to $d \leq 100\,\mu m$ we broaden the absorption bandwidth significantly. Figure 2.15 represents the absorption coefficient for those cases. We notice the highest bandwidth $\alpha \geq 0.4$ for the frequency range $400\,Hz$ to $3\,kHz$ for case 1. In general, perforation in the µm area leads to a broadened absorption bandwidth. The air gap is assumed constant with $D = 5\,cm$.

Case	d [µm]	b [µm]	ϵ [%]	f_0 [Hz]	α_{max}	r'	Im$\{\underline{w}_{MPP}\}$
1	30	60	20	1676	0.99	1.21	-0.01
2	60	160	11	1615	0.91	0.55	-0.02
3	80	220	10	1615	0.74	0.33	-0.02
4	100	500	3.14	1435	0.97	0.71	-0.02
5	200	2000	0.79	953	0.98	0.77	-0.02

Table 2.9: Effect of ultra-micro perforation

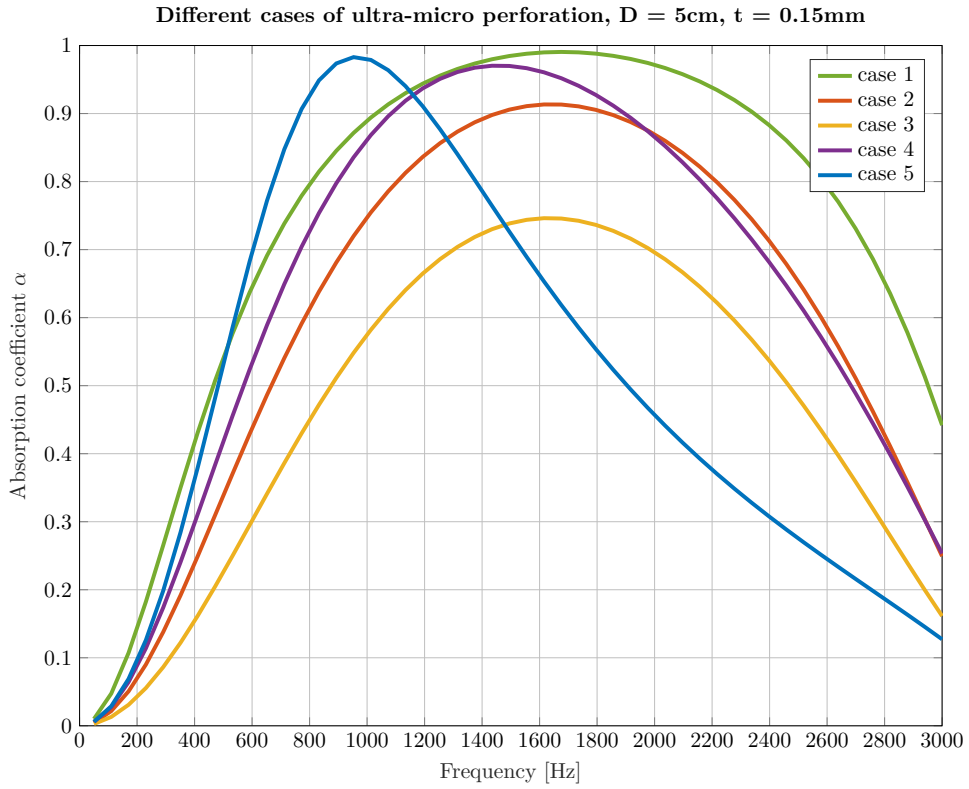

Figure 2.15: Five cases of ultra-micro perforation

Effect of perforation shape

As manufacturing circular holes in submillimetric size can be very challenging, the model of micro slit absorbers (MSA) is sometimes used instead. In this section we show the absorption curve for panels with slit perforations.
In Tab. 2.10 and Fig. 2.16 we compare the model for slit perforation with the model for circular holes by using the same design parameters $D = 5\,cm, t = 0.15\,mm, l = 3\,cm, d = 0.2\,mm$. The perforation ratio is kept constant with $\epsilon = 0.79\%$ and b adjusted accordingly. The range of the absorption coefficient ≥ 0.4 is considered as the absorption bandwidth. Reduced bandwidth and the weaker absorption peak for perforation with slits can be observed. Also the center frequency is shifted towards lower frequencies. Additionally, also the impact of the corrective term is shown. If we apply the same corrective term K_m as for circular shaped perforation to the MSA model, the center frequency f_0 differs only slightly from the model with circular holes. No end correction applied leads to a further frequency shift towards higher frequencies and further reduces the absorption peak. While the imaginary part of the normalized impedance $\mathrm{Im}\{\underline{w}_{MPP}\}$ does not change significantly, we notice the reduced values for the real part r' and the corresponding decrease of the absorption peak.

	f_0 [Hz]	α_{max}	Bandwidth [Hz]	r'	$\mathrm{Im}\{\underline{w}_{MPP}\}$
MPP	953	0.98	410 - 2100	0.77	-0.02
MSA with K_m for slits	652	0.74	490 - 880	0.33	-0.07
MSA with K_m for holes	1013	0.76	600 - 1700	0.34	0.07
MSA no K_m	1194	0.66	720 - 2000	0.27	-0.02

Table 2.10: Slit perforation (MSA) vs. circular holes (MPP), impact of end correction

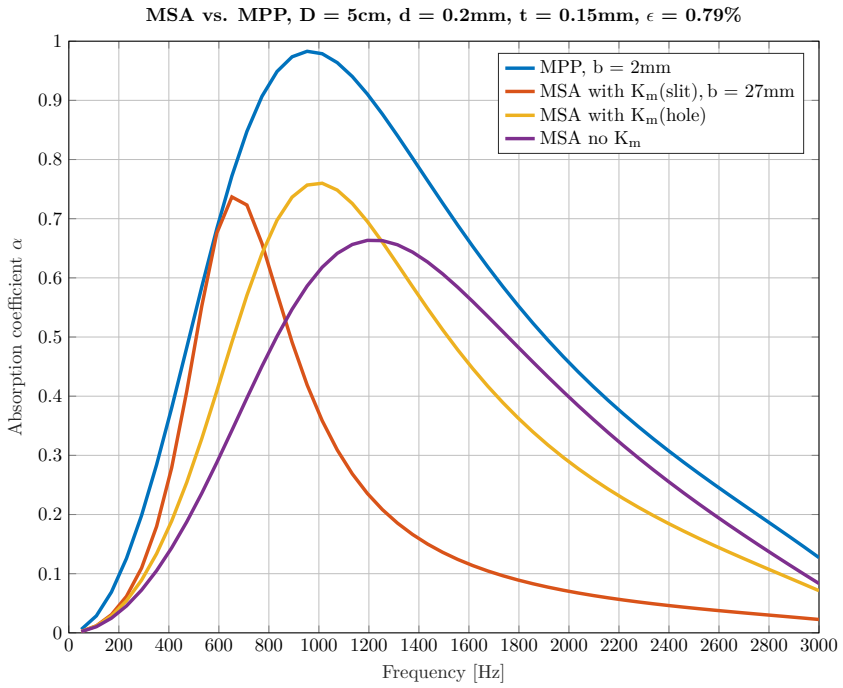

Figure 2.16: Slit perforation (MSA) vs. circular holes (MPP), impact of end correction

2.4.3 Multi layer design

Many studies have been conducted on improving the sound absorption performance of MPP absorbers. A compound absorber can be used to broaden the absorption bandwidth by adding a second layer of MPP to the primary one in tandem. The double-layer design can extend the absorption bandwidth to lower frequencies, but at the cost of occupying more space due to the extra layer construction. Previous work showed, that double-leaf MPP configurations improve broadband absorption [Sakagami et al., 2010]. Figure 2.17 shows a sketch of a double-layer design. They additionally inserted honeycomb partitioning between the two layers to force plane wave behavior between the perforated layers. Comparing the results, with and without the honeycomb structure, one can observe that the resonance peak is enhanced and shifted to lower frequencies. Also, the air cavities behind the MPPs have an impact and the overall performance can be improved significantly if this cavity is portioned and varied in depth [Herrin et al., 2017]. In this section, we discuss how to design and model a broadband multi-layer MPP absorber.

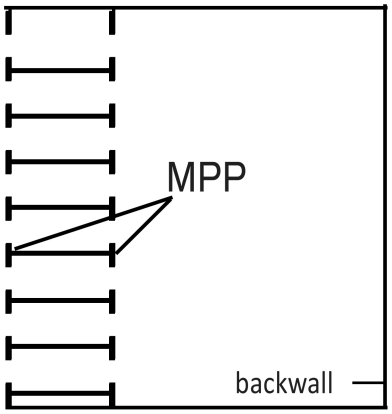

Figure 2.17: Scheme of a double-leaf MPP (sketch, draw.io)

An absorber system with multiple microperforated layers n, different geometrical parameters for each layer $[t_i, d_i, \epsilon_i]$ that are separated by n air gaps with variable or constant cavity depth $[D_i]$, can be estimated by the approach of solving the equivalent electrical circuit. Figure 2.18 shows a sketch of this arrangement. For simplicity we rewrite the impedance of the individual perforated panels as $\underline{Z}_1$ to $\underline{Z}_i$, the impedance used for modelling the air gap $\underline{W}_D$ to $\underline{W}_{D_i}$.

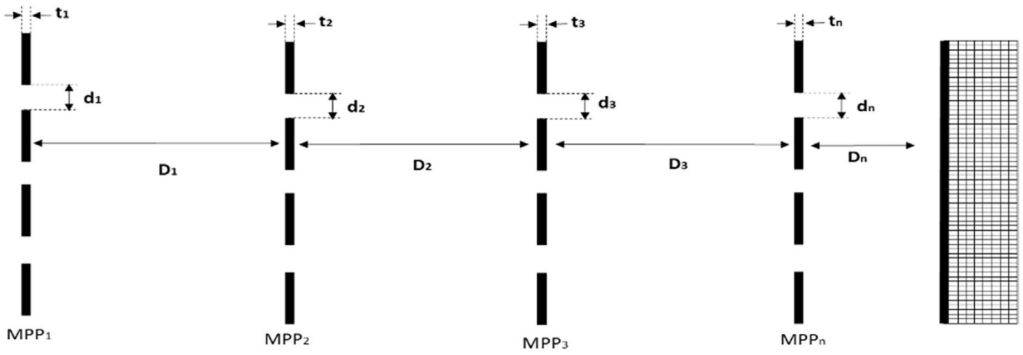

Figure 2.18: Multiple Layer MPP absorber model [Bucciarelli et al., 2019]

First, the acoustic impedance $\underline{Z}_i$ for each layer is estimated by:

$$\underline{Z}_i = \underline{Z}_{hole_i} + \underline{Z}_{edge_i} \quad i = 1, n. \tag{2.51}$$

Then, the total acoustic impedance is estimated solving sequentially the serial and parallel network with the starting point:

$$\underline{W}_{serial_1} = \underline{Z}_n + \underline{W}_{D_n} \tag{2.52}$$

$$\underline{W}_{serial_{i+1}} = \underline{Z}_{n-i} + \underline{W}_{parallel_i}, \quad \text{for} \quad i = 1, n-1, \tag{2.53}$$

$$\underline{W}_{parallel_i} = \Big(\frac{1}{\underline{W}_{D_{n-i}}} + \frac{1}{\underline{W}_{serial_i}}\Big)^{-1}, \quad \text{for} \quad i = 1, n-1, \tag{2.54}$$

As an example, we look closer at the impedance of a double layer MPP system. Figure 2.19 shows the sketch of an equivalent electrical circuit.

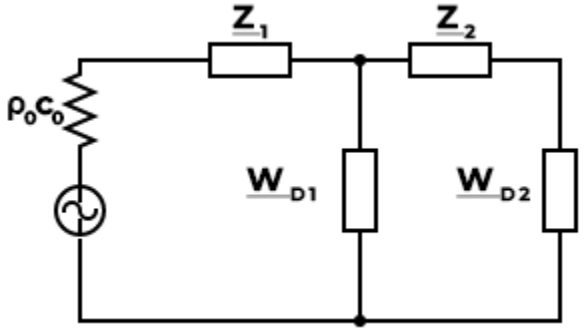

Figure 2.19: Equivalent electrical circuit analogy of a MPP with two layers in front of a rigid wall.

For a system with two layers ($n = 2$), the starting point yields to the impedance of the MPP closest to the rigid wall.

$$\underline{W}_{serial_1} = \underline{Z}_2 + \underline{W}_{D_2} \tag{2.55}$$

Then, this impedance $\underline{W}_{serial_1}$ will be in parallel with the impedance $\underline{W}_{D_1}$ resulting from the previous air cavity D_1. It can be written as:

$$\underline{W}_{parallel_1} = \frac{\underline{W}_{D_1}\underline{W}_{serial_1}}{\underline{W}_{D_1} + \underline{W}_{serial_1}} \tag{2.56}$$

By adding the impedance of panel 1 $\underline{Z}_1$ to $\underline{W}_{parallel_1}$ we obtain the total impedance $\underline{W}_{MPP}$:

$$\underline{W}_{MPP} = \underline{W}_{serial_2} = \underline{Z}_1 + \underline{W}_{parallel_1} \tag{2.57}$$

The expected behaviour of two multi-layer arrangements shall be examined. Figure 2.21 and Fig. 2.22 show the absorption coefficient for $n = 2$ and $n = 3$. They are modelled with a total depth of 7 cm for the double layer MPP and 6 cm for the triple layer MPP. The setup is shown in Fig. 2.20. Compared to the single layer MPP, an increased bandwidth can be achieved. Also, there is a slightly enhanced absorption to lower frequency range. We notice a constant absorption coefficient $\alpha \geq 0.4$ for more than 4 octaves between $250\,Hz$ and $\geq 5\,kHz$ for the

double layer configuration. The triple layer configuration further improves the absorption peak with an absorption coefficient $\alpha \geq 0.85$ for a frequency range from $800\,Hz$ to $\geq 5\,kHz$. As this multi-layer system relies on 8, respectively 12 design parameters, a proper algorithm has to be found, to obtain the parameters needed for a given frequency range. Research by [Pedro and Simón, 2019] addresses the question for a well suited algorithm to find optimal parameters. They propose a simulated annealing algorithm which is a stochastic global search optimization algorithm.

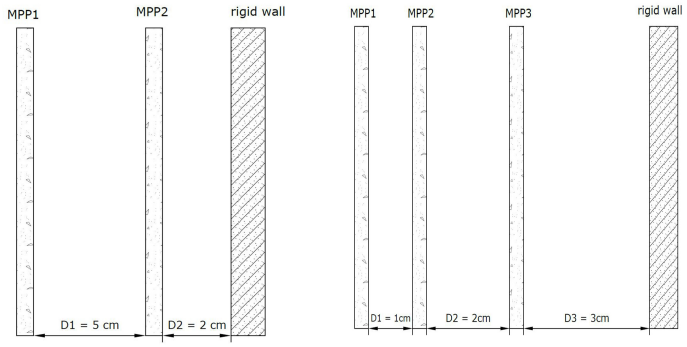

Figure 2.20: Sketch of double layer- and triple layer MPP setup.

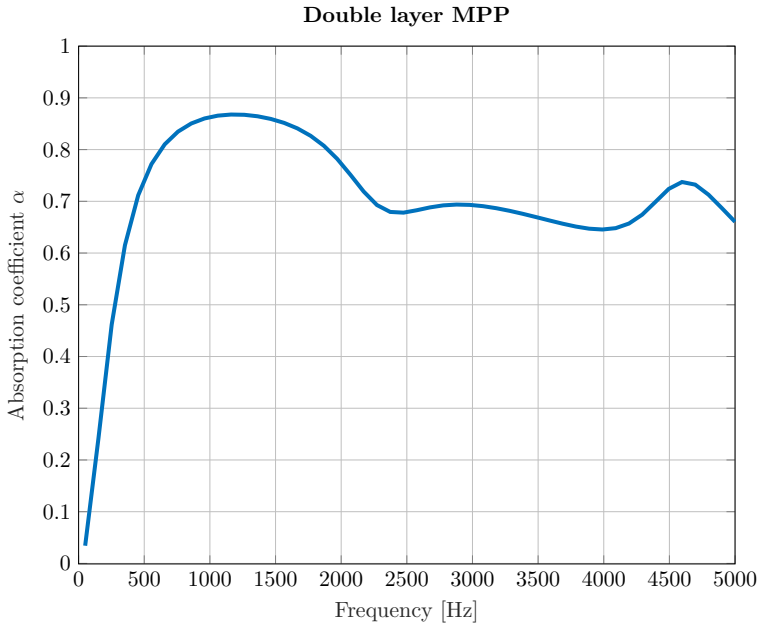

Figure 2.21: Absorption coefficient of a double layer MPP.

d_1 [mm]	t_1 [mm]	ϵ_1 [%]	D_1 [cm]	d_2 [mm]	t_2 [mm]	ϵ_2 [%]	D_2 [cm]
0.1	1	7	5	0.1	1	19.6	2

Table 2.11: Double layer MPP, design parameters

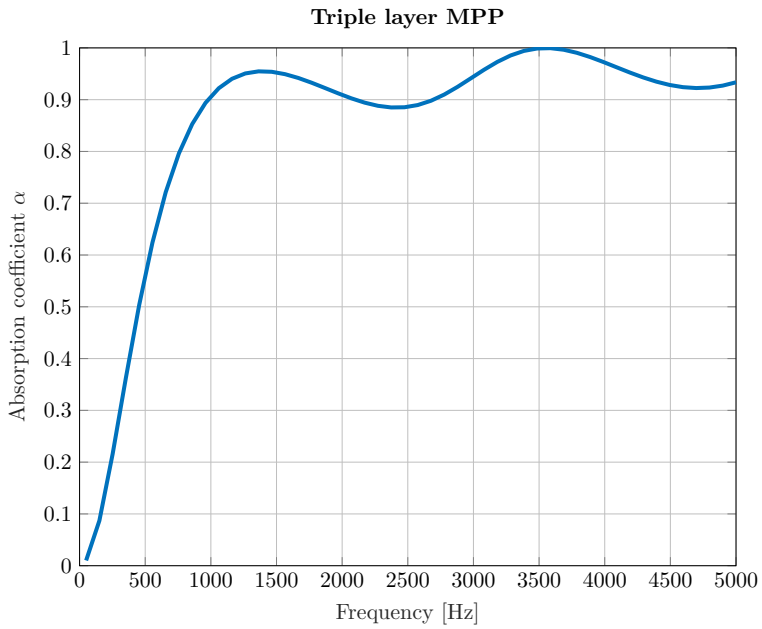

Figure 2.22: Absorption coefficient of a triple layer MPP.

d_{1-3} [mm]	t_{1-3} [mm]	ϵ_1 [%]	D_1 [cm]	ϵ_2 [%]	D_2 [cm]	ϵ_3 [%]	D_3 [cm]
0.15	1	15	1	10	2	10	3

Table 2.12: Triple layer MPP, design parameters

2.4.4 Applications

We find microperforated acoustic absorbers often in applications when used as an alternative to standard porous absorbers. These occur when certain design considerations or performance requirements need to be met. A few scenarios where microperforated acoustic absorbers may be preferred are:

- Limited space: In some situations, the thin-panel requirement is a big advantage. MPP provide comparable absorption performance while occupying less physical depth.
- Aesthetics: They can be fabricated with various shapes and patterns, allowing for better visual integration into a surrounding space. Even optical transparent products are possible.
- Moisture resistance, ease of cleaning: MPPs can be handled more easily and this is beneficial in spaces where cleanliness and hygiene are prioritised or high humidity levels are expected.

Figure 2.23 shows MPPs made of three different materials namely cotton, acrylic glass and wood with perforation applied. The microperforated fabric (a) can be used as a ceiling panel with a special frame made of aluminium [Maier, 2010]. The honeycomb glass absorber (b) consists of two layers of glass with embedded honeycomb structure to enforce plane wave propagation and improve acoustic properties. The wooden panel with circular holes and a hole size of $0.5mm$ (c) is available in all different colors and is often used in concert halls or conference rooms.

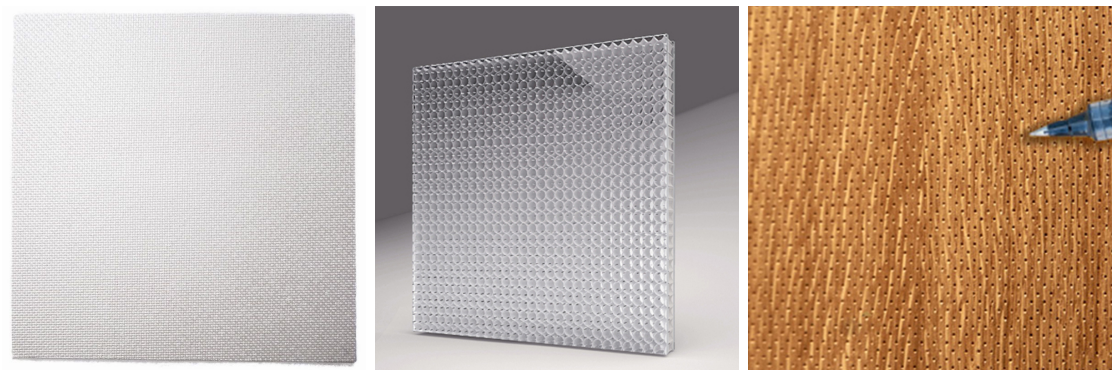

(a) Fabric with microperforation [HELIOACOUTEX, 2023]

(b) Glass absorber, two layers with honeycomb structure [Acoustic, 2023]

(c) Wooden panel, hole size o.5mm [Wood, 2023]

Figure 2.23: Examples of microperforated panels made of cotton, glass and wood.

In modern architecture, there are a few trends which underline the ever growing demand for quality transparent acoustic solutions for building interiors. Especially the lack of transparent sound absorbers encourages further research. The limitations in design become more and more neglectable. Apart from basic and straight panels also curved constructions from glass, transparent films and existing room elements like doors are suitable for microperforation as Fig. 2.24 shows. The most common technique for glass perforation is the use of a laser cutter.

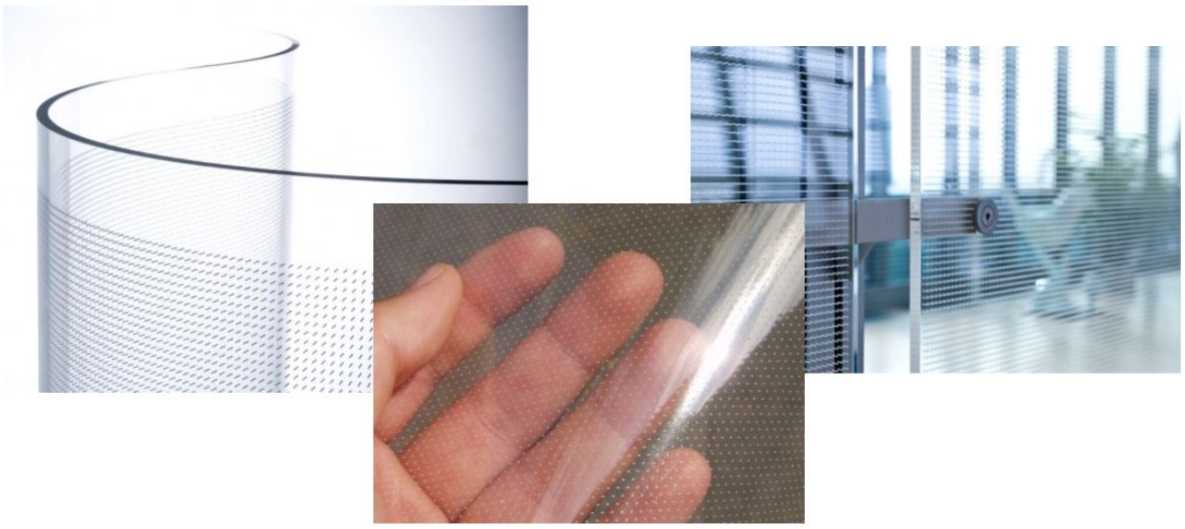

Figure 2.24: Various transparent sound absorbing materials that exist in the market made out of plastics or acrylics [Tourlomousi, 2017].

Figure 2.25 shows an example of an absorber film positioned at the ceiling of the office innovation center (OIC) at Fraunhofer Institut (Stuttgart, Germany).

Figure 2.25: Microperforated foil as sound absorber [Wack and Fuchs, 2004].

The effect on the reverberation time by applying the optically transparent microperforated foil under the roof is clearly visible in Fig. 2.26. Here a double-layered microperforated foil was installed and provides sufficient absorption for a frequency range of 125 Hz and above. The sail is carried by a steel wire net.

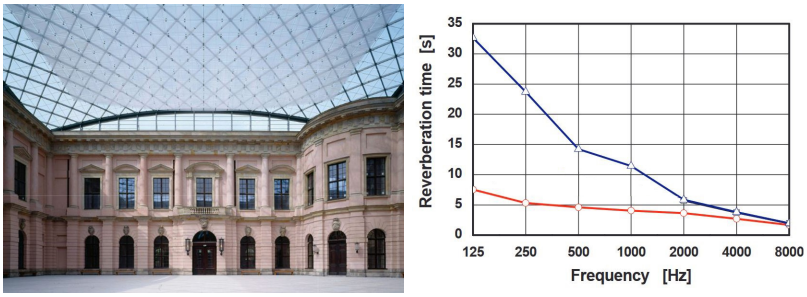

(a) Translucent sail of microperforated foil under concave-curved roof.

(b) Reverberation times before (triangle) and after (circular) installation of the foil absorbers.

Figure 2.26: Microperforated foil on ceiling [Wack and Fuchs, 2004].

Further applications of microperforated panels are shown on Fig. 2.27. MPPs are also applicable for noise control problems e.g. in the engine compartment of a boat (a), or as a design element in the reception area of a hotel (b). Image (c) shows a silencer consisting of microperforated metal sheet that are used inside ducts.

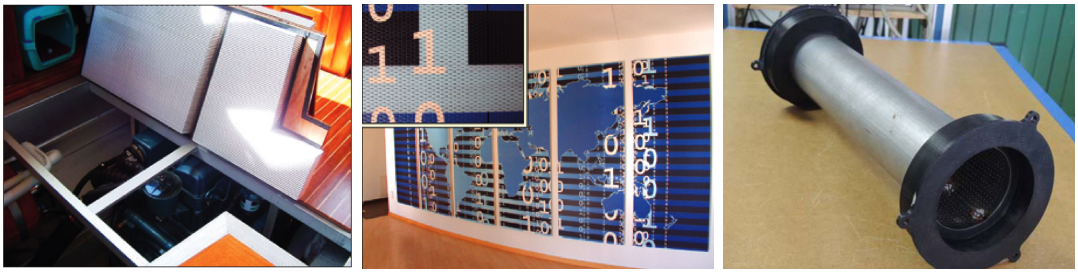

(a) MPP used in engine compartment of a boat [Herrin et al., 2011]

(b) MPP used in reception area of a hotel [Herrin et al., 2011]

(c) MPP used inside a duct silencer [Bravo et al., 2014]

Figure 2.27: Further applications of MPP absorbers.

However, due to the escalating plastic crisis and its impact on the environment, Industries are actively looking into different options like biodegradable polymers, plant-based materials and recycled substances to see if they can replace products made from regular plastics. This is also true for acoustic solutions. In the upcoming chapter, after a short overview of existing acoustic solutions based on sustainable materials, the preparation of the first translucent absorber prototype is presented. Therefore we experiment with thin layers of alginate forming a transparent film that behaves like plastic. In general a translucent sound absorber is a type of acoustic panel or material that is designed to absorb sound while allowing light to pass through. These materials are often used in architectural and design projects where both sound control and natural light are desired. Translucent absorbers can be used in a variety of applications such as in offices, schools, conference rooms, and other commercial spaces where natural light is desired, but control of the reverberation time is also important. As wall or ceiling panels they can be installed in different spaces. For microperforated panels from acrylic glass, the optical transmittance is about 80% which leads to a transparent surface. The holes become more apparent at oblique viewing angles. The translucent sound absorbers can also be customized with different colors, patterns, or designs to match the aesthetic of the surrounding space. So far, MPP absorbers were more expensive than traditional materials and considered too costly for commercial use. However, modern production techniques allow for lower-cost MPP absorber materials. In this thesis we search for a sustainable, lower-cost alternative for transparent MPP absorbers.

3

Sustainable materials in acoustics

As the need for sustainable materials and eco-friendly manufacturing increases, a variety of materials has occurred also for acoustic applications. These materials refer to materials that are environmentally friendly, renewable, and have a low impact on the environment. Big annual exhibitions like the **MaterialDistrict** in Utrecht (NL) underline the importance of research towards new materials. What can we make from 'waste', what are the latest 'plant-based' materials that can be used for architectural project, which products are made from recycled material are some of the big questions asked by designers, researchers, industry representatives and students with in total more than 4.500 participants. The suitability for acoustic applications plays a big role and the benefit for the acoustics is stated by almost all of the exhibitors [Utrecht, 2023]. Figure 3.1 shows a new compound material made from clay and mycelium that has the characteristics of a porous material (a) while (b) represents a 3D printed prototype of a passive destructive interference absorber with a series of tubes in varying lengths and diameters. It allows addressing the low frequency area from 190 Hz to 400 Hz by using computational design resulting in a total panel thickness of only a few centimeters [Setaki et al., 2023]. A sound barrier made from a double layered textile with added volume is shown on (c). A certain stitch and knitting technology creates a three dimensional, dense and stable panel [sound barrier, 2023]. All three of them rely on sustainable materials.

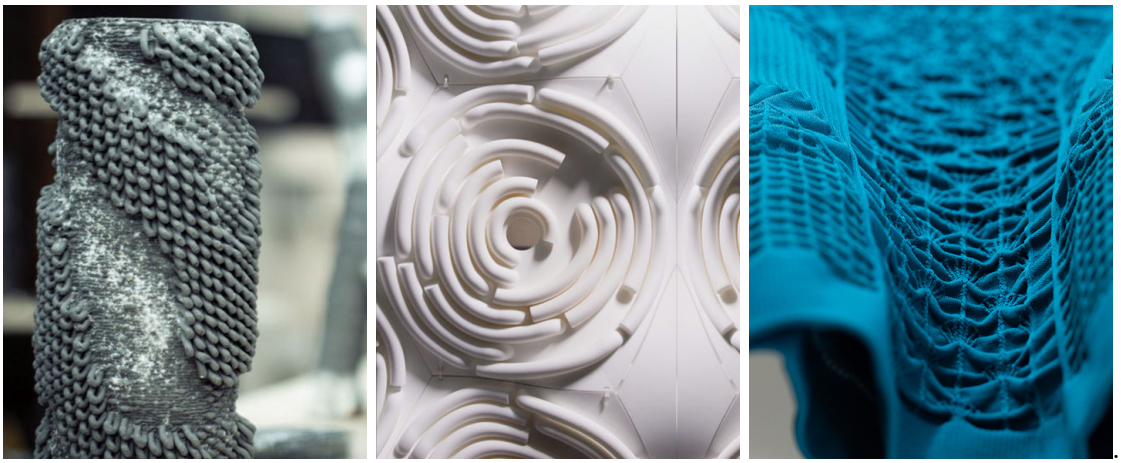

(a) Novel 3D printing material [Utrecht, 2023].

(b) Compact sound absorber addressing lower frequencies, 3D printed [Setaki et al., 2023].

(c) Double layered textile sound barrier, knitted and stitched [sound barrier, 2023]

Figure 3.1: Innovative examples of modern sound absorbers.

Those innovative materials can be used in the construction of buildings and other structures to improve the acoustical properties and reduce noise pollution. Also for room acoustics, panel made of sustainable materials are more and more common. Some examples of sustainable materials that are used include:

- **Natural fibers**: Natural fibers such as coir, jute, and flax can be used to make sound-absorbing materials, such as insulation and wall panels. Also waste jute fibers and denim as basis material provide sound-absorbing properties [Raj et al., 2020]. Wool, woven or compressed, is another natural and renewable material that is known for its excellent sound-absorbing properties. It can be used as insulation or as a sound-absorbing material in walls and ceilings.

- **Cork**: Cork is a natural and renewable material that is often used as a sound-absorbing material in walls and floors. Previous research with cork panels showed a good value of the measured sound absorption coefficient, comparable to traditional panels made from foam products. Also their low cost makes cork panels attractive. A limitation in panel thickness is a drawback [Iannace et al., 2020].

- **Recycled materials**: Materials like recycled glass, recycled rubber, recycled cotton and recycled plastic bottles can be used to make sound-absorbing materials, such as insulation and wall panels. Research with alginate and recycled glass provided promising results by building a sustainable foam material as shown in Fig. 3.3. A foam with open pores was formed as a compound material of alginate gel and powdered glass and provided sound absorbing properties [Caniato, 2019].

- **Mycelium**: Mycelium is a biologically-based material made from the root structure of mushrooms. It can be used as a sound-absorbing material due to its porous structure and ability to control sound waves. An in-depth study on mycelium based acoustic boards has been made by [Pelletier et al., 2013]. They showed, that in comparison to the traditional petroleum based foams, mycelium based absorbers show promise to provide a low cost but also high performing alternative to traditional foam based acoustic boards. Figure 3.2 shows a sample of these foams. Previous research on sustainable materials showed that in comparison to similar petroleum based foams, they reach a good level of sound absorption [Hemmer, 2022].

Figure 3.2: Porous sample of a foam made of mycelium and sawdust.

Sustainable materials may not always have the same level of sound-absorbing properties as traditional materials, so it is often necessary to use a combination of sustainable and traditional materials to achieve the desired acoustical performance. Also, the preparation of natural fiber based panels might need a tremendous amount of energy in the production process which is a big drawback.

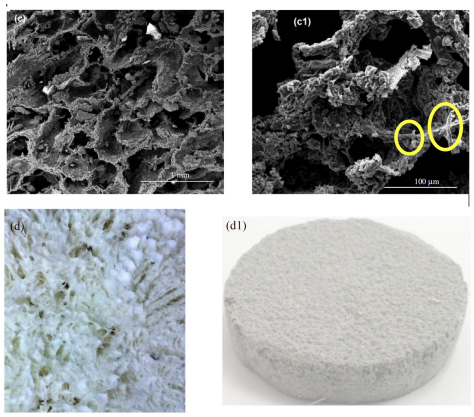

Figure 3.3: Foam of alginate and recycled glass under EM, (c) 50x, (c1) 500x detailed shot with enclosed glass fibres (d) structure of the samples (d1) specimen for measurements [Caniato, 2019]

3.1 Alginate - Sustainable absorber from seaweed

Another sustainable material that builds the basis for lots of material science is **alginate**. Therefore, the specimen of microperforated films investigated in this thesis are made from sodium alginate, in short alginate. **Sodium alginate** is a natural polysaccharide derived from brown seaweed and found in the oceans all over the world. Even forests of algae with a height of up to 4 meters occur as shown in Fig. 3.4 (a) and (b) pictures a shoe sole made of alginate. Alginate forms a gel-like substance when mixed with water and calcium ions, making it useful in the production of various products. Sodium alginate can be used in a variety of applications, including:

- Thickener: Sodium alginate can be used to thicken liquids, such as soups and gravies, as well as to create a more stable texture in some foods, such as ice cream.
- Gelling agent: used to create a gel-like texture in foods. When combined with calcium ions, it forms a gel-like substance known as a "calcium alginate gel".
- Emulsifier: Sodium alginate can be used to help mix oil and water-based ingredients together, creating a stable emulsion.
- Pharmaceuticals: used as a binder in some tablets and capsules, and it can also be used as a thickener in some liquid medications.
- Textile printing: used as a thickener in textile printing to create a paste-like consistency in the ink, which helps to improve the print quality.
- Textile industry: Some designers like Aaaron Nesser ([AlgiKnite, 2023]) developed a weavable yarn that can be machine or hand knitted.

(a) Algae or kelp forest [kelp forest, 2020].

(b) AlgiKick- shoe [AlgiKnite, 2023]

Figure 3.4: From seaweed to sneakers.

Brown seaweed, also known as **brown algae** can be found in a wide range of habitats, including rocky shores, sandy beaches, and subtidal environments all over the world. It is characterized by its brown color, which is caused by the presence of pigments called *fucoxanthin* and *phaeophytin* [Bold et al., 1987]. One of the most important aspects of seaweed in general is their filtering ability. Apart from filtering toxic substances from water, their enormously rapid growth and the effective photosynthesis make them responsible for almost 50 % of the world's oxygen demand [Smetacek, 1991]. In order to use alginate as a gel-forming agent, the powdered form, so called sodium alginate has to be extracted. Figure 3.5 shows the slightly yellowish alginic acid sodium salt, known as sodium alginate.

Figure 3.5: Sodium alginate, powder

The process to obtain the powder includes the following steps, as shown in Fig. 3.6:

- **Pre-extraction:** Washing and grinding to remove any salt or particles,
- **Neutralization:** Filtration and separation of any residues by adding $NaOH$,
- **Purification:** Extraction to separate the alginate from other components.conversion to sodium alginate by mixing it with a solution of sodium hydroxyde. Further drying to reduce its moisture content. The resulting product is a white, powdery substance that is ready for use.

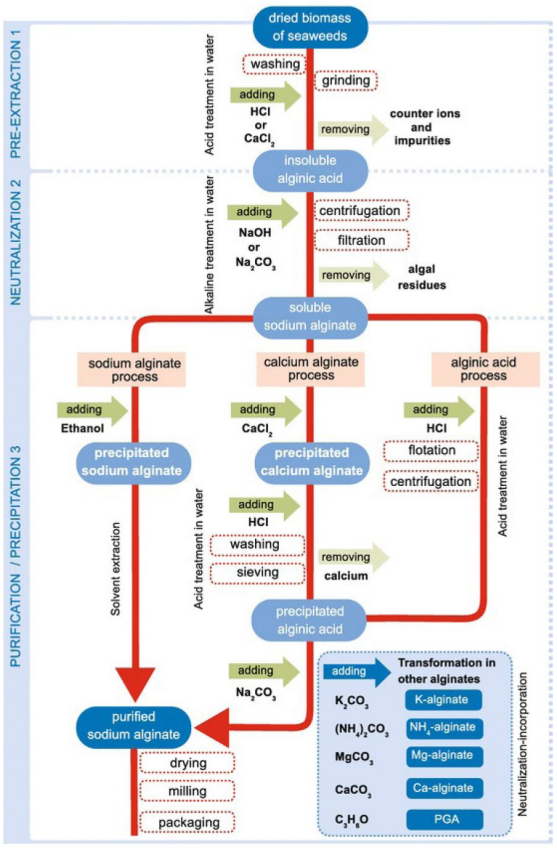

Figure 3.6: Schematic process of the extraction of sodium alginate [Rehm and Moradali, 2018].

For room acoustic purposes, alginate is suitable as a base material in multiple ways. Thin microperforated films are producible as well as the use of fine fibers that are machine woven. Alginate can also be used as the starting material for insulation foams. The focus of this thesis relies on the production and design process of microperforated films based on alginate.

3.2 Preparing acoustic samples from alginate

First, the thin layers of alginate should be made for further investigation in the impedance tube. To start the first phase of the experiments, we begin by creating a solution consisting of distilled water and sodium alginate powder. By dissolving the sodium alginate powder in water, we aim to achieve a homogeneous gel. Based on previous work [Marjanović, 2022] only the following materials are needed to start with the preparation of the films:

- Sodium Alginate
- Distilled water

However, the following additional substances are used for proper sample preparation:

- Calcium Chloride Dihydrat $CaCl2.2H2O$ ($> 99\%$), as a stabilizer and cross-linking agent
- Calcium Carbonate $CaCO_3$ ($> 98,5\%$), for applying perforation
- Glycerol ($99,5\%$), as plasticizer and softener
- Hydrochloric acid, HCl, for applying perforation by etching

In contrast to previous work, we now use sodium alginate powder that is produced for medical- and biochemical purposes and has a higher degree of purity than the one used for cooking. In order to make the first series of thin films, it is not necessary to use more than sodium alginate and distilled water. Later, additional substances are used to obtain more tear resistance and to further optimize the properties of the final alginate film.

3.2.1 Specimen with only sodium alginate

First, a sodium alginate solution (2 %, w/w) was prepared by dissolving 2 g of sodium alginate in 100 g of distilled water. As the powder does not dissolve immediately on the first contact with water, further stirring is required. The measuring cup containing the liquid was clamped in a stirrer for about 50 min with 800 rpm until complete dissolution. A viscous slightly yellowish solution was produced. Figure 3.7 shows the production process. While (a) presents the sodium alginate in powdered form, we see the 2 g of alginate in a weighing dish (b) and finally the solution in the stirrer (c). During this first stirring time, the yellow color cast can not be observed. We notice that stirring time and speed has an impact on the homogeneity of the final film.

(a) Sodium alginate (b) Sodium alginate, 2 g (c) Solution in stirrer

Figure 3.7: Sodium alginate powder mixed with distilled water.

The mixture was then poured into round petri dishes, 10 cm in diameter and 1.5 cm in height until they were completely full as shown in Fig. 3.8 (a). To speed up the drying process, the dishes were put into the laboratory vacuum oven for 48 hours. In Fig. 3.8 (b) we see the first result, a transparent film made of alginate.

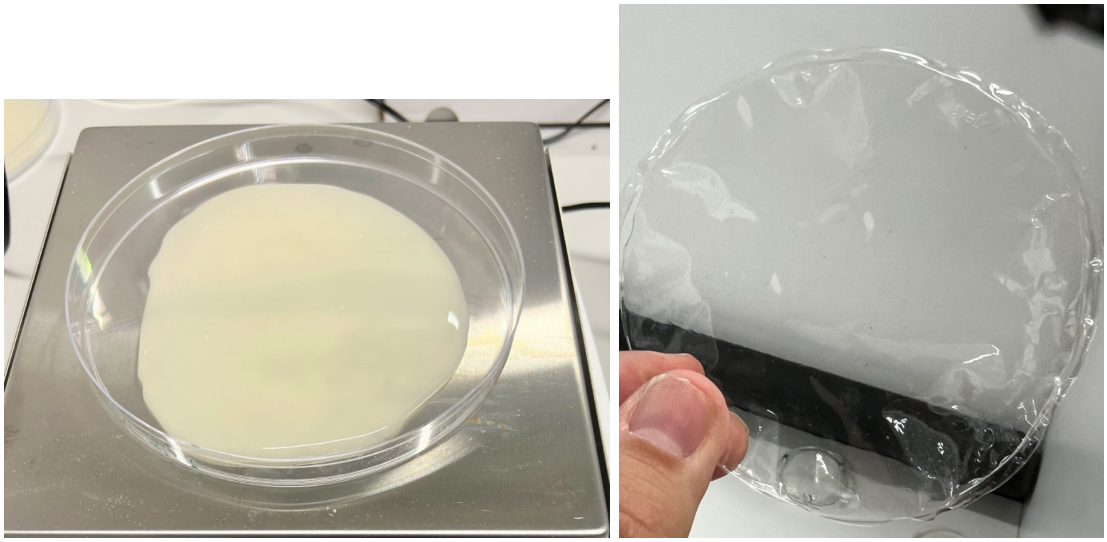

(a) Suspension of alginate poured into petridish. (b) Thin film of alginate.

Figure 3.8: From suspension to transparent film.

Although it looked perfectly transparent, the film seemed very unstable, and formed some bubbles on the edges. The stirring time or speed should be increased to reach a more homogeneous state. It felt not very solid and the film might tear easily. Sample thickness was only about 0.07 mm. Now it was important to improve stability of the alginate-film. A first idea to improve the stability is the concept of *crosslinking*.

3.2.2 Crosslinking

Crosslinking is a process in which chemical bonds are formed between the molecular chains of a polymer to improve its mechanical properties. This process results in the formation of a three-dimensional network within the polymer, which increases its strength, stiffness, and thermal stability. Crosslinking can be achieved by various methods, including chemical crosslinking agents, heat, radiation, or a combination of these methods. In our case, we use the salt *Calcium Chloride Dihydrat*, CaCl2.2H2O, as a crosslinking agent.
The degree of crosslinking can be controlled by adjusting the concentration, the reaction time, and the reaction temperature and must be tested empirically. Chemical crosslinking is widely used in various applications, including coatings, adhesives, elastomers, and biomedical materials, to improve their performance and durability [Arora et al., 2017]. We extended the process of the first sample fabrication and after the mixture was clamped onto the stirrer, we added different amounts of the salt as shown in Tab. 3.1. Then we continued stirring for 1.5h. Figure 3.9 shows the crosslinking agent.

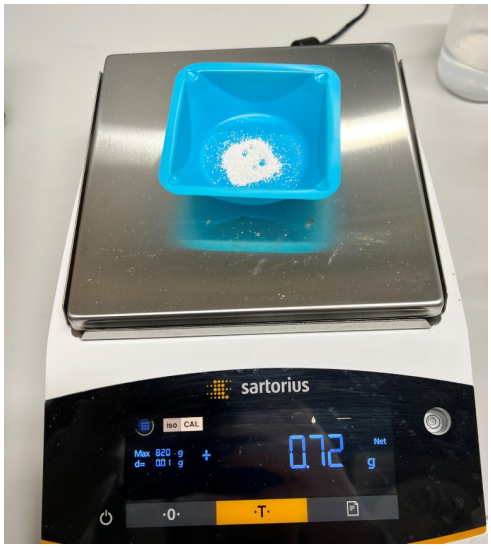

Figure 3.9: Crosslinking agent Calcium Chloride Dihydrat (salt)

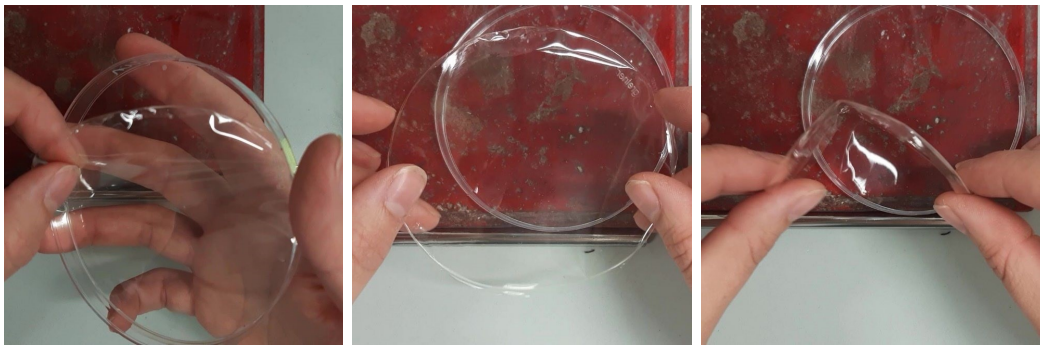

(a) (b) (c)

Figure 3.10: Examples of films with additional crosslinking, picture taken by Cornelia Ott.

	$CaCO_2$ [g]	Observation
01	0.018	Unstable film, transparent.
02	0.038	Stable film, transparent.
03	0.058	Stable film, plastic-like consistency, transparent.
04	0.078	Stable film, a little bit stiff, slightly yellow hue.
05	0.098	Stable film, medium stiffness, medium yellow hue.
06	0.108	Stiff, hardened film, medium yellow hue.
07	0.118	Stiff, hardened film, strong yellow hue.

Table 3.1: Different amounts of cross-linking agent $CaCO_2$, Alg = 2%.

Figure 3.10 shows pictures of the new alginate film. After the drying time of about 48 hours, the dried alginate film is transparent and flexible. A special observation was the sensitivity to unevenness of the surface. The film even replicates the tiny logo printed on the petri dish very detailed and copied the letters from the brand “Greiner” as seen on the top right corner of (b). Overall, it showed a good flexibility in all directions and behaves like plastic. Unfortunately, as soon as it gets in touch with water, the film dissolves immediately. Further tests were needed to find out the appropriate amount of the salt. Initially we started with an amount of 0.018 g $CaCl_2$. As we continue to increase the amount added, the transformation of the final appearance of the film becomes increasingly noticeable. We increased the amount in steps of 0.02 g. After

a certain amount of around 0.06 g we noticed a gradual shift in color, transitioning from its initial clarity to a subtle yellow hue. The impact of the salt does not only affect the visual characteristics. The stiffness of the material also increases as we add more salt. Figure 3.11 shows three different states ranging from clear and plastic-like film (a) to a medium flexibel film (b) until reaching the state of a very stiff almost hardened sheet (c).

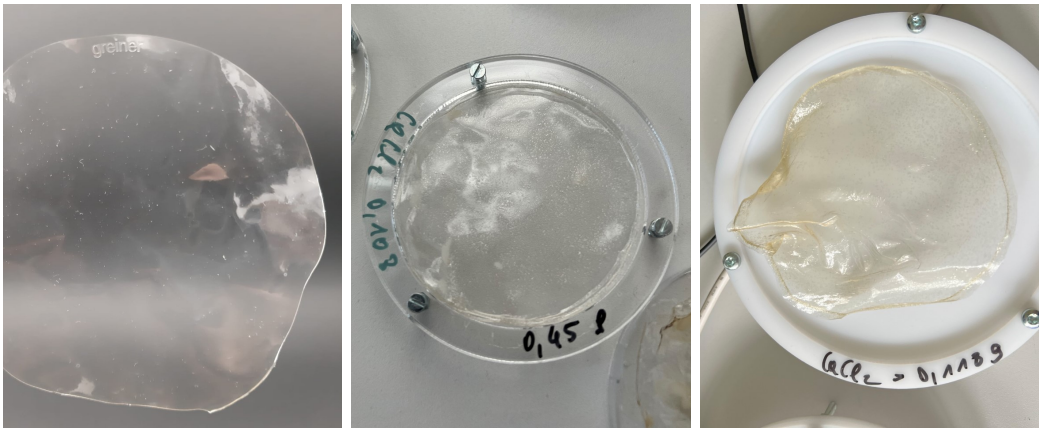

(a) Photo taken by Cornelia Ott (b) (c)

Figure 3.11: $CaCl_2$ affecting the stiffness and color cast.

Further testing led also to an increase of the alginate concentration to 4 % to achieve a thicker film. The best result of a stable film that was optically almost transparent and did not show a yellowish hue could be achieved with 0.04 g of calcium chloride. Three different specimen can be seen in fig. 3.12 (a) to (c). On the optical reflections in (c) we notice that the films could be a little bit more soft to provide a flat surface. For this reason small amounts of Glycerol were added (1 ml) to the suspension to soften the foil.

(a) (b) (c)

Figure 3.12: Clear film, 4 % alginate, 0.04 % calcium chloride.

3.2.3 Perforation methods

In order to provide acoustic absorption, the films must be perforated as described in the theory of microperforated panel absorbers in Ch. 2.4. Although the theory behind microperforated absorber materials is known for about 50 years, applying the submillimetric perforation onto a surface was always a difficult barrier to overcome. An advancement in industrial techniques gives us a couple of options to apply the holes. In this thesis, a variety of perforation techniques was examined. First, we tried to perforate the films with salt crystals. Therefore, we bring powder of **$CaCO_3$** into the suspension. The particles with known size should then be removed by washing them out in a bath of hydrochloric acid (**HCl**). What should remain is the perforated surface of the film. Figure 3.13 shows the $CaCO_3$ powder (a), the suspension with visible crystals (b) and an example of the dried film (c).

(a) (b) (c)

*Figure 3.13: Added **$CaCO_3$** powder.*

Here we faced two problems: First, the second drying process after the bath in **HCl** made the films totally unstable. Secondly the pores appeared to be still closed, open perforation could not be achieved as the holes were encased in a thin layer of alginate. Figure 3.14 (a) and (b) are different enlarged views of the pores that are still enclosed in alginate.

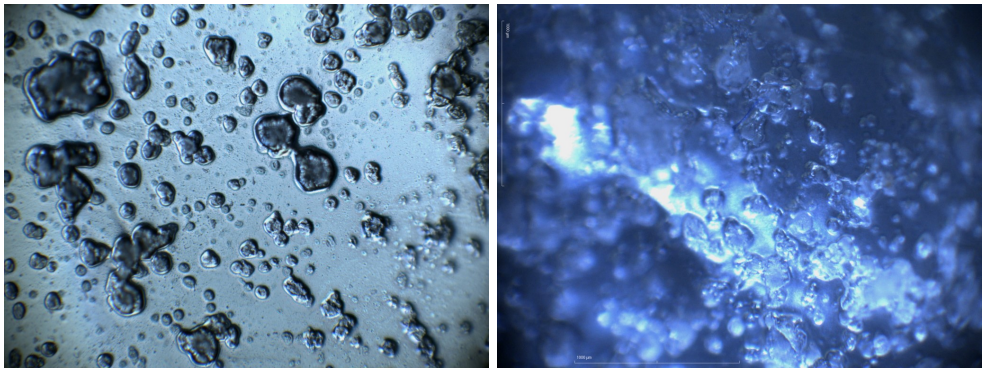

(a) sample after 24h in HCl bath (b) enlarged view

Figure 3.14: Alginate film under Electron microscope, closed pores visible.

Another approach to get the perforation into the film is casting the suspension directly onto a surface with small needles. Figure. 3.15 shows a 3D printed sample surface structure with a needle diameter of 0.15 mm and a spacing of 2 mm. Due to the small diameter, the needles broke while trying to pour the suspension onto the template.

With more expertise on the 3D printer, this method can definitely be improved.

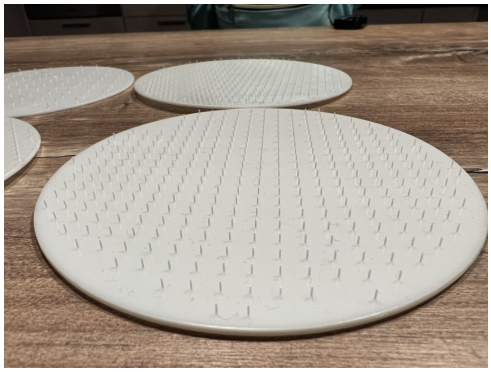

Figure 3.15: 3D printed perforation tools.

We then decided to try applying perforation by the use of a micro needling tool as these are used in the beauty industry a lot. Figure 3.16 shows the device and also first examples. The process can be very challenging and the success of perforation depends heavily on the pressure applied and the underlying ground. For best results the ground should be a hard surface as it is easier to destroy the sample of the films. A big drawback are the fixed dimensions of the commercially available needle roller. During the tests we asked for an industrial solution with customized micro needling device (customizable needle thickness and spacing) but this turned out to be extremely costly.

(a) Roller for micro needling [MNLRoller, 2023]

(b) Micro needling applied, photo by Cornelia Ott.

Figure 3.16: Experimenting with a needle roller with 540 needles, 0.15mm needle thickness.

For now, the most promising method for us was the use of a laser cutter to cut small holes into the films. Laser drilling is a non-contact method that uses a focused laser beam to create holes. The high-energy laser beam vaporizes or melts the material, resulting in a hole and offers high precision. It can create even sub-millimeter-sized holes with any pre-designed pattern. Timing and power of the laser must be tested before usage because although it is not highly flammable, the alginate film gets damaged and burned slightly if too much heat occurs. In Fig. 3.17 the process is shown. On (a) and (b) we see the laser working on a specimen of alginate which is covered in two sheet of paper to flatten the surface. To avoid big differences in the hole size, a flat surface of the films is needed.

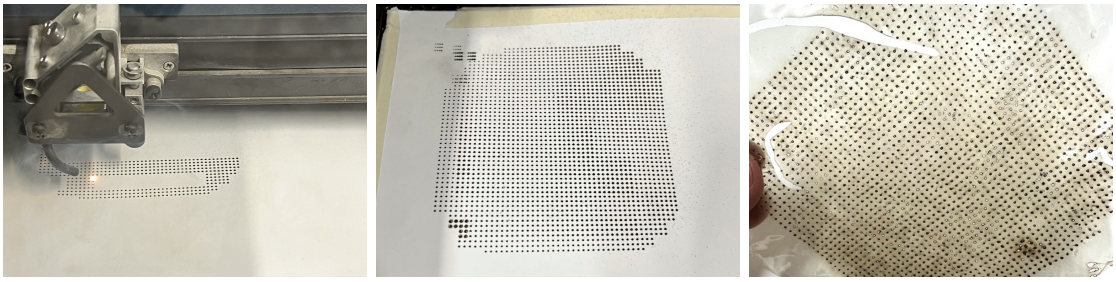

(a) (b) (c)

Figure 3.17: Laser cutter in use to obtain perforation.

For our purpose we used both laser-cutting machines from the IAM at TU Graz. A more detailed perforation grid could be machined with the Epilog Fusion M2 Laser. Figure 3.18 (a) shows the device, the process without covering the alginate film (b) and the predefined Rhino file which determines the position and sizes of the holes. Settings for strength and speed of the Laser have a huge impact on the results. We used a speed setting of 100 % and 9 % for strength to reduce burned edges.

(a) (b) (c)

Figure 3.18: Laser cutter in use to obtain perforation 2.

Although this method works best to achieve micro perforation, we face two big drawbacks. The first drawback of this technique is the limitation of the hole size by the smallest resolution the laser tip has. For our purposes, 0.2 mm is the smallest hole size the laser applies which is enough though. The second drawback is the reduced optical transparency as the edges of the holes get burned. These burned edges and also the unevenness of the hole sizes due to a non-flat surface during the drilling process can be seen on Fig. 3.17 (c). However, the charred area can be cleaned with a cotton swab.

3.3 Fabrication process summary

To create alginate films that provide the basis for microperforated films, the first specimen were made by mixing alginate powder with distilled water and pouring it into petri dishes. The film was then dried, resulting in an unstable sample that teared easily. To improve its stability, the crosslinking process is introduced using $CaCl_2$ as a crosslinking agent. The amount of salt affects the appearance and stiffness of the resulting film. For a transparent but also a tear-resistant result, values between 0.04 % and 0.07 % were ideal. The next step involved perforating the dry films to provide acoustic absorption. Several methods are explored, including the use of salt crystals, casting the suspension onto a template with small needles, and the use of a micro-needle roller. These perforation techniques did not provide suitable results. However, the most promising method is applying perforation by laser cutting, which offers high precision and the ability to create sub-millimetric-sized holes. Although there are drawbacks such as limited hole size due to the tip of the laser and reduced optical transparency due to burned edges, these issues can be neglected. Improving the settings of the machine might also reduce the edge burning effect. Although multiple sets of sample films were prepared on each new composition, only some of them were suitable and picked for further measurements. Figure 3.19 shows a series of images of various stations in the sample production.

(a) The shrinkage of the film after the bath in HCl was clearly visible. It reduced its size by 4 times.

(b) With the thickness measuring gauge the thickness of the individual samples was measured.

(c) Shows the mixture of alginate, water, and Glycerol. Initially, the suspension has a noticeable strong yellow color cast. However, during the drying process, this color cast gradually disappears, resulting in a clearer appearance. This is important as it affects the final aesthetic quality of the film.

(d) The suspension is poured into the petri dish. The pouring process hast to be slow to ensure an even distribution of the suspension on the surface of the dish.

(e) Shows a drying specimen with added $CaCO_3$ powder. This was one of the tested perforation techniques. The salt crystals are clearly visible within the film.

(f) Dry state of (e).

(g) Shows a sample with enclosed bubbles and a stiff surface due to a concentration above 0.12 % of the cross-linking with $CaCl_2$. The bubbles occur if no time for degasification was given after the suspension is stirred. We observed 12 hrs of degasification time to work best.

(h) By adding Glycerol to the mixture of alginate, destilled water and $CaCl_2$, the film gets softened and a cling film-like behaviour. It has to be added in small amounts ($\approx$ 1 ml on 100 ml) as it can get too soft very soon and also very sticky.

(i) Shows various samples six weeks after the first production run in the laboratory. We noticed that on all cross-linked samples, whether there was $CaCl_2$ or $CaCO_3$ added, a strong yellow hue occurred. It got more obvious if it was not clearly transparent after the first drying time of 24 hrs. The optically transparent films after the first drying time remained transparent. Some of the very stiff samples broke or they got small cracks.

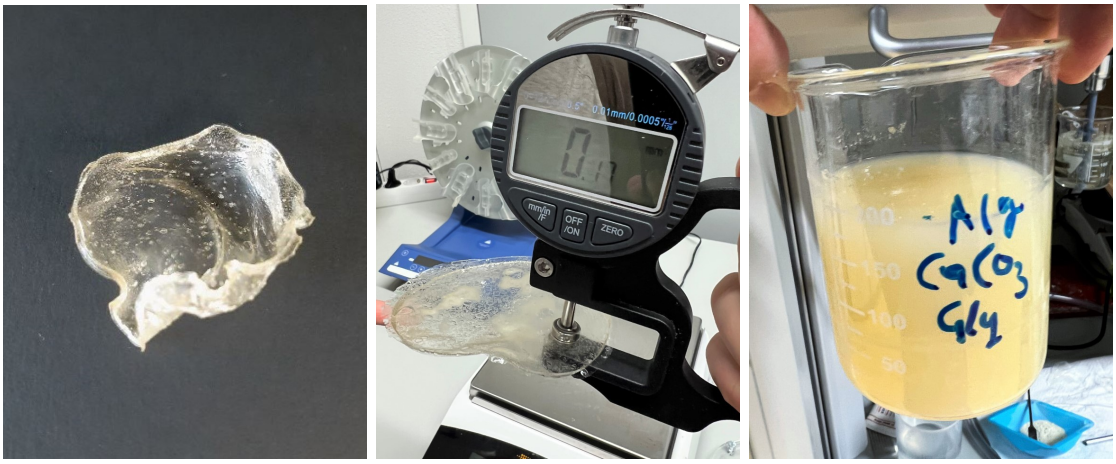

(a) Sample after HCl bath (b) Thickness measurement (c) Suspension

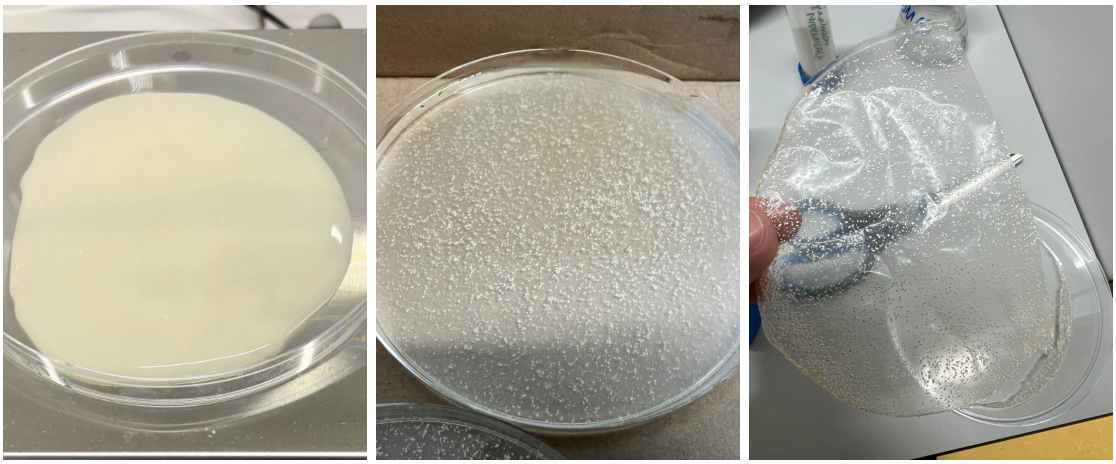

(d) Poured in petridish (e) Drying suspension (f) CaCO3 sample

(g) Cross-linked sample (h) Added plasticizer Glycerol (i) Overview of different specimen

Figure 3.19: Different experiments with alginate suspensions.

4 Measurements and results

To evaluate samples made from alginate, the absorption coefficient is measured in the impedance tube. It is a long, narrow tube with a speaker at both ends and four microphones placed along the tube. This is also known as four microphone method. In this method, the microphones are positioned along the length of the tube, with each measuring the pressure at a different location. The pressure signals from all four microphones are then used to calculate the sound transmission loss of the material. This provides a more comprehensive and accurate measurement of the material's acoustical properties, including any variations or inhomogenious areas along the length of the tube. Figure 4.1 shows the typical setup. In our case, we measure the absorption coefficient. The measurements were performed by using the Matlab based script CATS8 from the SPSC Institute of TU Graz. It also allows to simulate different values for the parameter air gap (D), which was used for the measurements. Predicted absorption behaviour and the corresponding calculated values for the absorption coefficient use the equations of Chap. 2. Therefore, different scripts were written in Matlab to implement the approaches for calculating the impedance of microperforated absorbers, resonant absorbers and porous absorbers.

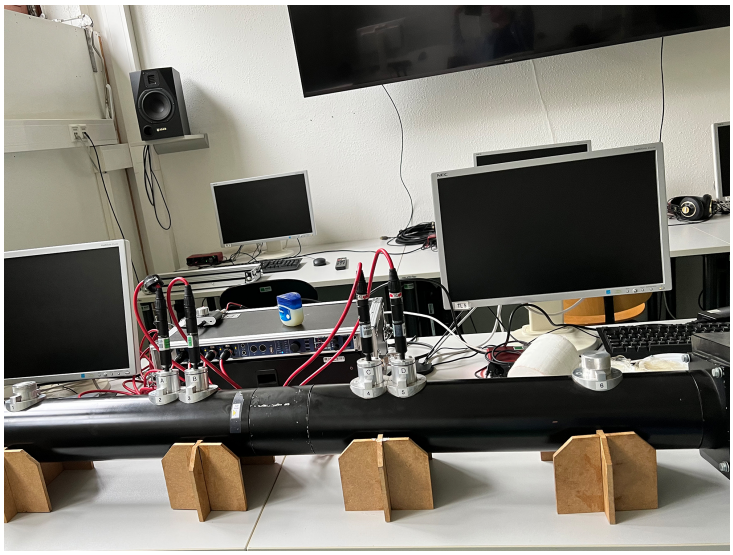

Figure 4.1: Impedance tube measurement setup.

4.1 Single layer absorber

To get a better insight into state-of-the-art microperforated absorber solutions, the absorption coefficient of a known material, a sample of a microperforated film was measured in the impedance tube that served as a reference measurement. Therefore, a piece of the film was cut out in a circle with diameter ø = 10 cm to fit into the tube. As a mounting device, a circle of plexiglas was used as shown in Fig. 4.2 to fix the sample. The frame consists of two parts while the films to be tested were clamped in between. Three small screws were used for further fixing. The commercial MPP film with the trade name OPALWHISPER ® [Haverkamp, n.d.] is made of teflon, a synthetic thermoplastic polymere and has the following specifications according to the design parameter for microperforated absorber films according to Chap. 2.4.2:

- **d = 0.2 mm, b = 2 mm, t = 150 µm, D = 5 cm**

In Fig. 4.2(a) the perforation with very small holes on the translucent film is visible. The holes are in circular shape and homogeneous spread on the surface. Figure 4.3 and Tab. 4.1 contain the measured results compared to the predicted theoretical absorption coefficient by using the model by Maa [D. Y. Maa, 1975]. The tear resistance or tear strength is a measure of how well a material can withstand the effects of tearing. From the datasheet, we obtain a value of $400\frac{N}{mm}$ for the film.

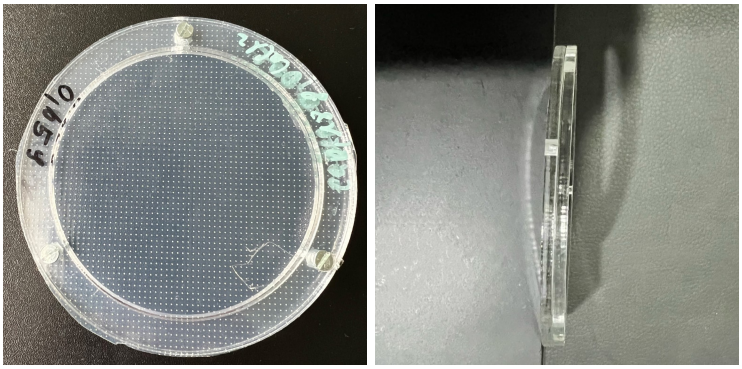

(a) Commercial MPP film, OPALWHISPER ® in a plexiglas mounting device

(b) Mounting device, side view

Figure 4.2: Commercial MPP film to be evaluated.

	f_{res} [Hz]	α_{max}	bandwidth [Hz]
MPP measured	891	0.95	400 - $\geq$ 2000
MPP calculated	970	0.98	420 - $\geq$ 2000

Table 4.1: MPP film, calculated [Eq. 2.45] and measured results.

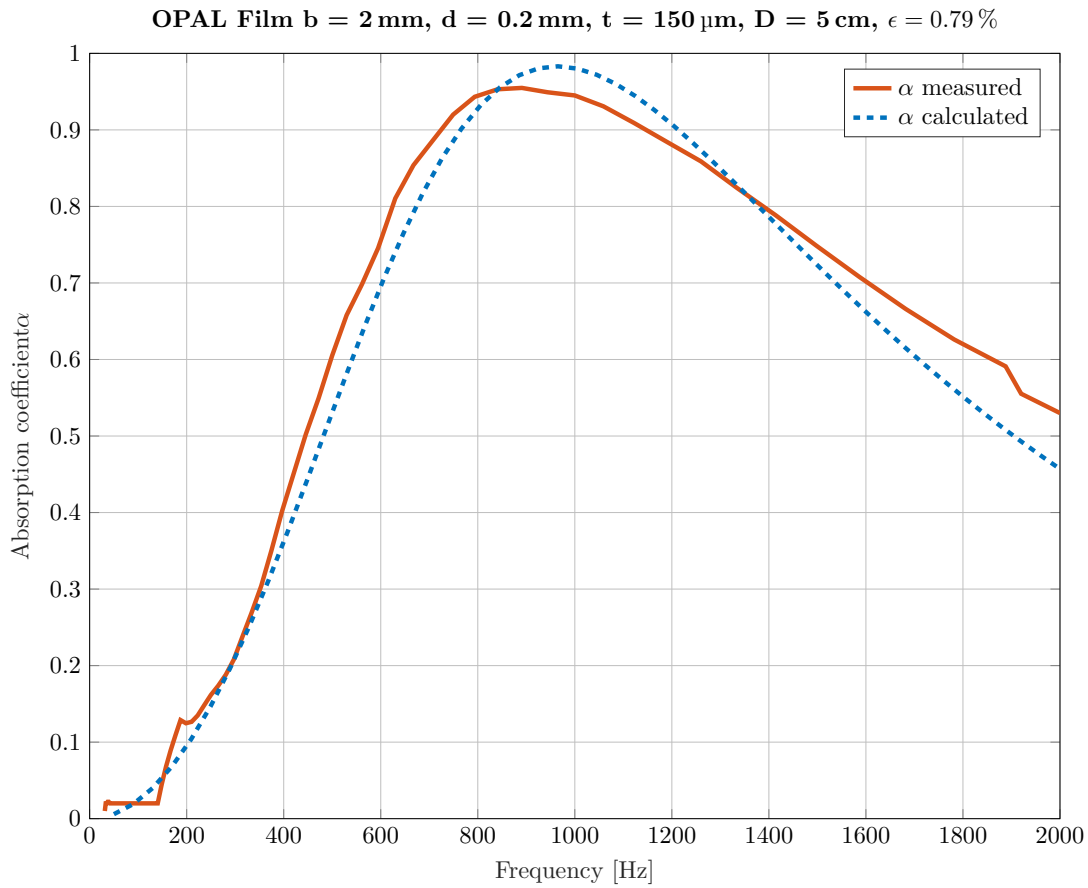

Figure 4.3: Absorption curve MPP film.

The measured absorption coefficient of the film shows typical MPP behavior with an absorption coefficient of $\alpha \geq 0.4$ in the frequency range $400\,Hz - \geq 2000\,Hz$. Compared to the predicted values, we notice a slight shift of the center frequency towards lower frequencies from $f_{res} = 970\,Hz$ to $f_{res} = 891\,Hz$ and also a broadened absorption bandwidth. This may be due to the production tolerance of the hole diameter and spacing. Examined with the electron microscope (EM), the hole diameter is $d = 0.2\,\text{mm} \pm 0.1\,\text{mm}$. Also further examination of the surface of the material show small craters rise. This could be attributed to the punching process with an industrial needle roller. It is possible that the edge effects have an impact on the absorption maximum and that the end correction term applied in the calculation is not accurate as proposed from Eq. 2.45. Figure 4.4 shows the EM photo series of the film. On (a) we see a perforation pattern of four equidistant holes, (b) shows an enlargement of one hole in particular from above and (c) is a 3D representation of the surface. On the bottom of the material it shows the crater around the pinched hole.

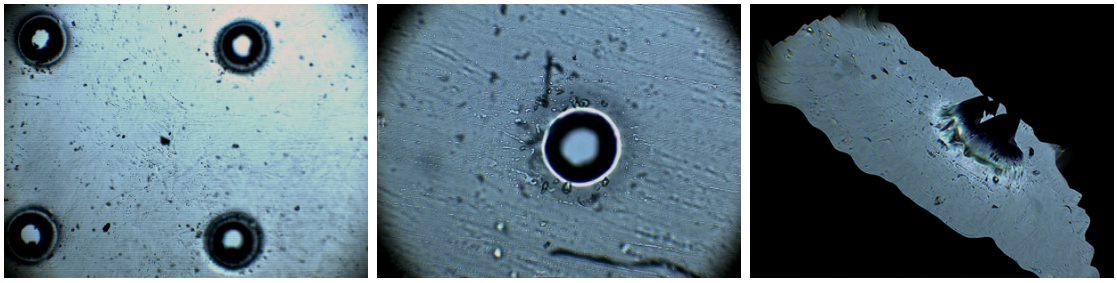

(a) MPP film, 7x (b) MPP film, 10x (c) 3D-view, 10x

Figure 4.4: MPP film examined with an EM.

4.1.1 Alginate film 01 (AL01)

The first sample of our alginate films that led to a stable sample is shown in Fig. 4.5, with a clear film with a slightly yellowish cast. In the manufacturing process the cross-linking agent $CaCl_2$ was added to the alginate suspension. This led to a rather stiff and inflexible membrane which can be observed on (a). Image (b) shows the mounting device made from plexiglas with the three screws attached and the sample holder of the impedance tube. The bubbles inside the film occurred randomly during the stirring process and did not vanish during drying time of 48 hours. (c) shows the measurement of the sample thickness. A piece with diameter $\varnothing = 10\,\text{cm}$ was cut out and put into the mounting device of plexiglas.

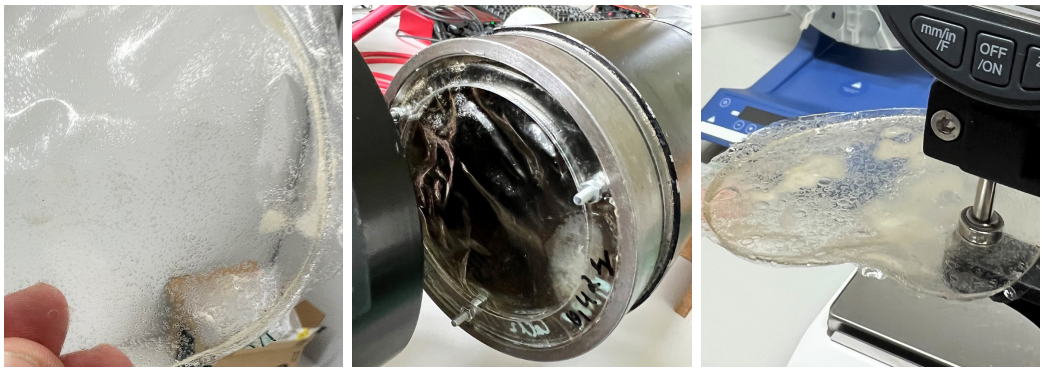

(a) Stiff membrane (b) Mounting frame with sample in impedance tube (c) Measurement of sample thickness

Figure 4.5: First sample made from alginate.

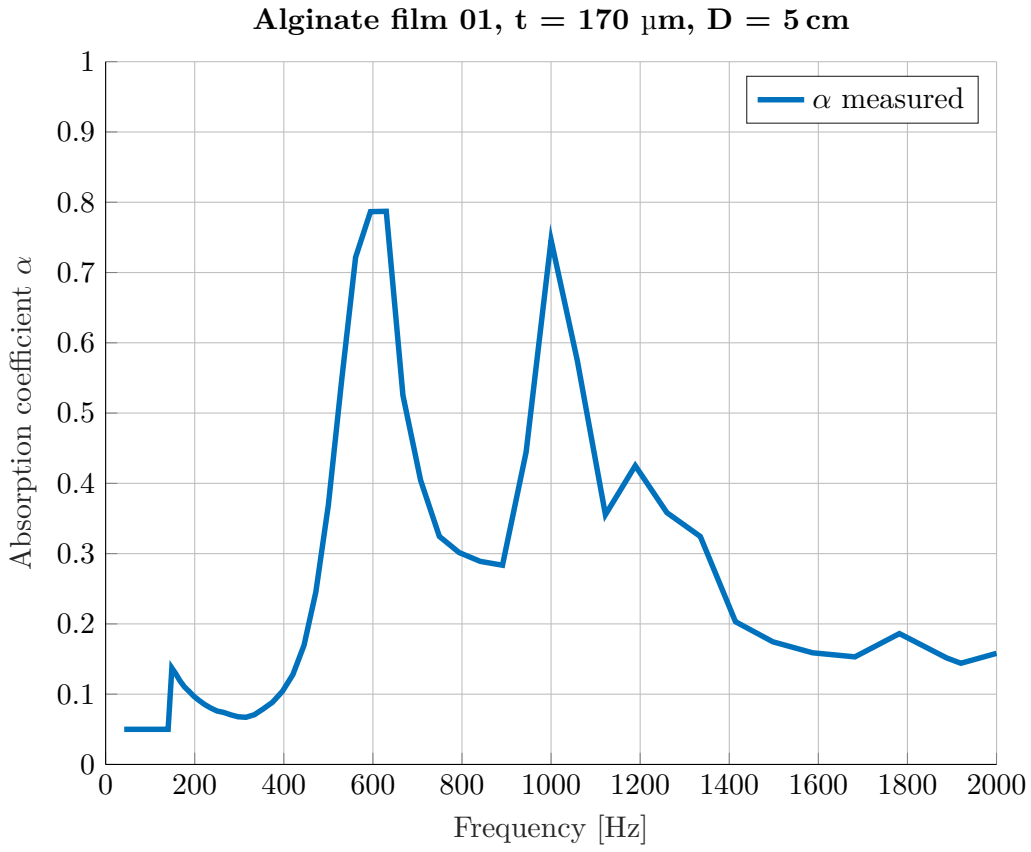

Figure 4.6: Absorption curve AL01.

	m [g]	a [cm^2]	m' [$\frac{g}{cm^2}$]	ϵ [%]	f_{res} [Hz]	α_{max}
f_1 meas.	1.45	78.54	0.185	-	630	0.78
f_2 meas.	1.45	78.54	0.185	-	1000	0.75
f_1 calc.	1.45	78.54	0.185	-	625	-
$f_{Helmholtz}$	-	-	-	1.49	1000	-

Table 4.2: Alginate film 01, calculated [Eq. 2.18, Eq. 2.26] and measured results.

Figure 4.6 shows the measured absorption coefficient α for the first sample made of alginate. We notice two narrow peaks occurring at $f_1 = 630\,Hz$ and $f_2 = 1000\,Hz$. The sample does not show characteristic MPP behaviour and the air bubbles in the film do not appear to be open pores. Air cannot pass through as it would with micro perforation applied and therefore perforation would be necessary to increase the absorption bandwidth. The sample film shows **characteristics** of a **membrane absorber**. This is also compared with the theory of Chap. 2.3 in the calculations of Tab. 4.2.
By using the mass per unit area (m') from a measurement of the weight (m), the cavity depth (D) and Eq. 2.18 we calculate f_1 for a membrane absorber. The calculated resonance frequency $f_1 = 625\,Hz$ lies slightly below the measured $f_1 = 630\,Hz$. However, this does not explain the measured peak $f_2 = 1000\,Hz$. As a thought experiment, we consider the enclosed air bubbles to be open and look at the peak on f_2 as a theoretical Helmholtz absorber. The consideration comes from the observation, that the enclosed air bubbles visible on Fig. 4.5 are only covered by an extremely thin layer of alginate. With Eq. 2.26 we use the peak at $f_2 = 1000\,Hz$ to further calculate the perforation ratio $\epsilon = 1.49\,\%$. This could be a reasonable result, but as the enclosed air bubbles are not evenly spread the perforation ratio is not determinable.

Manufacturing specifications

- **t = 170 µm, D = 5 cm**
- **Sodium alginate concentration:** 3 %
- **Cross linking agent:** $CaCl_2$, 0.108 g on 100 ml
- **Stirring time:** 2,5 hrs
- **Degasification time:** -
- **Drying:** 48 hrs, room temperature (20°C)
- **Material properties:** After the drying time a shrinkage of $\sim 5\,\%$ can be observed. The material is quite stiff compared to the reference material and tears easily. A measurement of the tear resistance was not possible at this point. The sample is not water resistant and sensitive to high humidity.
- **Acoustic properties:** It shows behaviour of a membrane absorber with $f_1 = 625\,Hz$ calculated and probably forms a Helmholtz absorber with $f_{Helmholtz} = 1000\,Hz$. Two peaks at the measured absorption coefficient occur at $f_1 = 630\,Hz$ and $f_2 = 1000\,Hz$, the film is not applicable for broadband absorption.

4.1.2 Alginate film 02 (AL02)

As the enclosed bubbles have no positive impact which yields MPP behaviour, we further enhanced the manufacturing process and added time for the suspension to degasify after stirring and before the cross-linking agent was added. This led to a homogeneous film without air bubbles enclosed. The second film to be measured was manufactured with a different cross-linking agent, namely Calcium carbonate ($CaCO_3$). Figure 4.7 (a) and (c) show the resulting very transparent film with $CaCO_3$ particles. On (b) we see the suspension with the alginate and the cross-linking agent before the drying process.

(a) Sample with enclosed particles (b) Suspension (c) Dry film

Figure 4.7: Alginate films with $CaCO_3$.

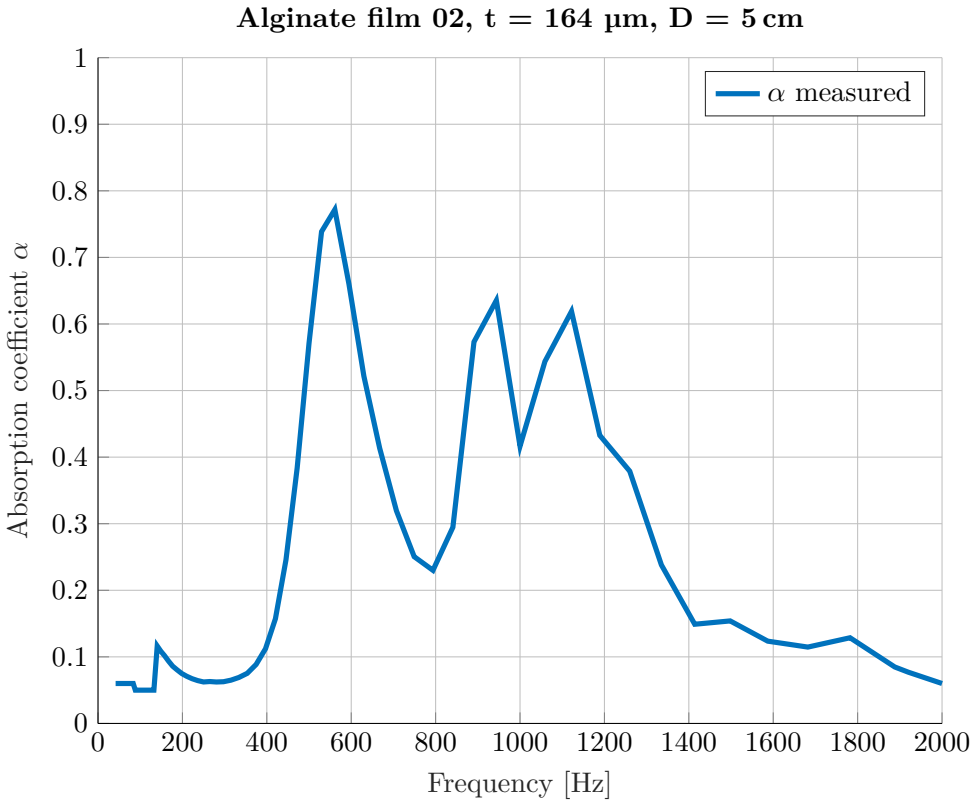

Figure 4.8: Absorption curve AL02.

	m [g]	a [cm^2]	m' [$\frac{g}{cm^2}$]	ϵ [%]	f_{res} [Hz]	α_{max}
f_1 meas.	1.77	78,54	0.225	-	561	0.77
f_2 meas.	1.77	78,54	0.225	-	943	0.63
f_3 meas.	1.77	78.54	0.225	-	1122	0.62
f_1 calc.	1.77	78.54	0.225	-	565	-
$f_{Helmholtz}$	-	-	-	1.72	943	-

Table 4.3: Alginate film 02, calculated [Eq. 2.18, Eq. 2.26] and measured results.

In the manufacturing process of sample **AL02** $CaCO_3$ and Glycerol [1 %] as plasticizer agent was added to the alginate suspension, which lead to a more gel-like membrane. The powder of $CaCO_3$ was evenly spread on the surface and should then be washed out in a bath of Hydrochloric acid (HCl) to obtain perforation and MPP behaviour. The small particles of $CaCO3$ are visible inside the film, on Fig. 4.7. One attempt to obtain micro-perforation was to immerse the dry films in a 5 % $CaCl_2$ ethanol/water bath containing 72 mM Hydrochloric acid for 5 min to be cross-linked. With the HCl, it is aimed to provide pores to the alginate gel.
Figure 4.8 shows the measured absorption coefficient α. We notice three narrow peaks occurring at $f_1 = 561\,Hz$, $f_2 = 943\,Hz$ and $f_3 = 1122\,Hz$. The sample film shows **characteristics** of a **membrane absorber**.
The measured resonance frequencies are compared with the calculated results in Tab. 4.3. The calculated resonance frequency $f_1 = 565\,Hz$ lies slightly above the measured $f_1 = 561\,Hz$. The third peak, measured at $f_3 = 1122\,Hz$ appears at twice the fundamental frequency and can be viewed as a harmonic. For the peak $f_2 = 943\,Hz$ we repeat the thought experiment of the previous measurement and assume Helmholtz behaviour due to air bubbles. With Eq. 2.26 we use the peak at $f_2 = 943\,Hz$ to calculate the perforation ratio $\epsilon = 1.72\,\%$. This could be a reasonable result, but as the enclosed air bubbles are not evenly spread the perforation ratio is not determinable. Also the corresponding thickness inhomogeneities could lead to the peak on f_2.
The sample does not show MPP behaviour as the pores in the film do not appear to be open. Further studies under the EM [Fig. 4.9] show, that these pores are enclosed and no statement can be made about the porosity: (a) and (b) are two different representations of the enclosed pores, the $CaCO_3$ particles are shown on (c). Therefore, this perforation technique is not suitable for optimizing the material for acoustic purposes.

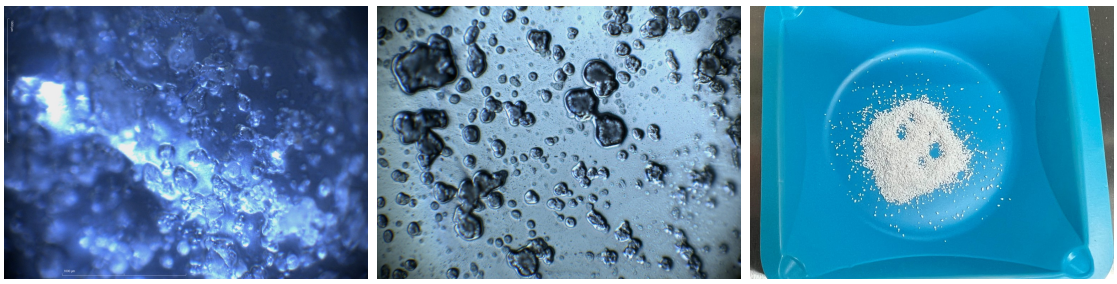

(a) Alg 02, EM - closed pores (b) Alg 02, EM - closed pores (c) $CaCO_3$ particles

Figure 4.9: Alginate film 02

Manufacturing specifications

- **t = 164 µm, D = 5 cm**
- **Sodium alginate concentration:** 2 %
- **Cross linking agent:** $CaCO_3$, 0.32 g on 100 ml

- **Plasticizer:** Glycerol, 1 %
- **Stirring time:** 2,5 hrs
- **Degasification time:** 24 hrs
- **Drying:** 48 hrs, room temperature (20°C)
- **Material Properties:** After drying, no visible shrinkage. The material is more gel like, due to the glycerol added and more flexible compared to the reference film. Tears easily. Not water resistant.
- **Acoustic properties:** It shows behaviour of a membrane absorber with $f_1 = 565\,Hz$ calculated and probably forms a Helmholtz absorber with $f_{Helmholtz} = 943\,Hz$. Three peaks at the measured absorption coefficient with narrow bandwidth occur at $f_1 = 561\,Hz$, $f_2 = 943\,Hz$ and $f_3 = 1122\,Hz$. Therefore, the film is not applicable for broadband absorption.

4.1.3 Alginate film 03 (AL03)

Alginate film 03 was perforated with the use of the needle roller. According to the manufacturer information the design parameters were **d = 0.1 mm, b = 1.5 mm**. Unfortunately, the thin and short needles were not able to pierce the films. Therefore we again expect the behaviour of a membrane absorber. Figure 4.10 shows the sample on (a) and the supposed to be perforated film on (b). Sample AL03 was made with added Glycerol [2 %] as a plasticizer agent. The drying time of 8 hours in the dehydrator led to a stable film with an increased thickness. Stirring time could be reduced to 30 minutes after adding the sodium alginate and 40 minutes after the cross-linking agent was added. As seen on (c), a thickness of 410 µm was measured.

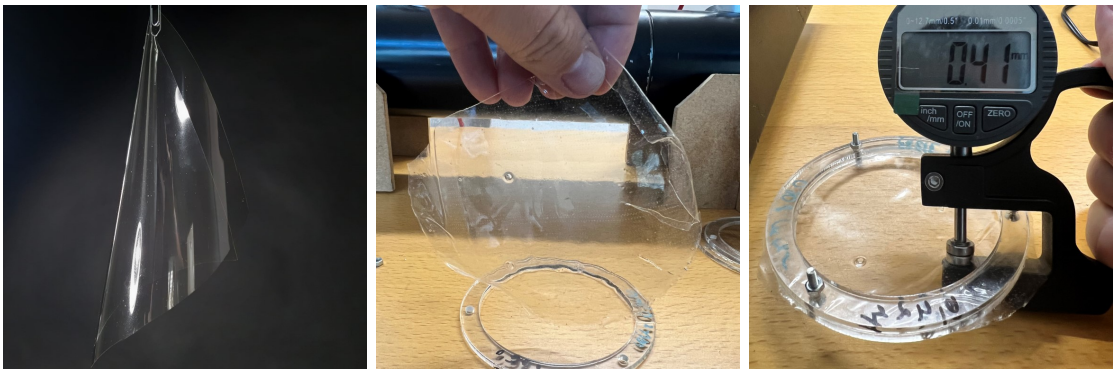

(a) AL03, Photo: C. Ott (b) Very transparent film (c) Measurement of thickness

Figure 4.10: Alginate film 03

	m [g]	a $[cm^2]$	m' $[\frac{g}{cm^2}]$	f_{res} [Hz]	α_{max}
f_1 meas.	7.16	78,54	0.9116	281	0.91
f_1 calc.	7.16	78.54	0.9116	281	1

Table 4.4: Alginate film 03, calculated [Eq. 2.17 and Eq. 2.18] and measured results.

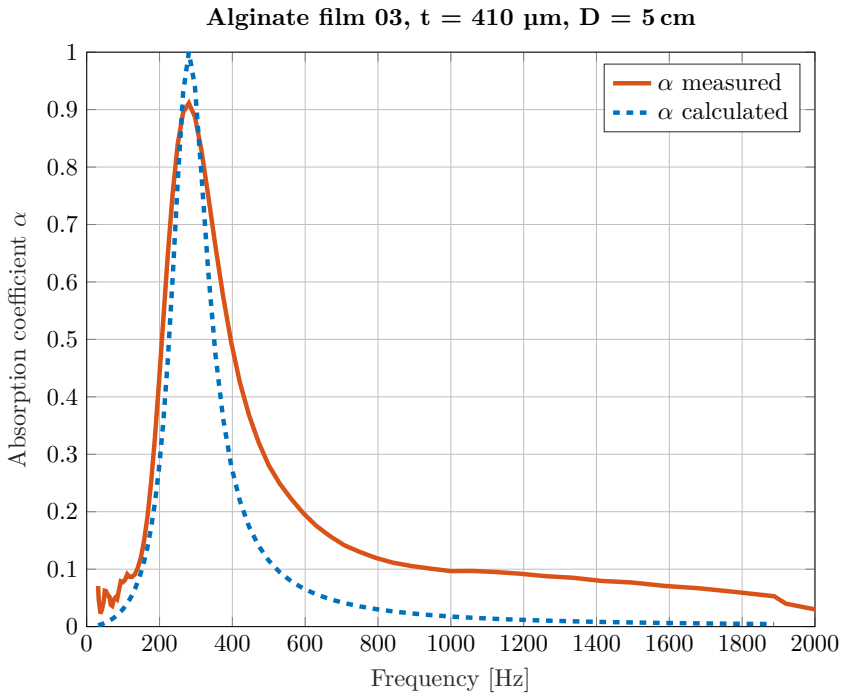

Figure 4.11: AL03 shows behaviour of membrane absorber.

Figure 4.11 shows the measured absorption coefficient α for **AL03**. The sample was perforated with a needle roller used for pharmaceutical purposes but the needles were not strong enough to pinch through the film and therefore expect the behaviour of a membrane absorber. The increased sample thickness of the film and the resulting increased mass per unit area shifts the resonance frequency to a lower frequency than AL02. We notice a narrow peak occurring at $f_1 = 281\,Hz$ with $\alpha = 0.91$. For the calculation of $\underline{W}$ with Eq. 2.17 we assume a matched impedance and therefore $r = Z_0$. The sample shows **characteristics** of a **membrane absorber**. The measured resonance frequency f_1 is compared with the calculation and with $f_1 = 281\,Hz$ it confirms the membrane behaviour.

Manufacturing specifications

- **t = 410 µm, D = 5 cm**
- **Sodium alginate concentration:** 3 %
- **Plasticizer:** Glycerol, 2 %
- **Cross linking agent:** $CaCl_2$, 0.02 g on 100 ml
- **Stirring time:** 30 min with sodium alginate, 40 min with added $CaCl_2$
- **Degasification time:** 1 hour sodium alginate suspension, 2 hrs with added $CaCl_2$
- **Drying:** 8 hrs, 37°C
- **Properties:** After drying, no visible shrinkage. The material feels and behaves like plastic but due to the added Glycerol it gets very soft and a little bit sticky. Tears more likely than previous samples. Not water resistant. The film is not entirely transparent and looks more like frosted glass.
- **Acoustic properties:** It shows behaviour of membrane absorber with $f_{res} = 281\,Hz$ with narrow bandwidth. Therefore the film is not applicable for broadband absorption.

4.1.4 Alginate film 04 (AL04)

Another sample to be measured was manufactured with the aim to receive a very transparent film, but also to improve its tear resistance leading to a thickness, that appears constant and homogeneous on the hole sample surface. Figure 4.12 (a) shows the clear film. The sample was then perforated using the Lasercutter. On (b) and (c) we see the film after the perforation pattern was applied. Compared to previous samples, this sample was not made in the laboratory of TU Graz but at home in the kitchen with a blender and dried in a dehydrator. To obtain a homogene surface without air bubbles, the alginate suspension with 4 % was left to degasify for 8 hours, before the cross-linking agent $CaCl_2$, 0.04 g on 100 ml was added to stabilize the film. In the next step, the suspension was left to degasify for another 24 hours. The higher concentration of sodium alginate led to the improved strength of the film. After casting into the petridish, the film is placed in the dehydrator for 6 hours at 37°C. The resulting film feels like a plastic film and does not tear as easily as previous films. As a drawback of the laser-cutter perforation technique, the film is not entirely transparent anymore as it gets burned on the edges.

(a) (b) (c)

Figure 4.12: Transparent alginate films with $CaCl_2$.

	d [mm]	t [µm]	f_{res} [Hz]	α_{max}	bandwidth [Hz]
f_1 ref. mat. meas.	0.2	150	891	0.95	400 - $\geq$ 2000
f_1 meas.	0.2	160	1260	0.49	1020 - 1620
f_1 calc.	0.2	160	1000	0.95	447 - $\geq$ 2000
f_1 calc.	0.32	160	1243	0.47	965 - 1572

Table 4.5: Alginate film 04, calculated [Eq. 2.45] and measured results.

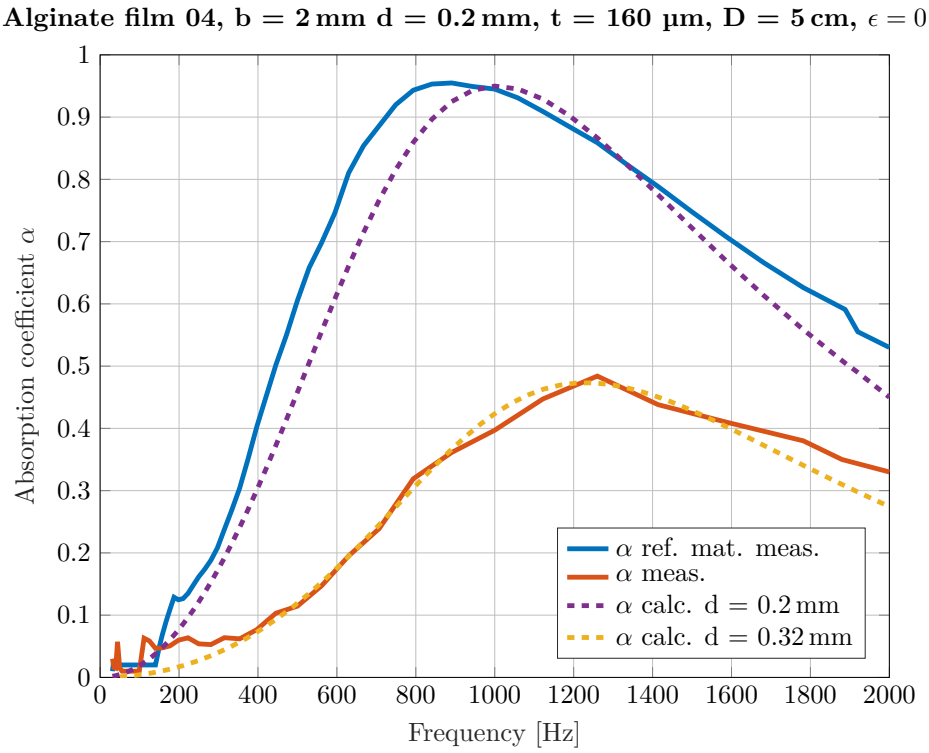

Figure 4.13: Absorption curve AL04.

Figure 4.13 shows the measured absorption coefficient α for the sample perforated with the laser cutter. The design parameters for the perforation pattern ($b = 2\,mm$, $d = 0.2\,mm$) were the same as for the reference material. Although we see MPP characteristics, the measured results differ significantly from the measured reference MPP film. We notice a broad absorption behaviour but with a lower peak found at $f_1 = 1260\,Hz$ and $\alpha = 0.49$. This could be attributed to variations in hole size d or in the hole distance b. The hole size seems to be above the desired $0.2\,mm$. One can observe that an assumed hole size of $d = 0.32\,mm$ fits the measured result more accurately. In comparison to the reference material, we notice the importance of keeping the design parameters in the desired range, as the acoustical performance of the reference material is clearly better. For more accuracy on the perforation with the laser cutter, the cutting process should further be optimized. An approach is to make sure that the surface of the film is even more flat during the cutting process and the focus of the laser must be set very precisely. Further optimization on the parameters of the laser cutter is necessary to obtain a more accurate hole size with less prominent variations.

Manufacturing specifications

- **t = 160 µm, D = 5 cm, d = 0.2 mm**
- **Sodium alginate concentration:** 4 %
- **Cross linking agent:** $CaCl_2$, 0.04 g on 100ml
- **Stirring time:** 30 min with sodium alginate, 40 min with added $CaCl_2$
- **Degasification time:** 8 hours sodium alginate suspension, 24 hours with added $CaCl_2$
- **Drying:** 6 hours, 37°C

- **Properties:** After drying, no visible shrinkage. The material feels and behaves like plastic. The film appears to be the most stable one made from alginate. However, it did not entirely reach the tear resistance of the reference material. The film is still not water resistant. Drawback: Although the use of a dehydrator speeds up the drying process, also time for degasification is needed.
- **Acoustic properties:** The characteristics of a microperforated absorber, and therefore broadband absorption can be observed, but with a relatively small absorption peak at $f_1 = 1260\,Hz$ and $\alpha = 0.49$. Perforation with laser cutter works as expected but hole size of d = 0.2 mm can not be achieved.

4.1.5 Alginate film 05 (AL05)

Alginate film 05 was a similar sample as the previous one but with an improved technique for the perforation with the laser-cutter. The transparent alginate film was covered with a thin sheet of cardboard to prevent the burned edges. Again the design parameter **b = 2 mm, d = 0.2 mm** were used to obtain the desired broadband absorption characteristics. Figure 4.14 shows the sample without perforation on (a) and the clamped film within the plexiglas circle on (b). Due to inaccuracy on the drying of the film, the sample was slightly thinner than the previous one, AL04 (c).

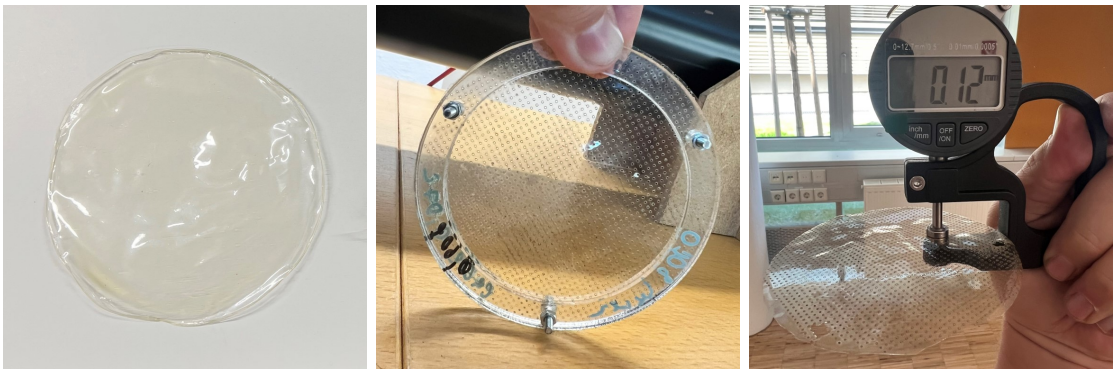

(a) (b) (c)

Figure 4.14: Alginate film 05

	d [mm]	f_{res} [Hz]	α_{max}	bandwidth [Hz]
f_1 meas.	0.2	1260	0.42	1150 - 1550
f_1 calc.	0.2	1000	0.94	447 - $\geq$ 2000
f_1 calc.	0.31	1260	0.44	1030 - 1498

Table 4.6: Alginate film 05, calculated [Eq. 2.45] and measured results.

Alginate film 05, b = 2 mm, d = 0.2 mm, t = 120 µm, D = 5 cm, $\epsilon = 0.79\,\%$

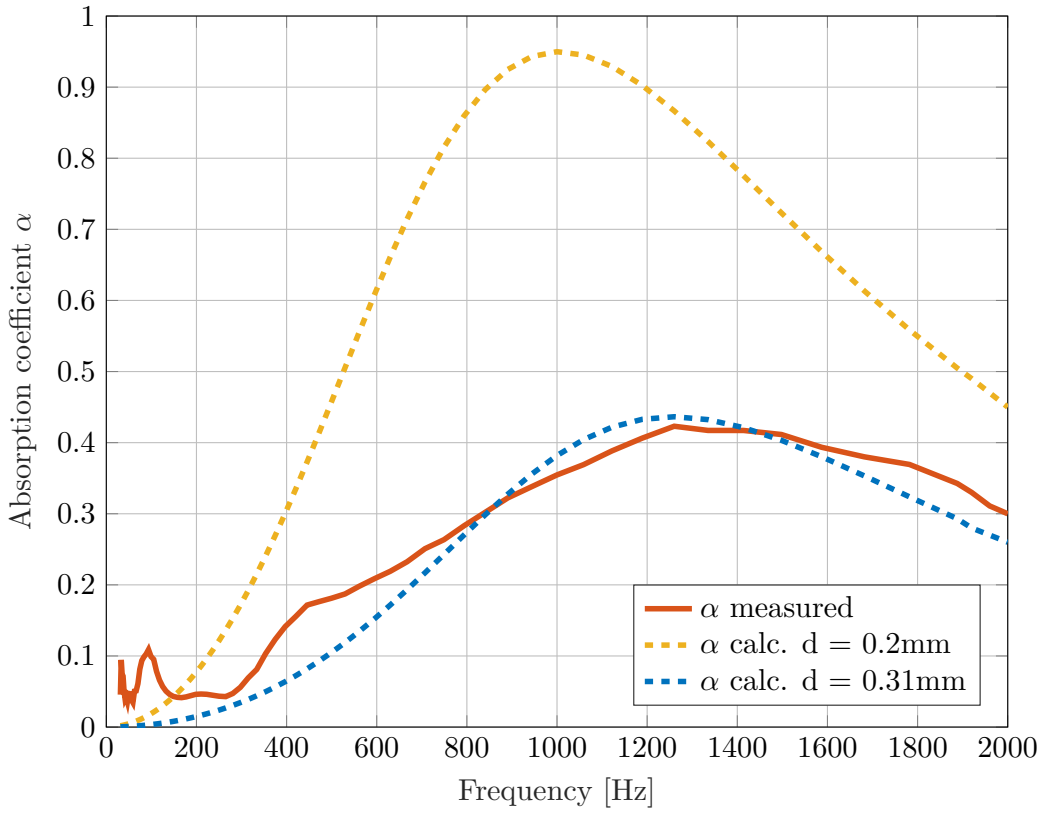

Figure 4.15: Absorption curve AL05 compared to calculated data.

Figure 4.15 shows the measured absorption coefficient α for Alginate film 05. The sample was perforated with the laser cutter and the design parameters ($b = 2\,mm, d = 0.2\,mm$) for the perforation pattern. Although we see MPP characteristics, the measured results differ significantly from the precalculated absorption curve. A low absorption peak is found at $f_1 = 1260\,Hz$ and $\alpha = 0.42$. However, due to the still remaining edge burning effect, the hole size **d** increases randomly on the film. One can observe in Fig. 4.15 that assuming a hole size of **d = 0.31 mm** fits the measurement significantly better.

Manufacturing specifications

- **t = 120 µm, D = 5 cm, d = 0.2 mm**
- **Sodium alginate concentration:** 4 %
- **Cross linking agent:** $CaCl_2$, 0.04 g on 100 ml
- **Stirring time:** 30 min with sodium alginate, 40 min with added $CaCl_2$
- **Degasification time:** 8 hours sodium alginate suspension, 24 hours with added $CaCl_2$
- **Drying:** 6 hours, 37°C
- **Properties:** After drying, no visible shrinkage. The material feels and behaves like plastic. A little less stiff and stable than the reference material although AL04 feels very similar. Less tear resistant than AL03. The sample is not water resistant.
- **Acoustic properties:** MPP absorption characteristics can be observed, but with decreased absorption peak compared to the expected value. Perforation with laser cutter works but reducing the hole size to **d ≤ 0.3 mm** is still an issue.

4.1.6 Alginate film 06 (AL06)

Alginate film 06 was a similar sample as AL 05 but with an improved technique for the perforation with the laser-cutter. Via the control software of the laser-cutter, the process should be improved by using different settings for intensity and speed of the laser. The transparent alginate film was covered with a thin sheet of cardboard to prevent the burned edges. Again the design parameter **d = 0.2 mm, b = 2 mm** were used. Figure 4.16 shows the sample on (a) without the perforation and the mounted film on the plexiglas circle on (b). Due to inaccuracy on the drying of the film, the sample was slightly thinner than the previous one (c).

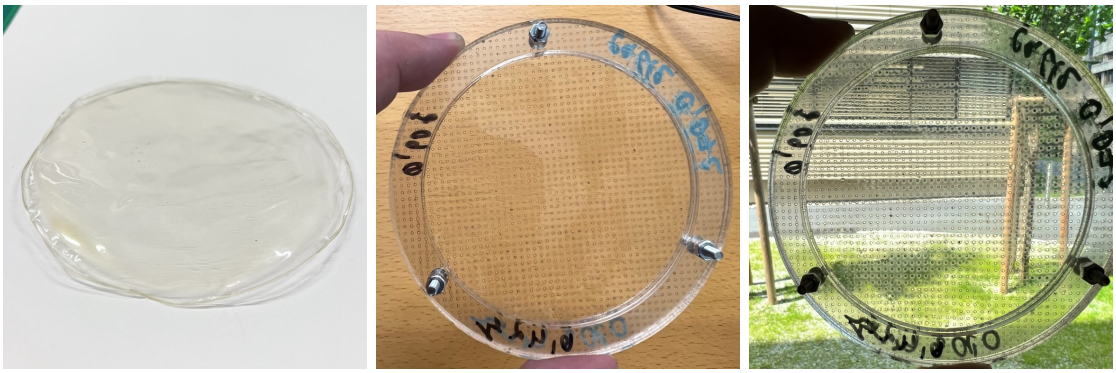

(a) (b) (c)

Figure 4.16: Alginate film 06

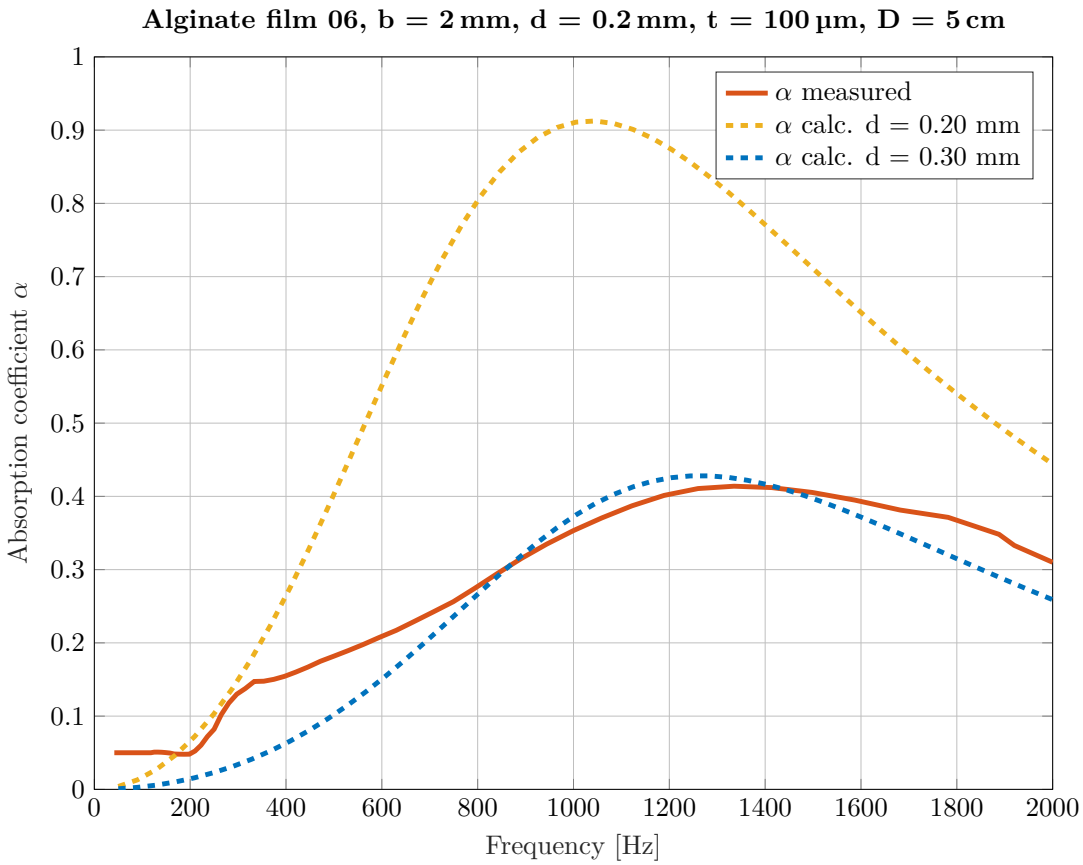

Figure 4.17: Sample 06 compared to simulated data.

	d [mm]	f_{res} [Hz]	α_{max}	bandwidth [Hz]
f_1 meas.	0.2	1335	0.42	1180 - 1498
f_1 calc.	0.2	1000	0.92	490 - $\geq$ 2000
f_1 calc.	0.3	1200	0.43	1050 - 1482

Table 4.7: Alginate film 06, calculated [Eq. 2.45] and measured results.

Figure 4.17 shows the measured absorption coefficient α for Alginate film 06. The sample was perforated with the laser cutter and the design parameters ($b = 2\,\text{mm}$, $d = 0.2\,\text{mm}$) for the perforation pattern. Although we see MPP characteristics, the measured results differ significantly from the precalculated absorption curve with an assumed $\mathbf{d = 0.2\,mm}$ and slightly from an assumed $\mathbf{d = 0.30\,mm}$ as shown in Tab. 4.7. The absorption peak can be found at $f_1 = 1335\,\text{Hz}$ with $\alpha = 0.42$, resulting in a bandwidth of $\alpha \geq 0.4$ in the frequency range $1180\,Hz - 1498\,Hz$. However, due to the still remaining edge burning effect, the hole size **d** increases randomly. One can observe in Fig. 4.17 that assuming a hole size of $\mathbf{d = 0.30\,mm}$ fits the measurement best.

Manufacturing specifications

- **t = 100 µm, D = 5 cm**
- **Sodium alginate concentration:** 4 %
- **Cross linking agent:** $CaCl_2$, 0.04 g on 100 ml
- **Stirring time:** 30 min with sodium alginate, 40 min with added $CaCl_2$
- **Degasification time:** 8 hrs sodium alginate suspension, 24 hrs with added $CaCl_2$
- **Drying:** 6 hrs, 37°C
- **Properties:** After drying, no visible shrinkage. The material feels and behaves like plastic. A little less stiff and stable than the reference material. From the samples that form an optically transparent film, AL06 was the weakest material and teared most easily. This is due to the thickness of only 100 µm.
- **Acoustic properties:** MPP absorption characteristics can be observed, but with a small absorption peak found at $f_1 = 1335\,\text{Hz}$ with $\alpha = 0.42$. Compared to the expected value perforation with laser cutter works but reducing the hole size to $\mathbf{d \leq 0.3\,mm}$ is still an issue.

4.1.7 Alginate film 07 (AL07)

Alginate film 07 was a sample of a compound material, with additional wool fibers in the alginate suspension to increase its mechanical strength. The sample was already premade by a material scientist and available at the IAM of TU Graz, therefore the fabrication process is partly unknown. The sample shows the possibilities of using alginate as a hardening material to create new material combinations. Chitosan powder, another biopolymer like sodium alginate, was added to the alginate suspension with the aim to glue the material together. Figure 4.18 shows the sample and the enclosed fibres are clearly visible on (a). As we see more clearly on (b), the sample looks and feels like a stiff membrane. It is still very thin with a thickness of $t = 2\,\text{mm}$. This time, no plexiglas circle was used because the sample was stable enough and as shown on (c) the sample fits directly into the impedance tube.

(a) (b) Photo by Milena Stavric (c)

Figure 4.18: Alginate film 07

	m [g]	a $[cm^2]$	m' $[\frac{g}{cm^2}]$	Ξ $[\frac{Pa*s}{m^2}]$	f_{res} [Hz]	α_{max}	bandwidth [Hz]
f_1 meas.	4.6	78,54	-	-	445	0.90	340 - 1700
f_1 calc.	4.6	78.54	0.586	-	351	1	-
f_1 calc.	4.6	78,54	-	25000	1650	0.41	1400 - 1920

Table 4.8: Alginate film 07, calculated [Eq. 2.17 and Eq. 2.18 for membrane, Eq. 2.16 for porous material] and measured results.

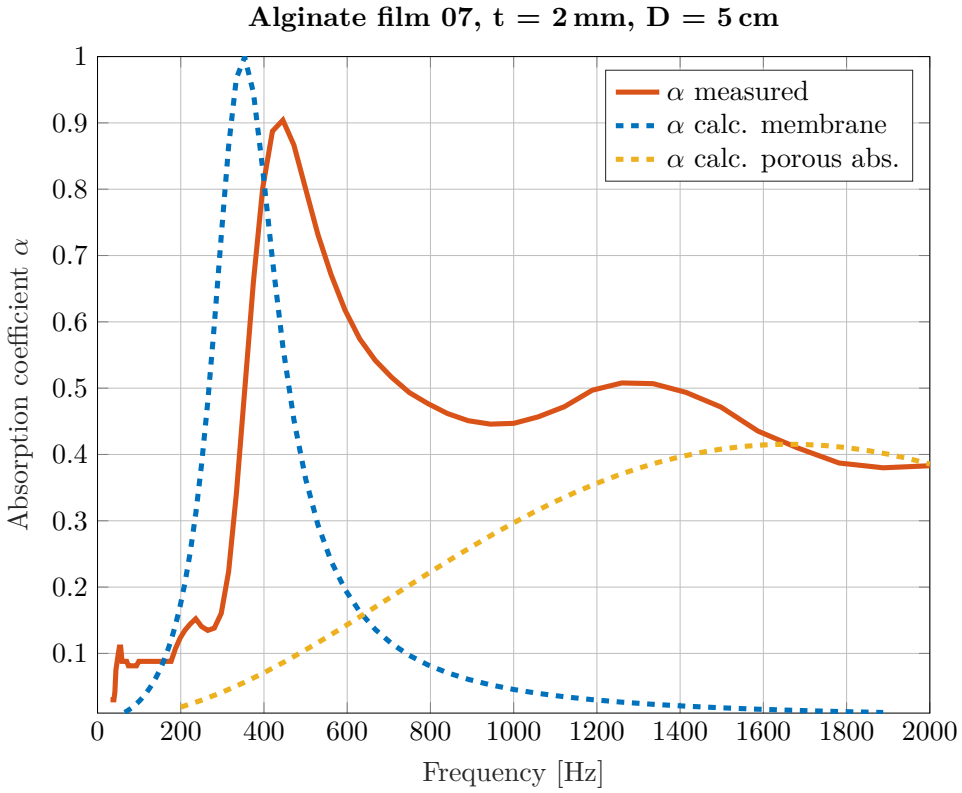

Figure 4.19: Absorption curve of AL07.

Figure 4.19 shows the measured absorption coefficient α for a sample made of alginate combined with wool fibres. We notice one narrow peak occurring at $f_1 = 445\,Hz$ with $\alpha = 0.90$. For the frequency range $340\,Hz$ to $1700\,Hz$ absorption with $\alpha \geq 0.4$ can be observed. As compressed wool can act as porous absorber, the panel with thickness, $t = 2\,\text{mm}$ with an assumed moderate flow resistivity $\Xi = 25000\ [\frac{Pa*s}{m^2}]$ is calculated, using the model of [Delany and Bazley, 1970] and implemented from Eq. 2.16. The obtained absorption coefficient leads into the direction of the measured curve and agrees approximately in the frequency range from $1200\,Hz$ to $2000\,Hz$. The flow resistivity is assumed to be similar to that of glass wool that feels a little more dense, like classic insulation panels. The sample **AL07** shows **characteristics** of a **membrane absorber** tuned to $f_1 = 445\,Hz$ and **broadband porous absorber** characteristics in the frequency range from $1200\,Hz$ to $2000\,Hz$. This is also compared with the calculation. For the calculation of $\underline{W}$ with Eq. 2.17 we assume a matched impedance and therefore $r = Z_0$. With Eq. 2.18 we calculate f_{res} for a membrane absorber. The calculated resonance frequency $f_1 = 351\,Hz$ lies below the measured $f_1 = 445\,Hz$. The added alginate and chitosan powder act like a glue with the fibres. To explain the absorption coefficient observed, further investigation is necessary.

Manufacturing specifications

- **Material properties:** With the added wool fibres, the material feels like hard felt. It is glued together with chitosan. Chitosan powder is a natural biopolymer derived from chitin, typically found in the shells of crustaceans. It is commonly used in pharmaceuticals, and cosmetics. At first glance, no air can pass through the sample.
- **Acoustic properties:** It shows behaviour of a membrane absorber with an absorption peak at $f_1 = 445\,Hz$. Some broadband absorption capabilities can be seen in the frequency range above, ranging from $1000\,Hz$ to $2000\ Hz$ with $\alpha \geq 0.4$. In total, the absorption coefficient lies above $\alpha \geq 0.4$ from $340\,Hz$ to $1700\,Hz$.

4.2 Double layer absorber

Now the absorption coefficient of double layer configurations were measured and then compared to the estimated absorption coefficient according to Chap. 2.4.3. The samples **AL03, AL04, AL05** and **AL06** were used.

4.2.1 Alginate film 05 and 04 (DL01)

First, a combination of AL05 and AL04 was measured. Therefore a special frame with long screws was built. This allowed the foils to be clamped into the frame and the distance between the two layers could be adjusted variably. Figure 4.20 shows the frame with two layers of the alginate film. A distance $D_1 = 6\,\text{cm}$ separates the two layers of alginate. The back layer (AL04) is assumed to be close to a rigid wall (b) with $D_2 = 1\,\text{cm}$. D_2 was a simulated air gap, implemented with the Software CATS8.

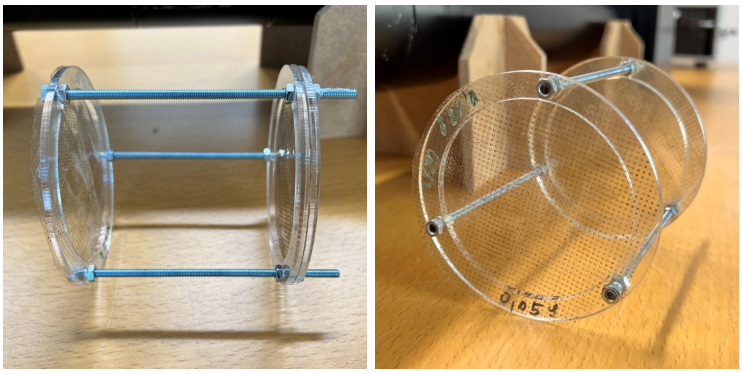

(a) (b)

Figure 4.20: DL01 setup.

	bandwidth [Hz]	D_1 [cm]	D_2 [cm]	α_{max}	f_{res} [Hz]
meas.	800 - 1408	6	1	0.54	1242
calc. d = 0.3 mm	800 - 1400	6	1	0.46	1050

Table 4.9: DL01 measurement and simulation data.

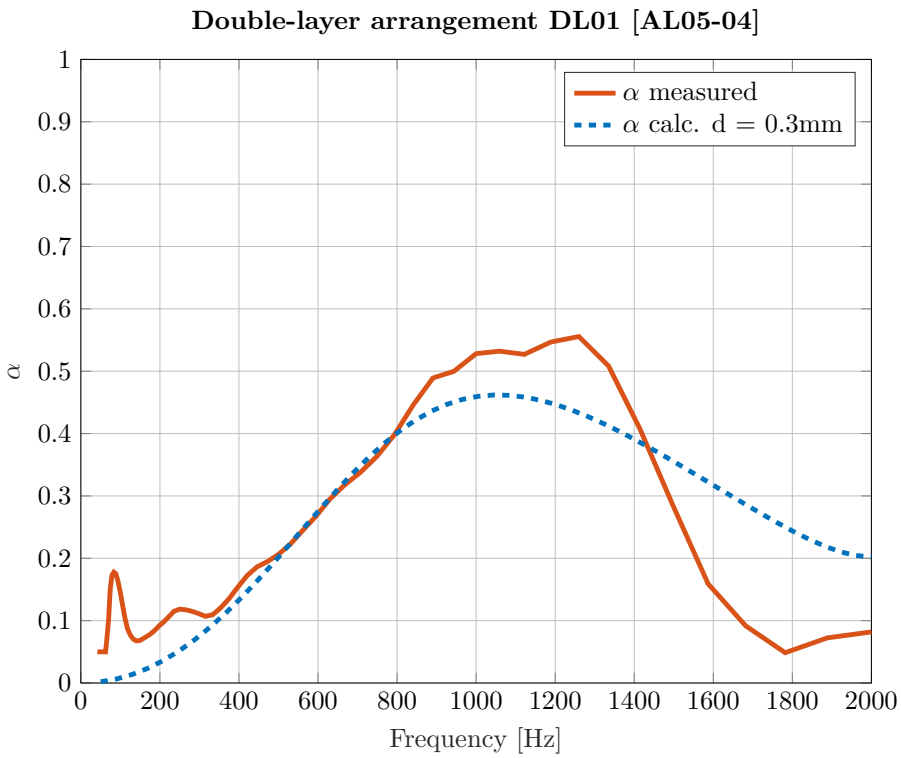

Figure 4.21: DL01 measurement compared to simulated data.

Figure 4.21 shows the measured absorption coefficient α for **DL01**. The configuration has the desired MPP characteristics with $\alpha \geq 0.4$ in the frequency range $800\,Hz$ to $1408\,Hz$. This measured absorption coefficient is compared with the simulation for a double-layer configuration. In difference to the calculated values, the absorption peak is slightly reduced and the absorption coefficient drops faster for frequencies above $1400\,Hz$. This can be either explained by an influence of the measurement setup or the two frames connected. Also inaccuracies on the perforation pattern of each layer and the resulting interaction of b and d might lead to the steeper absorption curve.

4.2.2 Alginate film 05 and 06 (DL02)

The same setup as for *DL01* was used. A distance $D_1 = 5\,\text{cm}$ separates the two layers of alginate. The front layer is AL05 while the back layer close to a rigid wall is AL06 with $D_2 = 1\,\text{cm}$. Also the influence of rotating AL05 by 120° is measured and discussed.

	bandwidth [Hz]	D_1 [cm]	D_2 [cm]	α_{max}	f_{res} [Hz]
measured	1059 - 1498	5	1	0.43	1260
meas. AL05 rotated	1020 - 1491	5	1	0.44	1260
calc. d = 0.31 mm	1055 - 1499	5	1	0.44	1189
calc. d = 0.25 mm	599 - 1850	5	1	0.70	1122

Table 4.10: DL02 measurement and simulation data

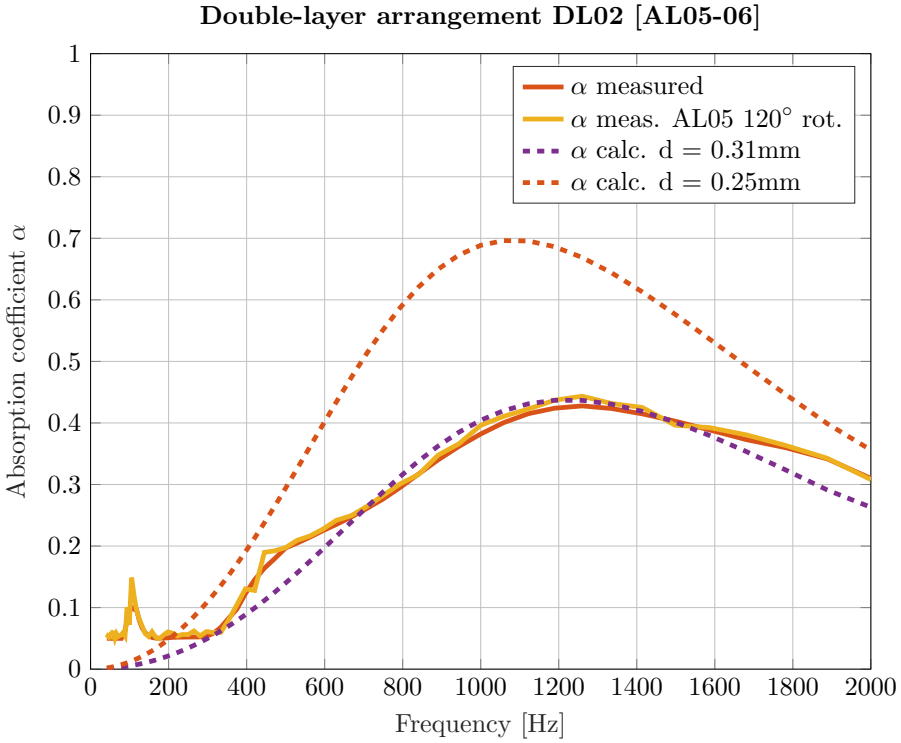

Figure 4.22: DL02 measurement and the first layer rotated by 120°.

Figure 4.22 shows the measured absorption coefficient α for **DL02**. The configuration has the desired MPP characteristics with $\alpha \geq 0.4$ in the frequency range $1059\,Hz$ to $1498\,Hz$. This measured absorption coefficient is compared with the simulation for a double-layer configuration. A second scenario with $d = 0.25\,\text{mm}$ for both films points out how much the acoustic performance can still be improved by reducing the hole size with a small $\Delta d = -0.06\,\text{mm}$. This would lead to a significantly increased bandwidth ranging from $599\,Hz$ to $1850\,Hz$. There is also an additional plot of the absorption curve for a rotated first layer of alginate (AL05) by 120 deg. The rotation does not affect the overall performance of the sample.

4.2.3 Alginate film 03 and 06 (DL03)

Now a configuration with one layer of alginate with membrane behaviour was measured. The same setup as for *DL01* was used. A distance $D_1 = 9\,\text{cm}$ separates the two layers of alginate. The front layer is AL03 while the back layer close to a rigid wall is AL06 with $D_2 = 1\,\text{cm}$. The samples were swapped afterwards and the measurement repeated.

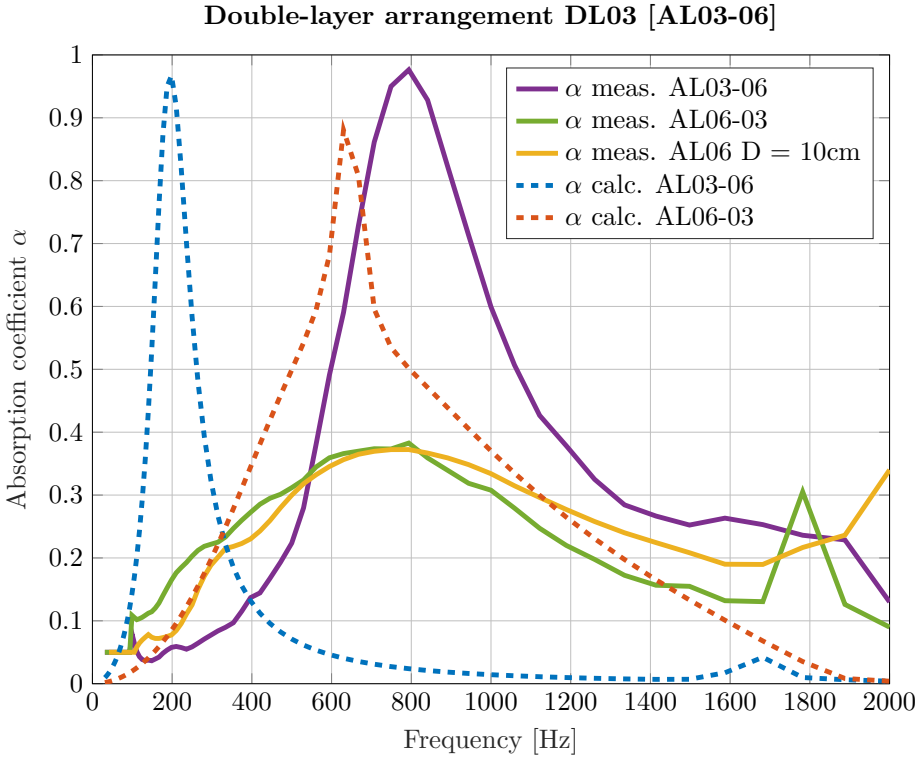

Figure 4.23: DL03 measurement compared to simulation.

	bandwidth [Hz]	D_1 [cm]	D_2 [cm]	α_{max}	f_{res} [Hz]
meas. AL03-06	562 - 1189	9	1	0.98	793
meas. AL06-03	-	9	1	0.38	793
meas. AL06	-	10	-	0.38	780
calc. AL03-06	140 - 280	9	1	0.97	198
calc. AL06-03	420 - 1000	9	1	0.88	630

Table 4.11: DL03 measurement and simulation data

Figure 4.23 shows the measured absorption coefficient α for **DL03**. With AL03 (membrane) in front and AL06 close to the rigid wall, the configuration has MPP characteristics with $\alpha \geq 0.4$ in the frequency range $562\,Hz$ to $1189\,Hz$ peaking at a high and relatively narrow $\alpha = 0.98$ with frequency $f_{res} = 793\,Hz$. For the flipped configuration we obtain no significant impact as the absorption curve stays below $\alpha \leq 0.4$. It is noticeable that both measurements indicate a peak at $793\,Hz$ that cannot be explained with the assumed simulations. For the simulated curves the impedance of the membrane layer is calculated according to Eq. 2.18. However, this does not seem to be the appropriate approach for this kind of layer configuration. The assumed characteristic peak for a membrane absorber does occur, but it is shifted from the expected $f_{res} = 198\,Hz$ to $f_{res} = 793\,Hz$. The expected peak fits the considerations, as an impermeable membrane should lead to this absorption coefficient. This indicates, that more air than expected gets through the first membrane layer which might be also caused by the measurement setup. For the flipped arrangement with the microperforated membrane in front, *DL03 [AL06-03]*, the characteristics of the simulated curve *calc. AL06-03* can be interpreted as similar to the measured result. However, the peak coming from the membrane does not occur in the measurement and an overall reduced absorption coefficient is noticed. The performance of only one layer *AL06* with the increased cavity depth of $D_1 = 10\,\text{cm}$ shows similar performance to the double layer arrangement. Therefore there is no benefit if two films are used.

4.3 Discussion

For a better comparison of the performance of the individual samples, Fig. 4.24 plots all absorption curves of the single layer measurements into one graphic. The parameters of each film are found in Tab. 4.12 and the following conclusions can be drawn:

- The samples can be divided into two categories. **AL01, AL02** and **AL03** show characteristics of a membrane absorber, although on AL01 a second and on AL02 even a second and third absorption peak occurs. It appears at a frequency of ≈ twice the resonance frequency, with an additional peak slightly below for AL02. **AL04, AL05** and **AL06** show the behaviour of a microperforated panel but with a reduced peak due to limited manufacturing accuracy. The sweetspot known from the parameter study cannot be reached.
- **AL03** acts like a membrane absorber with a strong absorption peak. The sample has an increased thickness compared to the other samples due to a shorter drying time and the added plasticizer Glycerol. The perforation approach with the needle roller had no noticeable impact.
- **AL04**, **AL05** and **AL06** almost entirely match the predicted behaviour with the limitation of an increased hole size $d = 0.3\,mm$. A hole size of $d = 0.2\,mm$ was desired according to the parameter study applied on earlier stage to obtain good broadband absorption between $500\,Hz$ and $2\,kHz$ with $\alpha \geq 0.4$. Further improvement on the perforation technique is necessary.
- The "perforation ratio" of **AL01** and **AL02** is hard to determine, as in both cases air is enclosed in small bubbles spread randomly over the alginate surface. However, due to the measurement it has an impact on the overall absorption curve that leads to an additional absorption peak.
- **AL07** is the only sample that consists of a compound material. The material is a mixture of alginate, wool fibres and chitosan. The resulting sample looks like a membrane and has an increased thickness of $2\,mm$. It shows a strong membrane absorption peak with $f_{res} = 445\,Hz$ and a total bandwidth of $340\,Hz$ to $1700\,Hz$. For higher frequencies this could be explained by an assumed porous structure.

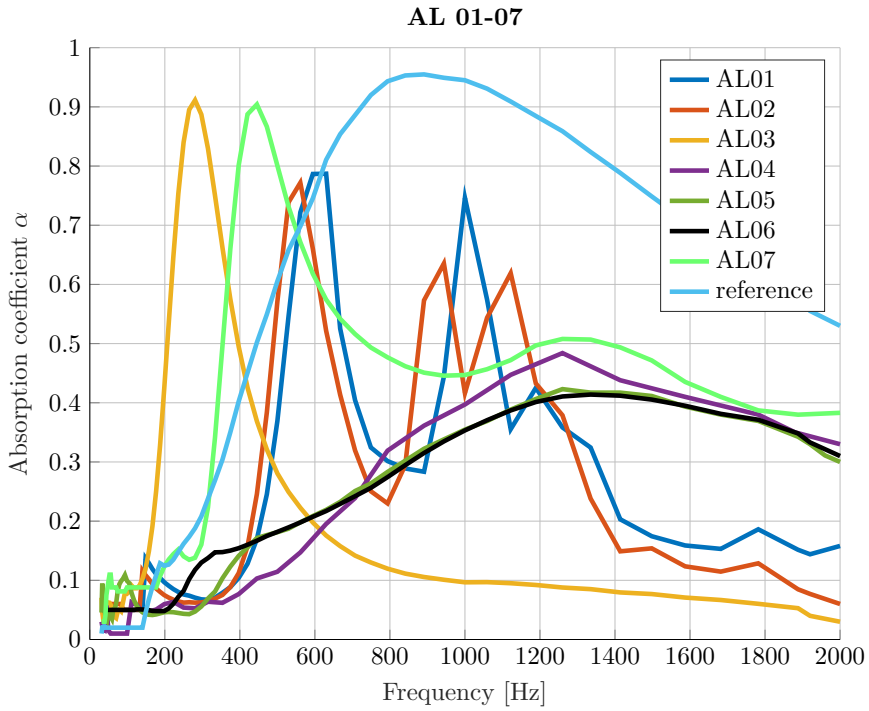

Figure 4.24: Absorption coefficient of all samples. $D = 5\,cm$

	d [mm]	b [mm]	t [mm]	bandwidth [Hz]	α_{max}	f_{res} [Hz]
AL01	-	-	0.170	-	0.78, 0.75	630, 1000
AL02	-	-	0.164	-	0.77, 0.63, 0.62	561, 943, 1122
AL03	-	-	0.410	-	0.91	281
AL04	0.32	2	0.160	1020 - 1620	0.49	1260
AL05	0.31	2	0.120	1150 - 1550	0.42	1260
AL06	0.30	2	0.100	1180 - 1498	0.42	1335
AL07	-	-	2	340 - 1700	0.90	445
reference	0.2	2	0.150	400 - $\geq$ 2000	0.95	891

Table 4.12: Overview of all single layer samples with their parameters.

Now we look at the results from the double layer measurements. For a better comparison of the performance of the individual samples, Fig. 4.25 plots all absorption curves of the double layer measurements into one graphic. The parameters of each film are found in Tab. 4.13 and the following conclusions can be drawn:

- **DL01** and **DL02** consist of two layers of microperforated films. Although the design parameters only differ slightly in hole size, we notice the following differences between the cases DL01 and DL02.
- **DL01** shows the characteristics of a microperforated absorber and comes close to the simulated result (Fig. 4.21). Overall absorption is increased in comparison to the single layer result of AL05 and AL04.

- **DL02** shows only little improvement against the single layer results AL05 and AL06. Rotating one layer against the second had no noticeable impact. From the simulation plot in Fig. 4.22 we notice the big impact the hole size of the layers has. Only a small reduction in size with $\Delta d = -0.06\,\text{mm}$ improves the bandwidth and the absorption coefficient significantly.
- **DL03** was a combined setup with one layer of alginate with the characteristics of a membrane absorber and one microperforated layer. However, using the model for multi-layer microperforated panels did not lead to comparable results with the measurement.

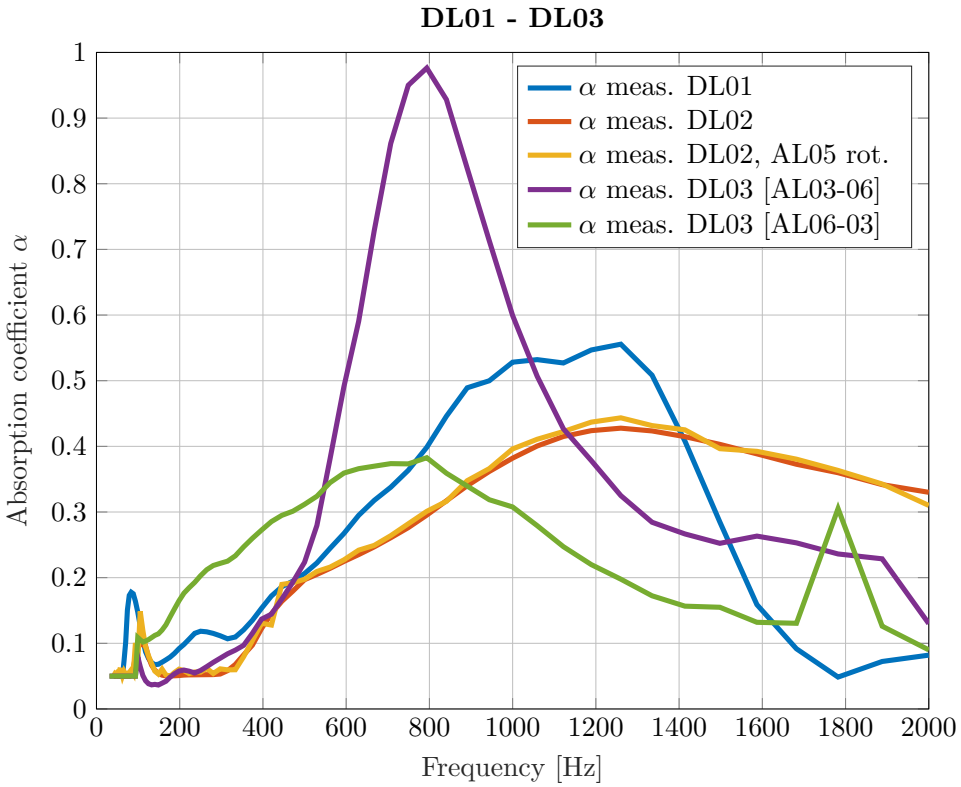

Figure 4.25: Absorption coefficient of all double-layer configurations.

	D_1 [cm]	D_2 [cm]	bandwidth [Hz]	α_{max}	f_{res} [Hz]
DL01	6	1	800 - 1408	0.54	1242
DL02	5	1	1059 - 1498	0.43	1260
DL02, AL05 rot.	5	1	1020 - 1491	0.44	1260
DL03 (AL03-06)	9	1	562 - 1189	0.98	793
DL03 (AL06-03)	9	1	-	0.38	793

Table 4.13: Overview of all double layer samples with their parameters.

5 Conclusion and outlook

Replacing environmentally harmful materials also for acoustic purposes is incredibly important and remains a subject of great interest. This work shows the capabilities of alginate as a great substitute for traditional materials. As we learn more about the impact of different materials on our environment, there is a growing need to find sustainable alternatives. Therefore, this work begins with the question of the possible uses of sustainable materials in acoustics. At the moment crude oil still plays a major role both in plastic production and for fiber production such as rock wool. As a welcome alternative some of the sustainable materials showed great potential for future usage in acoustic applications. From recycled materials like denim or cotton to plant based materials like mycelium, a variety of substances was presented until we finally reached the promising material *alginate*, that was chosen to be the basis for this work. The lack of optically transparent materials available further drew the attention towards alginate. However, to further evaluate the acoustic potential of this material extracted from seaweed, a theoretical framework was needed. Therefore the work started with sound propagation, the theory of membrane absorbers and finally reaching the big topic of microperforated absorbers. To get an insight on what kind of design parameters had to be tuned a parameter study was performed. This led to the following findings:

- The acoustic behaviour of microperforated films can be tuned by only four parameters. Material thickness t, the applied perforation with hole size d and hole spacing b and a certain distance D to a rigid wall. Circular holes provide best absorption properties.
- To obtain broadband absorption, a parameter set of $d \leq 0.2\,\mathrm{mm}$, $b \leq 2\,\mathrm{mm}$ and a thickness t between 100 µm and 200 µm allows for broadband sound absorption between $400\,Hz$ and $5000\,Hz$ by needing only a cavity depth D of $\approx 5\,\mathrm{cm}$.
- Structures with multiple layers of perforated sheets further improve the acoustic performance but the measured impact in this work was neglectable. Doubling the layer would also increase the costs.
- Although the framework is known for more than 40 years, due to the manufacturing difficulties when applying perforation in submillimetric size and below, this absorber type has great potential for future usage.

During the fabrication process of the alginate films an approach of trial and error was needed to achieve stable films. Starting with alginate powder and distilled water with only one or two additional ingredients, a plastic-like, stable and transparent film could be produced. However, there were still some challenges to address, particularly regarding the durability of the alginate and predictability of the resulting film thickness. The volume reduction during the drying process varied, and further investigation into possible additives to the alginate suspension is needed. The films on the one hand withstand higher air humidity after the process of cross-linking, but the samples are still not water-resistant. The moldering process is also harmful to the films. If the suspension is not dried out entirely before mold growth starts, the films get damaged. Therefore methods for a faster drying process or additives like a fungicide also require consideration.

At this point, the resulting films can be used as a transparent membrane absorber with a tear resistance that feels comparable to that of plastic. What makes alginate so unique, is the possibility to produce flat, optically transparent films with sheet thicknesses typically used for microperforated foils. However, a big part of the work involved figuring out the best way to apply the micro-perforations to the films. It turned out, that there is still great potential in finding new industrial tools with mechanical, chemical, or novel methods of applying the perforation pattern.
After trying to use a salt perforation method and a special needle roller used by the cosmetic industry, the best way to achieve microperforation was to use a laser cutter. Although this was the best method to apply these small hole sizes, we could not entirely reach the sweet spot for acoustic performance. A special barrier in our fabrication process was further reducing the hole size from $d = 0.3\,\mathrm{mm}$ to at least $d = 0.25\,\mathrm{mm}$ that would already have led to an expected doubled absorption peak and an increased absorption bandwidth to the frequency range of $600\,Hz$ to $5000\,Hz$. In this partly interdisciplinary work it was proven, that the biodegradable material alginate is suitable as a basis for acoustic applications. The most outstanding advantage is the possibility of replacing plastic and still obtaining a transparent material. Even without perforation applied alginate has great potential as the measurements showed that it also suits as a transparent membrane absorber.

Further topics of interest would be enhancing the durability of the transparent films, optimization of the fabrication and the composition and applying further perforation techniques. Also the question of extending the fabrication process to big acoustic panels for further measurements in the reverberation chamber is of great interest. Acoustics play a crucial role in various industries, from construction to entertainment. By using this eco-friendly alternative, that also provides a unique translucent design element, we can reduce waste and pollution while creating healthier and more sustainable spaces. Changing our habit to stop relying only on traditional materials can lead us towards a greener and more responsible future.

A
Appendix

List of Matlab files

RESONANT ABSORBER DEVICES	
Helmholtz_epsilon.m	calculate epsilon from measured f_res
membrane_f_res.m	calculate f_res from weight and size
membrane_ZtoAlpha.m	calculate curve α from weight and size
POROUS ABSORBER DEVICE	
por_abs.m	calculate α from thickness
delany_bazley.m	model of Delany Bazley
MPP ABSORBER DEVICES	parameter study, calculate α
mpp_compare_d.m	effect of hole diameter
mpp_compare_b.m	effect of hole spacing
mpp_compare_t.m	effect of panel thickness
mpp_compare_epsilon.m	effect of perforation ratio
mpp_compare_ultra_perf.m	further reduction of hole size and spacing
mpp_compare_slits.m	effect of perforation shape
mpp_multilayer_2layers.m	arrangement of two MPP layers
mpp_multilayer_3layers.m	arrangement of three MPP layers
EVALUATION OF SAMPLES	compare measured and predicted results
mpp_AL01.m	
mpp_AL02.m	
mpp_AL03.m	
mpp_AL04.m	
mpp_AL05.m	
mpp_AL06.m	
mpp_AL07.m	
mpp_DL01.m	
mpp_DL02.m	
mpp_DL03.m	
mpp_AL_ALL.m	
mpp_DL_ALL.m	
mpp_Opalfilm.m	

Bibliography

Acoustic, V. (2023). *Visacou acoustic* [S-plasticon]. Retrieved May 16, 2023, from https://s-plasticon.gr/materials/visacou-honeycomb-acoustic/

AlgiKnite. (2023). *Algiknite*. Retrieved June 2, 2023, from https://www.keellabs.com/

Arora, B., Tandon, R., Attri, P., & Bhatia, R. (2017). Chemical crosslinking: Role in protein and peptide science. *Current Protein & Peptide Science*, *18*(9). https://doi.org/10.2174/1389203717666160724202806

Bold, H. C., Alexopoulos, C. J., & Delevoryas, T. (1987). *Morphology of plants and fungi* (5th ed). Harper & Row.

Bravo, T., Maury, C., & Pinhède, C. (2014). Micro-perforated panels for silencers in ducted systems.

Bucciarelli, F., Malfense Fierro, G., & Meo, M. (2019). A multilayer microperforated panel prototype for broadband sound absorption at low frequencies. *Applied Acoustics*, *146*, 134–144. https://doi.org/https://doi.org/10.1016/j.apacoust.2018.11.014

Byrd, P. F., & Friedman, M. D. (1971). *Handbook of elliptic integrals for engineers and scientists*. Springer Berlin Heidelberg. https://doi.org/10.1007/978-3-642-65138-0

Caniato, M. (2019). Sound absorption performance of sustainable foam materials: Application of analytical and numerical tools for the optimization of forecasting model. *Applied Acoustics*, *161*. https://doi.org/10.1016/j.apacoust.2019.107166

Cox, T. J., & D'Antonio, P. (2009). *Acoustic absorbers and diffusers: Theory, design and application* (2nd ed) [OCLC: ocn227922698]. Taylor & Francis.

Crandall, I. (1926). *Theory of vibrating systems and sound*. Creative Media Partners, LLC. https://books.google.at/books?id=JvOJNAEACAAJ

Delany, M., & Bazley, E. (1970). Acoustical properties of fibrous absorbent materials. *Applied Acoustics*, *3*(2), 105–116. https://doi.org/10.1016/0003-682X(70)90031-9

Fuchs, H. V. (2007). *Schallabsorber und schalldämpfer: Innovative akustische konzepte und bauteile mit praktischen anwendungen in konkreten beispielen* (2., wesentlich erw. und bearbeitete Aufl) [OCLC: 164438580]. Springer.

Fuchs, H. V. (2017). *Raum-akustik und lärm-minderung: Konzepte mit innovativen schallabsorbern und -dämpfern* (4. Auflage). Springer Vieweg.

Fuchs, H. V., & Zha, X. (1997). Acrylic-glass sound absorbers in the plenum of the deutscher bundestag. *Applied Acoustics*, *51*, 211–217.

Haverkamp, D. (n.d.). *OPALFILM-whisper*. Retrieved February 21, 2023, from https://www.haverkamp.de/_data/downloads/productfiles/Folientechnologie/OPALVARIO/OPALFILM-Whisper_OPALWHISPER.pdf

HELIOACOUTEX. (2023). *Helioacoutex*. https://www.tuchler.net/en/1001766-membrane-helioacoutex-microperforated.html

Hemmer, D. (2022, February 28). *Absorbertheorien und materialforschung für den raumakustischen anwendungsbereich* (project thesis). TU Graz. https://download.spsc.tugraz.at/thesis/TIP_Hemmer.pdf

Herrin, D., Liu, J., & Seybert, A. (2011). Properties and applications of microperforated panels. *Sound and Vibration*, *45*, 6–9.

Herrin, D., Liu, W., Hua, X., & Liu, J. (2017). A guide to the application of microperforated panel absorbers. *Sound and Vibration*, *51*, 12–18.

Iannace, G., Ciaburro, G., Guerriero, L., & Trematerra, A. (2020). Use of cork sheet for room acoustic correction. *Journal of Green Building*, *15*, 45–55. https://doi.org/10.3992/1943-4618.15.2.45

Ingard, U. (1953). On the theory and design of acoustic resonators. *The Journal of the Acoustical Society of America*, *25*(6), 1037–1061. https://doi.org/10.1121/1.1907235

ISO 11654:1997. (1997). ISO 11654:1997. https://www.iso.org/standard/24883.html

kelp forest. (2020). *Kelp forest*. Retrieved February 1, 2023, from https://www.sportdiver.com/sites/sportdiver.com/files/styles/opengraph_1_91x1/public/images/2017/06/kelp1_istock-520593426.jpg?itok=bwAn7KyK

Kuttruff, H. (2019). *ROOM ACOUSTICS* [OCLC: 1129771363]. CRC Press.

Maa, D. Y. (1975). Theory and design of microperforated panel sound-absorbing constructions.

Maa, D.-Y. (1998). Potential of microperforated panel absorber. *The Journal of the Acoustical Society of America*, *104*(5), 2861–2866. https://doi.org/10.1121/1.423870

Maa, D. (2000). Theory of microslit absorbers. *Shengxue Xuebao/Acta Acustica*, *25*, 481–485.

Maier, A. (2010). Artikel SAIL 300 b1, 3.

Marjanović, I. (2022). *Alginat in der architektur* (Master Thesis). TU Graz.

MNLRoller. (2023). *Micro-needling roller*. Retrieved June 2, 2023, from https://www.amazon.de/gp/product/B08GJZ5XJP/ref=ppx_yo_dt_b_search_asin_title?ie=UTF8&psc=1

Oldfield, R. (2006, September). *Improved membrane absorbers* (Master Thesis). University of Salford. Salford, UK.

Org, B. t. b. (2023). *Backtoblue: Plastics consumption*. https://backtoblueinitiative.com/plastics-consumption/

PCal. (2023). *Porous absorber calculator*. http://www.acousticmodelling.com/porous.php

Pedro, C., & Simón, F. (2019). Multiple-layer microperforated panels as sound absorbers in buildings: A review. https://doi.org/10.20944/preprints201901.0248.v1

Pelletier, M., Holt, G., Wanjura, J., Bayer, E., & McIntyre, G. (2013). An evaluation study of mycelium based acoustic absorbers grown on agricultural by-product substrates. *Industrial Crops and Products*, *51*, 480–485. https://doi.org/10.1016/j.indcrop.2013.09.008

Qian, Y., Kong, D., Liu, S., Sun, S., & Zhao, Z. (2013). Investigation on micro-perforated panel absorber with ultra-micro perforations. *Applied Acoustics*, *74*, 931–935. https://doi.org/10.1016/j.apacoust.2013.01.009

Raj, M., Fatima, S., & Tandon, N. (2020). Recycled materials as a potential replacement to synthetic sound absorbers: A study on denim shoddy and waste jute fibers. *Applied Acoustics*, *159*, 107070.

Rayleigh, L. (1945). *Theory of sound*. Dover Publications.

Rehm, B. H., & Moradali, M. F. (Eds.). (2018). *Alginates and their biomedical applications*. Springer Singapore. https://doi.org/10.1007/978-981-10-6910-9

Sakagami, K., Yairi, M., & Morimoto, M. (2010). Multiple-leaf sound absorbers with microperforated panels: An overview. *Acoustics Australia*, *38*.

Setaki, F., Tian, F., Turrin, M., Tenpierik, M., Nijs, L., & Van Timmeren, A. (2023). 3d-printed sound absorbers: Compact and customisable at broadband frequencies. *Architecture, Structures and Construction*, *3*(2), 205–215. https://doi.org/10.1007/s44150-023-00086-9

Smetacek, V. (1991). Die primärproduktion der marinen plankton-algen. *Spektrum der Wissenschaften, Dez.1991*, 52–63.

sound barrier, T. (2023). *Materialdistrict utrecht* [Exhibition]. Retrieved May 16, 2023, from https://materialdistrict.com/material/3d-engineered-sound-barrier/

TA. (2023). Skriptum technische akustik, tu graz.

Tayong, R., Dupont, T., & Leclaire, P. (2011). Experimental investigation of holes interaction effect on the sound absorption coefficient of micro-perforated panels under high and medium sound levels. *Applied Acoustics*, *72*(10), 777–784. https://doi.org/10.1016/j.apacoust.2011.04.011

Tourlomousi, O. (2017). *Microperforated glass* (Master Thesis). TU Delft.

Utrecht, M. (2023). *Materialdistrict utrecht* [Exhibition]. Retrieved May 16, 2023, from https://materialdistrict.com/event/materialdistrict-utrecht-2023/

Wack, R., & Fuchs, H. (2004). On the use of micro-perforated sails in assembly rooms. https://publica.fraunhofer.de/handle/publica/346251

Wood, A. (2023). *Acoustic wood*. https://www.decustik.com/en/acoustic-panels/microperforated-acoustic-panels

Zwicker, E., & Zollner, M. (1993). *Elektroakustik*. Springer Berlin Heidelberg. https://doi.org/10.1007/978-3-642-58003-1

Zwikker, C., & Kosten, C. W. (1949). *Sound absorbing materials*. Elsevier Science.